INFORMATION TO USERS

UNIVERSITY OF CALIFORNIA

Santa Barbara

Carrier Dynamics in Self-Organized Quantum Dots

A dissertation submitted in partial satisfaction
of the requirements of the degree of

Doctor of Philosophy

in

Electrical and Computer Engineering

by

Gary Wang

Committee Members:

Professor John E. Bowers, Chairman
Professor James L. Merz
Professor Pierre M. Petroff
Professor Arthur Gossard

January 1997

UMI Number: 9727730
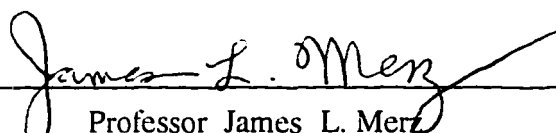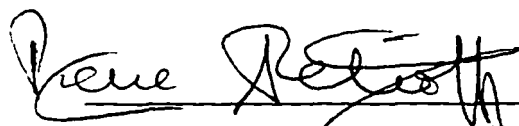
The dissertation of Gary Wang
is approved by

_____
Professor John E. Bowers

_____
Professor James L. Merz

_____
Professor Pierre M. Petroff

_____
Professor Arthur Gossard

January 1997

To my family and friends

Acknowledgements

The journey through graduate school has been a wonderful experience. I would like to thank not only those people who have assisted my research in this dissertation but also all my friends who I have met during the last six years. Prof. Bowers and Prof. Merz has provided me with plenty of support and encouragement. Prof. Gossard and Prof. Petroff have answered many fundamental questions I had on quantum structures. Their knowledge and insights have propelled my learning. Their demands for excellence have cultivated my success. Their generosities and enthusiasm have touched my heart.

This research could not be possible without the quantum dot samples from Devin Leonard. Rosa Leon, G. Medeiros-Ribeiro and Casper Reaves. I would also like to thank those who has provided me the much needed experimental expertise. Helga Weman and Julie Fouquet have taught me the photoluminescence and time-correlated single photon counting experiment. Simon Fafard has taught me PLE experiment. Judy Karin, Wenbin Jiang, Kirk Giboney, and Andy Hays have provided me with the essential knowledge of ultrafast lasers. Laura Smilowitz has assisted me in the understanding of streak camera measurement. Scott Crooker and Chi-Kwang Sun have answered many questions on the pump-and-probe measurement. I am also grateful to many useful discussions I had with Prof. Awschalon, Prof. Atac, Prof. Brewer, Rajeev Ram, Roger Helkey, Dennis Derickson, Dubravko Babic, Radha Nagarajan and others. The engineering staffs have provided me with numerous helps. Tom Reynolds has maintained many essential equipment in the lab. The supports of Jack Whaley, Dan Cone, Don Zak, Martin Vandenbroek, and staffs at QUEST and ECE have been wonderful.

I will always remember the supports from my friends Dane Venaas, Gordon Shaeffer, Patsy Dorsey, Lorraine Gersitz, Bruce Gunter, Nancy Clayton, and Anastasia Telesetsky. Thank you.

Vita

November 24, 1967:	Born Taipei, Taiwan.
June 15, 1990:	B.S., Physics, College of Creative Studies, University of California, Santa Barbara
June 15, 1990:	B.S., Electrical and Computer Engineering, University of Calfornia, Santa Barbara
June 12, 1992:	M.S., Electrical and Computer Engineering, University of Calfornia, Santa Barbara

Publications and Conference Presentations

D. Tauber, G. Wang, R. S. Geels, J. E. Bowers, and L. A. Coldren, "70 GHz Relaxation Oscillation in a Vertical Cavity Surface Emitting Laser," Device Research Conference, Boston, MA, June (1992).

L. Smilowitz, A. Hays, A. J. Heeger, G. Wang, and J. E. Bowers, "Picosecond Time Resolved Photoluminescence in MEHPPV-Solution, Film, Gel, and Blend," (International Conference on Science and Technology of Synthetic Metals, ICSM '92, Goteborg, Sweden, 12-18 Aug. 1992). Synthetic Metals, 15 March 1993, vol.55, (no.1):249-54.

L. Smilowitz, N. S. Sariciftci, C. Gettinger, A. J. Heeger, F. Wudl, G. Wang, and J. E. Bowers, "Photoexcitation Spectroscopy of Photoinduced Electron Transfer Conducting Polymer-Buckminsterfullerence Composites", (Non-Linear Optical Properties of Advanced Materials, Los Angeles, CA, USA, 20-21 Jan. 1993). Proceedings of the SPIE - The International Society for Optical Engineering, 1993, vol.1852:316-26.

A. Hays, L. Smilowitz, A. J. Heeger, G. Wang, and others. "Picosecond Photoluminescence from Poly (2-Methoxy,5-(2'-Ethyl-Hexyloxy)-P-Phenylene-Vinylene): Solutions, Gels, Films and Blends." (Nonlinear Optical Properties of Advanced Materials, Los Angeles, CA, USA, 20-21 Jan. 1993). Proceedings of the SPIE - The International Society for Optical Engineering, 1993, vol.1852:327-36.

D. Tauber, G. Wang, R. S. Geels, J. E. Bowers, and L. A. Coldren, "Large and Small Signal Dynamics of Vertical Cavity Surface Emitting Lasers", *Appl. Phys. Lett.*, 62(4), 325-327, January 25 (1993).

G. Wang R. L. Nagarajan, D. Tauber, and J. E. Bowers, " Picosecond Gain Dynamics in Vertical Cavity Surface Emitting Laser: Transient Carrier Heating and Gain Enhancement," Ultrafast Electronic & Optoelectronics Conference, San Francisco, CA, Jan. 25-27 (1993).

J. Bowers, D. Babic, G. Wang, D. Tauber, W. Jiang, and R. L. Nagarajan, "Vertical Cavity Laser High Speed Dynamics and Modeling," INVITED PAPER, Integrated Photonics Research Topical Meeting, Palm Springs, March 22-24 (1993).

L. Smilowitz, A. Hays, A. J. Heeger, G. Wang, and J. E. Bowers, "Time Resolved Photoluminescence from Poly (2-methoxy, 5-(2'ethyl-hexloxy)-p-phenylene-vinylene): Solutions, Gels, Films. and Blends", J. Chem. Physics , 98(8). 6504-6509. April 15 (1993).

G. Wang, R. L. Nagarajan, D. Tauber, and J. E. Bowers, "Reduction of Damping in High Speed Semiconductor Lasers", Photon. Tech. Lett., 5(6), 642-645, June (1993).

C. C. Barron, C. J. Mahon, B. J. Thibeault, G. Wang, L. A. Coldren, and J. E. Bowers, "Asymmetric Fabry-Perot Modulators with Millimeter-Wave (37 Ghz) Frequency Response," Post Deadline Paper VIB-9, 51st Annual Device Resarch Conference, Santa Barbara, CA June 21-23 (1993).

C. C. Barron, C. J. Mahon, B. J. Thibeault, G. Wang, W. Jiang, L. A. Coldren, and J. E. Bowers, "High-speed III-V Asymmetric Fabry-Perot modulators", (LEOS '93 Conference Proceedings. IEEE Lasers and Electro-Optics Society 1993 Annual Meeting, San Jose, CA, USA, 15-18 Nov. 1993). New York, NY, USA: IEEE, 1993. p. 658-9.

G. Wang, S. Farfard, D. Leonard, J. E. Bowers, P. Petroff, and J. Merz, "Time Resolved Photoluminescence in InGaAs Quantum Dots," IQEC, Anaheim, CA May 8-13 (1994).

G. Wang, S. Fafard, D. Leonard, J. E. Bowers, J. L. Merz, and P. M. Petroff, "Time Resolved Optical Characterization of InGaAs/GaAs Quantum Dots", Applied Physics Letters, 64(21), 2815-7, May 23 (1994).

C. C. Barron, C. J. Mahon, B. J. Thibeault, G. Wang, W. Jiang, L. A. Coldren, and J. E. Bowers, "Resonant-Cavity-Enhanced P-I-N Photodetector With 17 Ghz Bandwidth-Efficiency Product", Electronics Letters, 30(21) 1796-1797 October (1994).

G. Wang, C.-K. Sun, D. Leonard, G. M. Riberio, J. E. Bowers, P. M. Petroff, J. Oshinowo, and Y. Arakawa, "Exciton Dynamics in InGaAs/GaAs Quantum Dots," Postdeadline Paper, Quantum Optoelectronics Topical Meeting, Dana Point, CA, March 13-15 (1995).

C. C. Barron, C. J. Mahon, B. J. Thibeault, G. Wang, W. Jiang, L. A. Coldren, and J. E. Bowers, "Millimeter-Wave Asymmetric Fabry-Perot Modulators", *Journal of Quantum Electronics*, 31 (8), 1484-1493, August (1995).

C.-K. Sun, G. Wang, J. E. Bowers, B. Brar, H.-R Blank, H. Kroemer, and M. H. Pilkuhn, "Optical Investigations of the Dynamic Behavior of GaSb/GaAs Quantum Dots", *Applied Physics Letters*, 68 (11), 1543-1545, March 11, (1996).

G. Wang, C.-K. Sun, H. R. Blank, B. Brar, J. E. Bowers, H. Kroemer, and M. H. Pilkuhn, "Time Resolved Optical Investigation of Spatially Indirect Excitons in GaAs/GaSb Quantum Dots," CLEO/QELS '96, June 2-7 (1996).

R. J. Ram, C.-K. Sun, G. Wang, E. Goobar, J. Ko, M. Oestreich, J. E. Bowers, and A. Imamoglu, "Dynamics of Condensing Polaritons," IQEC '96, Sydney, Australia, July 14-19 (1996).

C.-K. Sun, G. Wang, M. S. Minsky, J. E. Bowers, S. Keller, B. Keller, and S. P. DenBaars, "Time-Resolved Photoluminescence Study in InGaN Single-Quantum-Well," Electronic Materials Conference, Santa Barbara, CA, June 26-28 (1996).

G. Wang, C.-K. Sun, J. E. Bowers, G. Medeiro and P. M. Petroff, "Ultrafast Carrier Dynamics in InAs Self-Organized Quantum Dots," Postdeadline Paper, IQEC'96, Sydney, Australia, July 14-19 (1996).

S. Fafard, S. Raymond, G. Wang, R. Leon, D. Leonard, S. Charbonneau, J. L. Merz, P. M. Petroff, and J. E. Bowers, "Temperature Effects on the Radiative Recombination in Self-Assembled Quantum Dots," (11th International Conference on the Electronic Properties of Two-Dimensional Systems, Nottingham, UK, 7-11 Aug. 1995). *Surface Science*, 20 July 1996, vol.361-362:778-82.

C.-K. Sun, S. Keller, G. Wang, M. S. Minsky, J. E. Bowers, and S. P. DenBaars, "Radiative Recombination Lifetime Measurements Of Ingan Single-Quantum-Well," *Appl. Phys. Lett.* 23 Sept. 1996, vol.69, (no.13):1936-8.

Abstract

Carrier Dynamics in Self-Organized Quantum Dots

by Gary Wang

Recent developments in the growth of self-organized quantum dots have provided opportunity to investigate the physics of zero- dimensional quantum structure. In this work, we investigate the carrier dynamics in the In(Ga)As/(Al)GaAs self-organized quantum dots using time-resolved photoluminescence and pump-and-probe spectroscopy. Three areas of carry dynamics are studied: radiative recombination, thermionic emission, and carrier relaxation. The measured radiative lifetime is compared to the published results. A reduced radiative transition rate is found. This increase in the PL decay time can be attributed to the localization of the exciton in the quantum dot. From the temperature dependent measurement, we find that the reduction of quantum dot photoluminescence efficiency at high temperature is attributed to the thermionic emission. The effect of thermionic emission process can significantly modify the potential quantum dot device properties such as optical gain and modulation bandwidth. From the transient absorption measurement, a fast carrier relaxation rate is deduced. The measured carrier relaxation time is an order of magnitude smaller than the theoretical prediction of the phonon bottleneck, indicating other relaxation mechanism might be dominant in these quantum dots.

Table of Contents

Temperature Effects on Radiative Recombination

Carrier Capture and Relaxation Processes in Quantum Dots

Chapter One

Introduction

1.1 Motivations: Small and Fast

Understanding the properties of novel materials is crucial to the ability to engineer the optoelectronic devices of the future. The rapid development of compound semiconductor technology over the last decade has spawned interest in the study of new materials to fuel the need for faster communication links and smaller electronic devices. The expectations to meet these desires have led the scientific community to search for the perfect quantum semiconductor materials on the nanometer scale. Materials such as quantum dots are intrinsically small and fast: small because of the inherent size that is required to observe the quantum effect, and fast because electrons can traverse the reduced distance in a shorter time.

In a 0-dimension (0D) quantum dot, the interaction of the electronic wavefunction with the boundary of the surrounding material leads to the quantization of the energy levels (Bastard, 1988). This situation is in sharp contrast to conventional bulk semiconductors where carrier energy levels are characteristically distributed in continuous bands and are insensitive to the size and shape of material. As a consequence of the quantization effect, quantum dot materials are expected to be characterized by a sharp linear optical absorption and a narrower gain spectrum relative to conventional bulk (3D) or quantum well (2D) material (Vahala, 1987). Unlike bulk material, the ability to tailor design the physical parameters of the dots will allow us to achieve greater engineering control

over the material properties and make large improvement for future generations of optoelectronic devices.

| 3D bulk | 2D well | 1D wire | 0D dot |
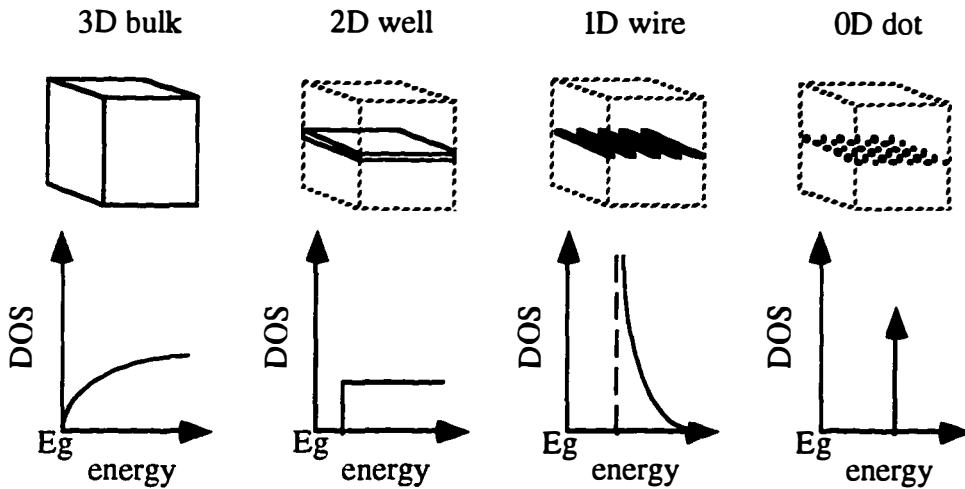
Figure 1.1   Density of States (DOS) in 3D, 2D, 1D, and 0D structures.

The success of quantum well materials has enabled us to significantly improve optoelectronic device performance today. This achievement is due partly to the enhanced density of states (DOS) near the bottom of the conduction band and the top of the valence band (Lee, 1992). The DOS is a material property which quantifies the number of carriers that are permitted to occupy a given energy state of semiconductor. Since most optoelectronic devices operate near the conduction band minimum, the DOS of semiconductor material imposes an intrinsic limitation on the number of carriers that are allowed to contribute to the device performance at one time. In a semiconductor quantum well laser, the benefit of a sharpened DOS allows a reduction of threshold current, an increase in the differential gain, an

improved temperature tolerance, and an enhancement of the modulation bandwidth; all of which are extremely desirable characteristics in an optical communication system (Asada *et al.*, 1986; Arakawa *et al.*, 1982; Zory, 1993). In the 0D quantum dot material, this fundamental advantage is further amplified. Figure 1.1 shows the sharpening of the DOS as the material structure's dimension reduces. Limited only by the packing density of the dots, quantum dot materials, unlike bulk and quantum well materials where the DOS are finite at the ground state energy, can offer a larger number of spatially separated states for carriers at a desired energy. Consequently, if one can realize the ideal quantum dot laser with high packing density, significant improvements over the performance of existing quantum well lasers can be achieved.

Despite the high potential expectations for the quantum dot material, these advantages are accompanied by physical limitations and intrinsic quantum phenomenon. The operation of a quantum dot laser will require sufficient material gain to compensate for the cavity loss. Due to the small volume nature of a dot, a large number of quantum dots will be required to achieve the conditions necessary for lasing. The difficulty attaining a high packing density of quantum dots with uniform size still presents a major technological challenge (Mirin *et al*, 1996; Moritz *et al.*, 1996). Additionally, the confinement of the carriers in a quantum dot should modify fundamental physical processes such as carrier-carrier scattering and carrier-phonon coupling. These processes can ultimately govern the efficiency of potential device applications. Benisty *et al.* (1991) and Bockelmann *et al.* (1991)

4
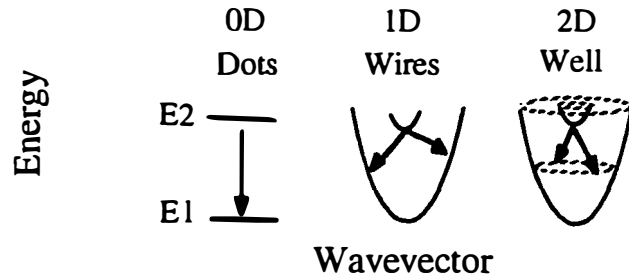
Figure 1.2a   Schematic illustrations of the reduced electron-phonon scattering in quantum structures. Scattering rate is proportional to the number of final states available. The final states in 2D quantum well are represented by states on a circle. In the 1D quantum wire, only two states are available. In quantum dots, efficient relaxation occurs only when E2-E1 is a multiple of the LO phonon energy.
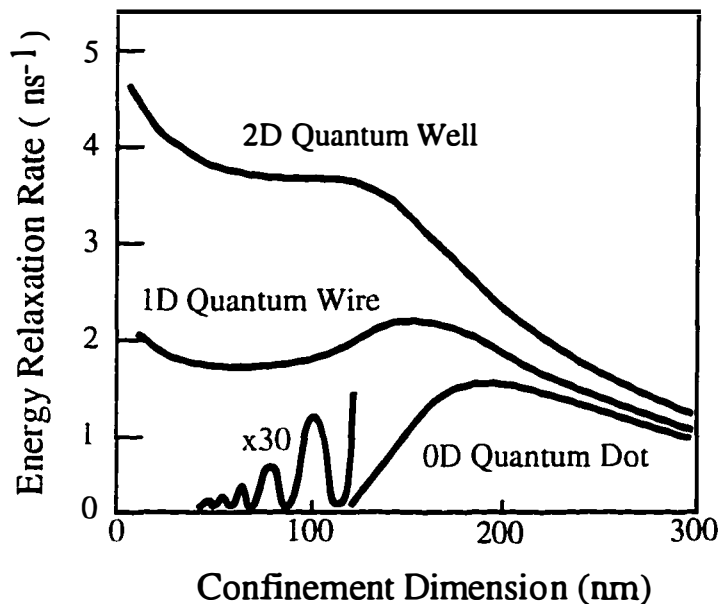
Figure 1.2b   Theoretical prediction of the reduction in the energy relaxation rate for quantum structures. Severe reduction of energy relaxation rate is predicted for 0D quantum dots. (Bockleman *et al.*, 1991)

have pointed out that a reduction in the carrier-phonon scattering rate may be expected in the 0D quantum structure as shown in Figure 1.2, and that the efficiency of the quantum dot devices can suffer from this consequence. These theoretical intuitions should require further experimental confirmation. It is the objective of this dissertation to study how these physical phenomenon are modified in the quantum dots materials and how such consequences will affect the performance of future optoelectronic devices.

1.2   Research on Quantum Dots

The major challenge in quantum dot research is to develop materials characterized by nanometer-scale structure definition and of sufficiently high quality so that the quantum dot effects are not obscured by surface and interface defects. Many approaches utilizing different technologies have been attempted with limited success and potential usefulness.

The nano-crystal precipitates grown from the liquid phase using chemical precursors have been a popular and successful method for achieving quantum confinement of electrons and holes (Ekimov, 1991). Crystals passivated in proper glass complexes have demonstrated efficient photoluminescence, enhanced exciton binding energy, and large non-linearity in optical absorption (Peyghambarian, 1989; Justus, 1991; Tokizaki, 1993; Caponemko et al., 1993). However, due to the passive nature of glass, the integration of nano-crystal materials with the existing solid state semiconductor device technology presents another uncertainty.

Because of the ease of integration with the established device research, quantum dot material that utilizes the existing compound semiconductor

technologies can offer potentially large returns for the scientific investments. Efforts to fabricate electronic gated quantum dot potentials have been used to successfully observe Coulomb blockade effect at low temperature (Heitmann and Kotthaus, 1993; Chakraborty, 1994). However, the induced confinement potential is restricted to the resolution of lithography technology which is typically on the order of 100 nm. The confinement potential generated from the biased gate is typically on the order of 10 meV (Chakraborty, 1994), which is still too shallow to provide a large intersubband spacing at room temperature. Furthermore, the optical application of those dots would require the confinement of both electrons and holes. The success in this area has been limited.

Wet and dry etching technologies have been employed to define dots at nanometer-scale using semiconductor quantum well material (Lehmann, 1985; Grambow, 1989). Even though the chemical etching processes are well understood and characterized, the optical properties of such dots are usually severely shadowed and obscured by the naturally large surface recombination of GaAs material and the etch-damaged defects on the side walls (Cheung, 1989; Mayer *et al.*, 1990). Passivation efforts have been used to reduce the surface recombination. However, the recombination dynamics of chemically etched dots are still dominated by the defects. Using etching technology to produce nanometer structure with a high optical quality is extremely difficult.

In order to study the intrinsic recombination dynamics of quantum dots, materials that are free of extrinsic defects must be used. Etch-free technologies such as epitaxial regrowth over patterned substrate show interesting and successful results (Mirin *et al*, 1992; Arakawa *et al.* , 1993). Using the step corners on a 311

GaAs substrate, Brandt *et al.* (1991) reports InAs quantum dots with high optical quality.

Strain-induced quantum dots are thoroughly studied by Kash *et al.* (1990) and Tan *et al.* (1992). Lateral quantum confinement within an AlGaAs quantum well is achieved utilizing the inhomogeneous strain from an etched InGaAs stressor on the surface. Since the strain-induced dots are buried beneath the surface, there is no etch-related defect, and the problem with surface recombination may be completely avoided.

Even though both the epitaxial regrown quantum dots and strain-induced quantum dots could produce efficient luminescence, the complicated fabrication steps involved to achieve the 3D quantum confinement effect still hinder their potential device application. Recent discovery on the growth of the self-organized quantum dots has shown yet another method to achieve quantum confinement (Leonard *et al.* , 1993) . Self-organized quantum dots are formed intrinsically as a natural epitaxial growth phenomenon. The lack of extrinsic processing steps makes the self-organized quantum dots material an ideal candidate for device integration. With no need for extra investments in the processing technology, the existing device fabrication processes will be easily adopted to utilize the benefits of this new quantum dot material, provided that the growth process is controlled and well understood.

1.3 Self-Organized Quantum Dots

Research on the epitaxial growth using lattice mismatch materials has provided new insights on the control of the structural properties in a material. Differentiated by the degrees of binding between the atoms and the surface of the substrate, heteroepitaxial crystal growth modes are characterized into three different regimes: island mode, layer-by-layer mode, and layer-plus-island mode (Herman and Sitter, 1989). These growth mode are illustrated schematically in Figure 1.3.

monolayer coverage	island Volmer-Weber	layer+island Stranski-Krastanov	layer Frank-van der Merwe
$\theta < 1$ ML			
$1 < \theta < 2$			
$2 < \theta$			
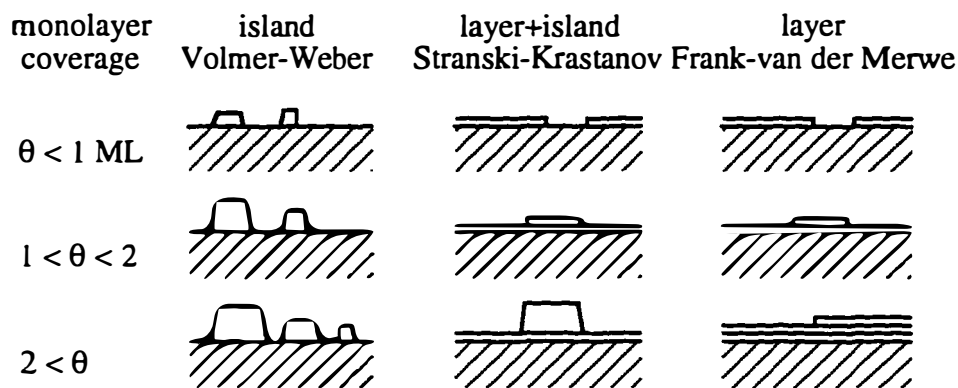
Figure 1.3 The growth sequence vs. monolayer coverage in the three expitaxial crystal growth modes. The coherent InAs/GaAs self-organized quantum dots are formed in the layer plus islands mode (Herman and Sitter, 1989).

In the island mode, or the Volmer-Weber (VW) mode, the atoms are more strongly bound to each other than to the substrate. This results in small clusters of lattice mismatched islands forming directly on the substrate. The VW growth, mostly considered as a nuisance during the growth of strained layer materials, usually yields material with a poor optical quality. In the layer-by-layer mode, or

Frank-Van der Merwe (FM) mode, the situation is directly opposed to the VW mode. The atoms are more strongly bound to the substrate rather than each other. Sequential two-dimensional (2D) monolayers completely covering the surface are achieved as long as the binding energy in the following layer decrease monotonically toward the value for the bulk crystal (Venables et al., 1984). High optical quality quantum well materials are obtained from the FM mode growth. The intermediate growth mode between 3D and 2D occurs when this monotonic decrease of the binding energy is disrupted, forcing coherent islands growth on the top of the monolayers. It is in this Stranski-Kranstanow (SK) growth mode that the self-organized quantum dots are formed (Stranski and Kranstanow, 1939).

Material Systems	Strain	Technology	Reference
InAs/GaAs $In_{0.5}Ga_{0.5}As$/GaAs	7.1 %	MBE, MOCVD	Lenoard et al., 1993 Oshinowo et al., 1994
$In_{0.3}Al_{0.7}As$/$Al_{0.3}Ga_{0.7}As$	4.4 %	MBE	Leon et al., 1995
InSb/GaAs GaSb/GaAs	8.1 %	MBE	Bennett et al., 1996 Sun et al., 1996
$In_{0.49}Ga_{0.51}P$/InP	3.2 %	MOCVD	Reaves et al., 1995
Si/Ge	4.1%	MBE	Schittenhelm et al., 1995

Table 1.1 Various self-organized quantum dot systems formed by Stranski-Kranstanow growth. All material systems exhibit significant strain between the dot and the barrier materials.

The self-assembled nature of the quantum dots is a result of a thermal equilibrium process principally driven by epitaxial strain between the substrate and the deposited atoms. All material systems with significant lattice mismatch are probable candidates for observation of SK growth. Table 1.1 summarizes the material systems that have demonstrated the formation of the self-organized quantum dots.

The InAs/GaAs quantum dots studied in this dissertation are grown using molecular beam epitaxy (MBE) using an Intervac Gen II system. Utilizing the long mean free path of an ultra high vacuum chamber (~ 1 x 10^{-10} Torr), MBE growth relies on two primary factors that govern the surface kinetics: the sample temperature and the molecular beam fluxes generated using the effusion cells. The quantum dots in the samples studied are grown at 530 °C with an As_2 overpressure of ~7 x 10^{-6} Torr to prevent re-evaporation of As from the samples. The islands are produced by pulsing the group V molecular beam in short cycles and using very low growth rate which allows precision control in the deposition of very small amounts of material. This is done until the transition from 2D growth to 3D growth is observed in the surface morphology, monitored using high energy electron diffraction (RHEED) technique (Theeten, 1975).

The amount of material required for the formation of the quantum dots is dependent on the strain involved in the material system. Leonard *et al.* (1995) has shown that the critical layer thickness (CLT) for the formation of InAs quantum dots on GaAs is 1.5 monolayers. The density of the quantum dots increases abruptly once the deposited InAs reaches the CLT. The parameters of the growth

condition can strongly affect the density and physical dimensions of these quantum

dots. An atomic force microscopy (AFM) image of the self-organized InAs

quantum dots without GaAs overgrowth is shown in Figure 1.4. Densities of

$1 \times 10^9 \, cm^{-2}$ to $1 \times 10^{11} \, cm^{-2}$ are obtained without introducing dislocation defects.
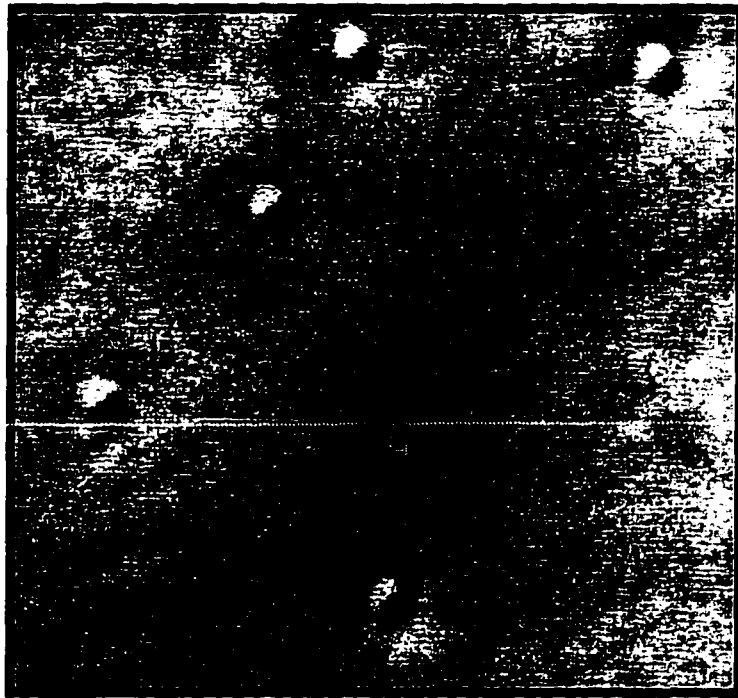
Figure 1.4   Atomic Force Microscope (AFM) image of InAs/GaAs quantum dots measured using Nanoscope III AFM. Dots density shown above is 1×10^9 / cm^2 . The average dot diameter is 20 nm (Leonard et al., 1994).

Leonard *et al.* (1995) report that the self-organized quantum dot has a physical

shape similar to a plano-convex lens, with the radius to the height aspect ratio of

2.27. The exact physical shape of self-organized quantum dot depends on both

growth and measurement parameters. Grundmann *et al.* (1995) have reported

pyramid geometry for the InAs/GaAs dots. Because of the nature of the self-

organizing process, the achieved quantum dot sizes exhibit a Gaussian distribution

as shown in Figure 1.5. The average size for the InAs dots is 20 nm in diameter

and 8 nm in height.

Dot Diameters   Dot Heights
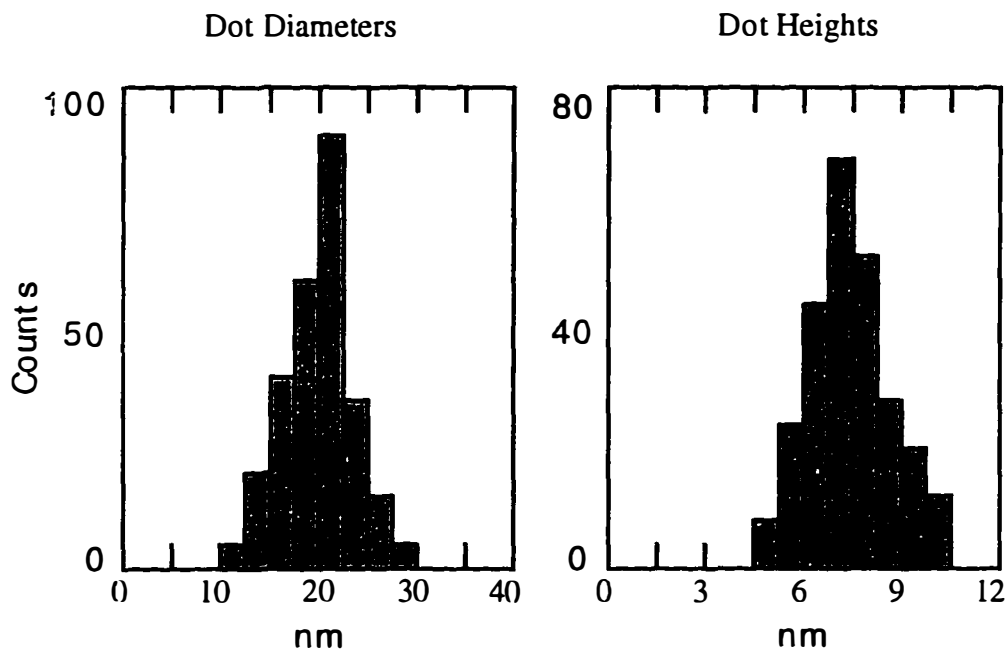
Figure 1.5 Histogram of size distribution for dot diameters and heights. Data is analyzed from an 1 μm x 1 μm AFM image. The average dot diameter is 20 nm with the standard deviation of 5 nm. The average dot height is 7 nm, with standard deviation of 1 nm (Leonard, 1994).

Immediately after the formation of the quantum dots, GaAs overgrowth is used to provide the top potential barrier required for optical studies. The physical dimensions of the self-organized quantum dot are not entirely the correct description of the confinement potential. Figure 1.6 shows the bright field cross-sectional transmission electron microscope (TEM) image of a self-organized InAs quantum dot. Strain field in the surrounding GaAs barrier is clearly visible from contrast between the bright and dark fields. It is well understood that the presence of strain can modify the semiconductor band structure (Pikus and Bir, 1960). Therefore, an exact picture of quantum dot potential will require a clear understanding of the strain field and the formation mechanism of the self-organized quantum dots.

Figure 1.6 Bright field cross-sectional Transmission Electron Microscope (TEM) image of a self-organized quantum dot. Contrast surround the dot is due to the strain between the InAs and the surrounding GaAs. (Leonard *et al.*, 1993)

The exact relation between the growth process, the strain field, and the electronic structure of the self-organized quantum dots can be thoroughly understood with the proper designs of growth experiments (Leonard, 1995) and theoretical models (Grundmann, 1995). Although the research on the growth

mechanics and the physical properties of these quantum dots can be intellectually interesting and scientifically challenging. However, the scope of this dissertation will focus on the photoluminescence properties and the carrier dynamics in the self-organized quantum dot materials.

1.4   Ultrafast Processes in Quantum Structures

The direction of this thesis is aimed at clarifying our understanding of the carrier scattering processes in the quantum dots. For bulk and quantum well devices, most of the involved physical processes have been thoroughly studied and well understood both theoretically and experimentally. However, due to the lack of quality materials, the experimental research on the dynamic processes in quantum dot devices is so far very limited. The past experimental ultrafast research in quantum well structures are summarized in Table 1.2.

The main concerns of this dissertation will address the ultrafast properties of self-organized quantum dots by investigating three areas of carrier dynamics: carrier capture (Chapter 5), thermal emission (Chapter 4), and radiative recombination (Chapter 3).

The carrier capture process involves the effect of carrier diffusion, quantum capture, and energy/momentum relaxation. These processes are required to transport carriers from the electrical contact to the active states in the quantum structure. Benisty *et al.* (1991) and Bockelmann *et al.* (1992) have proposed that the energy relaxation time in a quantum dot can be as slow as several nanoseconds due to the potential mismatch of the phonon energy with the discrete energy level spacing in a quantum dot. This proposed slow energy relaxation time can severely

Time	Scattering Processes	Quantum Well	Quantum Dot
100 fs	carrier thermalization	Knox, 1988	
	electron-hole scattering	Hopfel, 1986	
	carrier-LO phonon	Shah, 1985	
	carrier capture	Blom, 1990	
100 ps	acoustic phonon scattering	Pinczuk, 1988	
	radiative recombination[a]	Fouquet, 1986	this
	thermionic emission[b]	Bacher, 1993	dissertation

[a] As of the writing of this dissertation, various groups have also reported the photoluminescence lifetime of self-organized quantum dots. The report values are compared in Table 3.3.

[b] The temperature dependent experiments disscused in this dissertation follow the study of the quantum well material by Bacher *et al.* (1993). Some of the experiments are done in conjunction with Fafard *et al.* (1994).

Table 1.2 Summary of experimental ultrafast research on quantum well and quantum dot structures.

reduce the modulation bandwidth of the semiconductor laser (Nagarajan, 1992) and introduce non-linear effects such as spectral hole burning and carrier heating (Willatzen *et al.*, 1991; Gomatam *et al.*, 1988; Hall *et al.*, 1992). A pump-and-probe experiment will be used to show that the relaxation of the carrier in the self-organized quantum dots is as fast as values reported for the quantum well materials in the literature, indicating that the effect of phonon relaxation bottleneck may not be

not as severe as the existing theoretical prediction and that other energy relaxation mechanisms may be important.

The thermal emission process is essentially the reverse of the capture process where carriers are removed from the active states due to thermionic emission. The thermal emission time is controlled by the height of the confinement barrier. When the thermal energy of the lattice is larger than the confining potential, a fast carrier emission can occur. For a quantum well laser, a fast carrier escape time will reduce the differential gain (Nagarajan *et al.*, 1992). The temperature dependent photoluminescence and the time-resolved photoluminescence will be used to investigate the thermal emission properties of various self-organized quantum structures. The values for the confinement barrier heights will be extracted and compared to the results derived from the measured thermal emission time.

The radiative recombination process converts the carriers into photons, generating light for the optoelectronic applications. Although the fundamental process for the radiative recombination in quantum dots is similar to bulk and quantum well structures, the reported quantum dot carrier lifetimes in the literature vary from 10 ps to 1 ns (Mukai *et al.*, 1996; Schulzgen *et al.*, 1993; see Table 3.3). Using time-resolved photoluminescence, the carrier lifetimes in various self-organized quantum dots will be compared with the published values. The difference in the radiative recombination process among bulk, quantum well, and quantum dots will be clarified. Furthermore, the radiative recombination of the spatially indirect excitons are studied in the staggered band alignment GaSb/GaAs quantum dots. The radiative lifetime of exciton is found to be modified significantly as the

result of staggered band offset. A field dependent radiative processes is observed, indicating that the effect of space charge is important.

1.5 Carrier Dynamic Model

Although these three different processes may be individually studied, their combined effects will ultimately affect the characteristics of the optoelectronic device such as quantum efficiency and modulation response. The relationships among the capture, emission, and recombination processes can be understood using a simplified model. The model consists of a three level system, with the transport processes between each level characterized by time constants. This is illustrated in Figure 1.7.
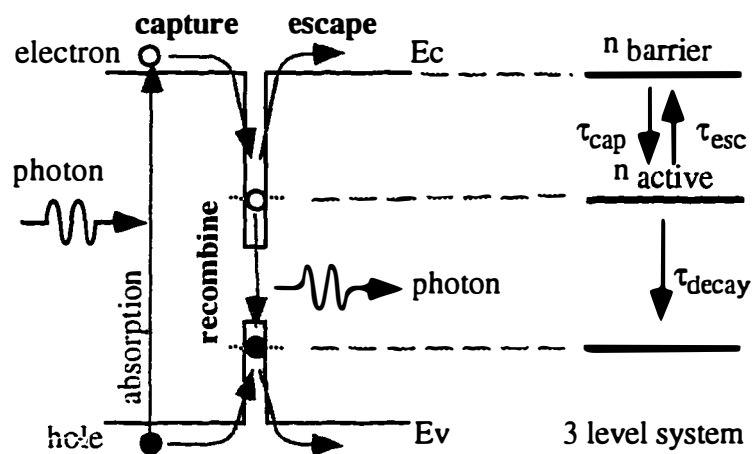
Figure 1.7 A carrier dynamics model describes the relationships between the carrier capture, escape, and recombination of the electrons and holes in quantum dots.

18

The capture and emission of electrons and holes are considered in an ambipolar picture (Deveaud *et al.*, 1988; Blom *et al.*, 1990). The effective time constants are determined by the average of the carriers in both the conduction band and valence band. Although a separated set of rate equations can be easily introduced for the electron and hole populations (Pickin *et al.*, 1990; Ridley, 1990), accurate identifications of these processes from optical experiments are difficult. In most cases, however, the relaxation of the hole is faster than the electron, and the dynamics of the electrons are usually the limiting bottleneck (Shah, 1996).

Using rate equation analysis, characteristics such as the photoluminescence decay (Equation 1.1 and 1.2; Bastard, 1989) and the modulation bandwidth (Equation 1.3; Nagarajan *et al.*, 1993) are obtained in terms of the time constants representing carrier capture ($\tau_{capture}$), thermal escape (τ_{escape}), and radiative recombination (τ_{decay}).

$$\frac{d}{dt} n_{barrier} = excitation - \frac{n_{barrier}}{\tau_{capture}}$$

$$\frac{d}{dt} n_{active} = \frac{n_{barrier}}{\tau_{capture}} - \frac{n_{active}}{\tau_{decay}} - \frac{n_{active}}{\tau_{escape}} \qquad (1.1)$$

$$PL(t) \propto e^{-t/\tau_{decay} - t/\tau_{escape}} - e^{-t/\tau_{capture}}, \qquad (1.2)$$

$$M(\omega) \propto \left(\frac{1}{1 + j\omega\tau_{capture}} \right) \frac{1}{\omega_r^2 - \omega^2 + j\omega\gamma}$$

$$\omega_r^2 \propto \frac{1}{\tau_{cavity}\tau_{stim}} \ ; \ \gamma \propto \frac{1}{\tau_{decay}}\left(1 + \frac{1}{\chi}\right) \ ; \ \chi = 1 + \frac{\tau_{capture}}{\tau_{escape}} \qquad (1.3)$$

1.6 Organization of Dissertation

The organization of this dissertation will be centered around the device model presented in section 1.5. Chapter 2 will introduce macroscopic optical properties such as the photoluminescence and absorption spectra of the quantum dots. Energy levels in a quantum dot are calculated considering a square dot under a uniform strain. The excellent radiative efficiency of the self-organized quantum dots indicates that the microscopic carrier dynamics probably are not mediated by extrinsic defects and surface recombination. Chapter 3 will discuss the time dependence of the radiative recombination in the quantum structures. Time-resolved photoluminescence reflecting the carrier lifetime in the quantum dots will be presented. The measured values will be compared to the reported quantum dot exciton lifetimes reported in the literature. The effects of carrier density and quantum dot size on the observed exciton lifetime in quantum structures will be clarified. Chapter 4 will address the temperature dependence of the radiative processes in quantum dots. The effects of acoustic phonon scattering and thermionic emission in quantum structures will be discussed by analyzing the temperature dependence of the time-resolved photoluminescence. Chapter 5 will focus on the carrier capture processes in the quantum dots. Energy relaxation

20

phenomenon and the theoretical prediction of the phonon bottleneck (Benisty *et al.*, 1991) will be investigated using femtosecond spectroscopy. Chapter 6 will analyze spatially indirect excitons in the GaSb/GaAs quantum dots. The carrier dynamics differences between the staggered band lineup GaSb/GaAs dots and the nest band lineup GaSb/AlGaAs dots will be explored. Space charge effects in the GaSb/GaAs quantum dots will be studied. Chapter 7 will conclude the study by discussing the performance implications for self-organized quantum dot devices based on the material parameters measured in the previous chapters.

References

1.   Y. Arakawa, K. Vahala, A. Yariv, K. Lau, *Applied Physics Letters* **47**, no.11 1142-4 (1 Dec. 1985).

2.   Y. Arakawa, Y. Nagamune, M. Nishioka, S. Tsukamoto, *Semiconductor Science and Technology* **8**, 6 1082-1088 (1993).

3.   Y. Arakawa, *Solid-State Electronics* **37**, 4-6 523-528 (1994).

4.   M. Asada, Y. Miyamoto, Y. Suematsu, *IEEE Journal of Quantum Electronics* **QE-22**, no.9 1915-21 (Sept. 1986).

5.   G. Bacher, H. Schweizer, J. Kovac, A. Forchel, H. Nickel, W. Schlapp, R. Losch, *Physical Review B-Condensed Matter* **43**, 11 9312-9315 (1991).

6.   G. Bastard, *Wave Mechanics Applied to Semiconductor Heterostructures* (Halsted Press, New York, 1988).

7.   H. Benisty, C. M. Sotomayor-Torres, C. Weisbuch, *Physical Review B (Condensed Matter)* **44**, no.19 10945-8 (15 Nov. 1991).

8.   B. R. Bennett, P. M. Thibado, M. E. Twigg, E. R. Glaser, R. Magno, B. V. Shanabrook, L. J. Whitman, *Journal of Vacuum Science & Technology B* **14**, 3 2195-2198 (1996).

9.   D. Bimberg, *et al.*, *Thin Solid Films* **267**, 1-2 32-36 (1995).

10.   D. Bimberg, *et al.*, *Japanese Journal of Applied Physics Part 1-Regular Papers Short Notes & Review Papers* **35**, 2b 1311-1319 (1996).

11.   D. Bimberg, *et al.*, *Physica Status Solidi B-Basic Research* **194**, 1 159-173 (1996).

12.   P. W. M. Blom, R. F. Mols, J. E. M. Haverkort, M. R. Leys, J. H. Wolter, *Superlattices and Microstructures* **7**, no.4 319-21 (1990).

13.   U. Bockelmann, T. Egeler, *Physical Review B-Condensed Matter* **46**, 23 15574-15577 (1992).

14.   U. Bockelmann, *Physical Review B-Condensed Matter* **48**, 23 17637-17640 (1993).

15.   U. Bockelmann, K. Brunner, G. Abstreiter, *Solid-State Electronics* **37**, 4-6 1109-1112 (1994).

22

16. U. Bockelmann, P. Roussignol, A. Filoramo, W. Heller, G. Abstreiter, K. Brunner, G. Bohm, G. Weimann, *Physical Review Letters* **76**, 19 3622-3625 (1996).

17. O. Brandt, L. Tapfer, K. Ploog, R. Bierwolf, M. Hohenstein, F. Phillipp, H. Lage, A. Heberle, *Physical Review B-Condensed Matter* **44**, 15 8043-8053 (1991).

18. O. Brandt, L. Tapfer, K. Ploog, R. Bierwolf, F. Phillipp, M. Hohenstein, *Surface Science* **267**, 1-3 204-208 (1992).

19. V. Bresslerhill, C. M. Reaves, S. Varma, S. P. Denbaars, W. H. Weinberg, *Surface Science* **341**, 1-2 29-39 (1995).

20. T. Chakraborty, *Current Science* **67**, 11 858-860 (1994).

21. P. Chen, Q. Xie, A. Madhukar, L. Chen, A. Konkar, *Journal of Vacuum Science & Technology B* **12**, 4 2568-2573 (1994).

22. R. Cheung, Y. H. Lee, C. M. Knoedler, K. Y. Lee, T. P. Smith III, D. P. Kern, *Applied Physics Letters* **54**, no.21 2130-2 (22 May 1989).

23. R. M. Delacruz, S. W. Teitsworth, M. A. Stroscio, *Superlattices and Microstructures* **13**, 4 481-486 (1993).

24. S. P. Denbaars, C. M. Reaves, V. Bresslerhill, S. Varma, W. H. Weinberg, P. M. Petroff, *Journal of Crystal Growth* **145**, 1-4 721-727 (1994).

25. A. I. Ekimov, *Physica Scripta* **T39**, Vt39 217-222 (1991).

26. S. Fafard, S. Raymond, G. Wang, R. Leon, D. Leonard, S. Charbonneau, J. L. Merz, P. M. Petroff, J. E. Bowers, *Surface Science* **362**, 1-3 778-782 (1996).

27. J. E. Fouquet, A. E. Siegman, R. D. Burnham, T. L. Paoli, *Applied Physics Letters* **46**, no.4 374-6 (15 Feb. 1985).

28. J. E. Fouquet, R. D. Burnham, *IEEE Journal of Quantum Electronics* **QE-22**, no.9 1799-810 (Sept. 1986).

29. P. Grambow, T. Demel, D. Heitmann, M. Kohl, R. Schule, K. Ploog, *Microelectronic Engineering* **9**, no.1-4 357-60 (May 1989).

30. M. Grundmann, O. Stier, D. Bimberg, *Physical Review B-Condensed Matter* **52**, 16 11969-11981 (1995).

31. M. Grundmann, *et al.*, *Superlattices and Microstructures* **19**, 2 81-95 (1996).

32. D. Heitmann, K. Kern, T. Demel, P. Grambow, K. Ploog, Y. H. Zhang, *Surface Science* **267**, 1-3 245-252 (1992).

33. Herman, Sitter, *Molecular Beam Epitaxy* (Springer-Verlag, New York, 1989).

34. R. A. Hopfel, J. Shah, A. C. Gossard, *Physical Review Letters* **56**, no.7 765-8 (17 Feb. 1986).

35. B. L. Justus, M. E. Seaver, J. A. Ruller, A. J. Campillo, *Proceedings of the SPIE - The International Society for Optical Engineering* **1409**, 2-8 (1991).

36. K. Kash, R. Bhat, D. D. Mahoney, P. S. D. Lin, A. Scherer, J. M. Worlock, B. P. Vandergaag, M. Koza, P. Grabbe, *Applied Physics Letters* **55**, 7 681-683 (1989).

37. K. Kash, *Journal of Luminescence* **46**, 2 69-82 (1990).

38. N. Kirstaedter, *et al.*, *Electronics Letters* **30**, 17 1416-1417 (1994).

39. N. Kirstaedter, *et al.*, *Applied Physics Letters* **69**, no.9 1226-8 (26 Aug. 1996).

40. W. H. Knox, D. S. Chemla, G. Livescu, J. E. Cunningham, J. E. Henry, *Physical Review Letters* **61**, no.11 1290-3 (12 Sept. 1988).

41. W. H. Knox, C. Hirlimann, D. A. B. Miller, J. Shah, D. S. Chemla, C. V. Shank, *Physical Review Letters* **56**, no.11 1191-3 (17 March 1986).

42. N. N. Ledentsov, *et al.*, *Solid-State Electronics* **40**, Si 785-798 (1996).

43. S. J. Lee, N. H. Shin, J. J. Ko, M. J. Park, R. Kummel, *Semiconductor Science and Technology* **7**, 8 1072-1079 (1992).

44. H. W. Lehmann, *Journal of Vacuum Science & Technology B (Microelectronics Processing and Phenomena)* **6**, no.6 1881-4 (Nov.-Dec. 1988).

45. R. Leon, S. Fafard, D. Leonard, J. L. Merz, P. M. Petroff, *Applied Physics Letters* **67**, 4 521-523 (1995).

24

46. D. Leonard, M. Krishnamurthy, C. M. Reaves, S. P. Denbaars, P. M. Petroff, *Applied Physics Letters* **63**, 23 3203-3205 (1993).

47. D. Leonard, K. Pond, P. M. Petroff, *Physical Review B-Condensed Matter* **50**, 16 11687-11692 (1994).

48. F. Leonavila, H. Rodriguezcoppola, F. Comas, *Physica Status Solidi B-Basic Research* **189**, 1 107-116 (1995).

49. A. Madhukar, Q. Xie, P. Chen, A. Konkar, *Applied Physics Letters* **64**, 20 2727-2729 (1994).

50. G. Mayer, B. E. Maile, R. Germann, A. Forchel, P. Grambow, H. P. Meier, *Applied Physics Letters* **56**, no.20 2016-18 (14 May 1990).

51. R. P. Mirin, I. H. Tan, H. Weman, M. Leonard, T. Yasuda, J. E. Bowers, E. L. Hu, *Journal of Vacuum Science & Technology A-Vacuum Surfaces and Films* **10**, 4 697-700 (1992).

52. R. Mirin, A. Gossard, J. Bowers, *Electronics Letters* **32**, no.18 1732-4 (29 Aug. 1996).

53. A. Moritz, R. Wirth, A. Hangleiter, A. Kurtenbach, K. Eberl, *Applied Physics Letters* **69**, 2 212-214 (1996).

54. R. Nagarajan, M. Ishikawa, T. Fukushima, R. S. Geels, J. E. Bowers, *Journal of Quantum Electronics* **28**, 10 1990-2008 (1992).

55. J. Oshinowo, M. Nishioka, S. Ishida, Y. Arakawa, *Applied Physics Letters* **65**, 11 1421-1423 (1994).

56. P. M. Petroff, A. C. Gossard, R. A. Logan, W. Wiegmann, *Applied Physics Letters* **41**, no.7 635-8 (1 Oct. 1982).

57. N. Peyghambarian, B. Fluegel, D. Hulin, A. Migus, M. Joffre, A. Antonetti, S. W. Koch, M. Lindberg, *Journal of Quantum Electronics* **25**, 12 2516-2522 (1989).

58. W. Pickin, J. P. R. David, *Applied Physics Letters* **56**, no.3 268-70 (15 Jan. 1990).

59. G. E. Pikus, G. L. Bir, *Sov. Phys. -Solid State* **1**, 1502 (1960).

60. G. E. Pikus, G. L. Bir, *Symmetry and Strain-Induced Effects in Semiconductors* (Wiley, New York, 1974).

61. A. Pinczuk, S. Jagdeep, A. C. Gossard, *Solid-State Electronics* **31**, no.3-4 477-9 (March-April 1988).

62. S. Raymond, S. Fafard S; P. J. Poole, A. Wojs, P. Hawrylak, S. Charbonneau, D. Leonard, R. Leon, P. M. Petroff, and J. L. Merz.*Physical Review B (Condensed Matter)* **54**, 16 11548-11554 (1996).

63. S. Raymond, S. Fafard, S. Charbonneau S, R. Leon R, D. Leonard, R. Leon, P. M. Petroff, and J. L. Merz. *Physical Review B (Condensed Matter)* **52** 24 17238-17242 (1995).

64. C. M. Reaves, V. Bresslerhill, W. H. Weinberg, S. P. Denbaars, *Journal of Electronic Materials* **24**, 11 1605-1609 (1995).

65. B. K. Ridley, *Physical Review B (Condensed Matter)* **41**, no.17 12190-6 (15 June 1990).

66. S. Ruvimov, *et al.*, *Physical Review B-Condensed Matter* **51**, 20 14766-14769 (1995).

67. P. Schittenhelm, M. Gail, G. Abstreiter, *Journal of Crystal Growth* **157**, no.1-4 260-4 (Dec. 1995).

68. O. G. Schmidt, *et al.*, *Electronics Letters* **32**, no.14 1302-4 (4 July 1996).

69. J. Shah, A. Pinczuk, A. C. Gossard, W. Wiegmann, *Physica B & C* **134B+C**, no.1-3 174-8 (Nov. 1985).

70. J. Shah, *Ultrafast Spectroscopy of Semiconductors and Semiconductor Nanostructures* (Berlin ; New York : Springer, 1996)

71. G. S. Solomon, M. C. Larson, J. S. Harris, *Applied Physics Letters* **69**, 13 1897-1899 (1996).

72. I. N. Stranski, L. V. Krastanow, *Akad. Wiss. Let. Mainz Math-Natur.Kl IIb* **146**, 797 (1939).

73. C. K. Sun, G. Wang, J. E. Bowers, B. Brar, H. R. Blank, H. Kroemer, M. H. Pilkuhn, *Applied Physics Letters* **68**, 11 1543-1545 (1996).

74. I. H. Tan, R. Mirin, V. Jayaraman, S. Shi, E. Hu, J. Bowers, *Applied Physics Letters* **61**, 3 300-302 (1992).

75. I. H. Tan, Y. L. Chang, R. Mirin, E. Hu, J. Merz, T. Yasuda, Y. Segawa, *Applied Physics Letters* **62**, 12 1376-1378 (1993).

26

76. Y. S. Tang, C. M. S. Torres, R. A. Kubiak, T. E. Whall, E. H. C. Parker, H. Presting, H. Kibbel, *Journal of Electronic Materials* **24**, 2 99-106 (1995).

77. J. B. Theeten, *Acta Electronica* **18**, no.1 39-45 (Jan. 1975).

78. T. Tokizaki, T. Kataoka, A. Nakamura, N. Sugimoto, T. Manabe, *Japanese Journal of Applied Physics Part 2-Letters* **32**, 6A L782-L784 (1993).

79. K. J. Vahala, Y. Arakawa, A. Yariv, *Applied Physics Letters* **50**, no.7 365-7 (16 Feb. 1987).

80. K. J. Vahala, J. A. Lebens, C. S. Tsai, T. F. Kuech, P. C. Sercel, M. E. Hoenk, Z. Hal, *Proceedings of the SPIE - The International Society for Optical Engineering* **1216**, 120-9 (1990).

81. J. A. Venables, G. D. T. Spiller, M. Hanbueken, *Rep. Prog. Phys.* **47**, 339 (1984).

82. C. Weisbuch, J. Nagle, *Science and Engineering of One- and Zero-Dimensional Semiconductors. Proceedings of a NATO Advanced Research Workshop* , 309-16 (1990).

83. Q. H. Xie, A. Madhukar, P. Chen, N. P. Kobayashi, *Physical Review Letters* **75**, 13 2542-2545 (1995).

84. Q. H. Xie, A. Kalburge, P. Chen, A. Madhukar, *Photonics Technology Letters* **8**, 8 965-967 (1996).

85. P. S. Zory, *Quantum Well Lasers* (Academic Press, Boston, 1993).

27

Chapter Two

Photoluminescence Properties of the Self-Organized Quantum Dots

2.1 Introduction

The interaction of light with matter is the fundamental force that drives the advances in the field of optoelectronics. Optical absorption and photoluminescence (PL) are the two important physical processes that reflect the characteristics of optoelectronic materials. In semiconductors, optical absorption occurs when an incident photon excites an electron from the valence band to the conduction band. The thermalized electron-hole pair relaxes to the bottom of the band and recombines by emitting a photon via photoluminescence. The process is depicted in Figure 2.1.
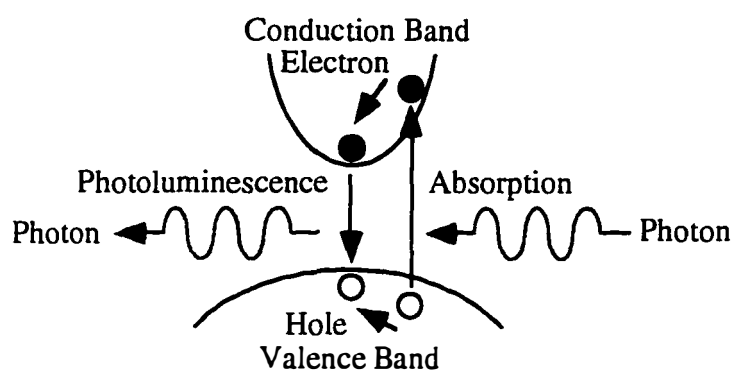
Figure 2.1 Schematic illustration of the photoluminescence and the absorption processes in bulk semiconductors.

The absorption strength and PL intensity at a given energy is characterized by the oscillator strength, the density of states available in the conduction and valence bands, and the electron and hole energy distribution. Because radiative recombination competes with other non-radiative processes, the intensity of PL is an indicator of material's optical quality and radiative efficiency. Other information such as the structure quality and the properties of excitons can be revealed from the linewidth of PL emission spectra (Srinivas *et al.*, 1992).

Since PL utilizes the optical absorption to populate carriers in the excited states of the semiconductor, it can naturally be employed to measure the absorption spectrum of a material. Photoluminescence excitation (PLE) spectroscopy is a technique where the strength of the absorption at a higher energy state is measured from the ground state PL intensity. By scanning the energies of the incident photons and monitoring the PL intensity at the ground state of the system, an indirect measurement of absorption spectrum is obtained. The obtained PLE spectrum can be different from the direct abosorption measurement because the complicated carrier relaxation processes involved in the intermediate steps.

In this chapter, we pave the foundation for the study of carrier dynamics in quantum structure by introducing the PL and PLE measurements of the self-organized quantum dots. The analysis of these measurements will provide strong evidences for the 0D density of states and the enhanced quantum confinement. The excellent optical and structure quality of these quantum dots will be demonstrated.

The low temperature PL of the self-organized quantum dots will be presented in Section 2.3. An extremely simplified model for the PL emission

energy will be presented in Section 2.4. Using a zeroth order approximation for the quantum dot confinement potential, the model will provide a reasonable agreement with the measured optical properties. The evidences for the 0D density of states and the presence of the lateral confinement in the quantum dots will be observed from the narrow PL linewidth (Section 2.5) and the PLE spectra (Section 2.6). The observed excited state absorption in the PLE spectra is analyzed in Section 2.7. A good agreement is obtained with the calculation in Section 2.4. The effect of the excited states on the PL is studied in Section 2.8. Interesting resonances are observed in the PL when the PL excitation energy is moved below the energy position of the wetting layer. In Section 2.9, a larger binding energy for the exciton in the quantum dots is deduced from the the enhanced radiative efficiency at higher temperatures.

2.2 Experimental Considerations

In the continuous wave PL and PLE experiments, an intensity regulated output of a tunable Spectra Phyiscs Ti:sapphire laser, pumped by the 514.5 nm line of a Coherent 15 W Ar$^+$ laser, was used as the excitation source. The PL was dispersed through a SPEX double grating spectrometer, and then detected using either a liquid nitrogen cooled Ge detector or a thermal electric cooled photomultiplier tube (PMT) depending on the wavelength sensitivity that was needed. To achieve a higher sensitivity and a faster response time at longer wavelengths, an AgO PMT with a S-1 spectral response rather than the GaAs PMT

was used. The sample was placed in a variable temperature Janis flow cryostat and cooled with liquid helium.

Two types of quantum dot samples are studied in this chapter. The first sample consists of $In_xGa_{1-x}As$ quantum dots surrounded by GaAs (Leonard *et al.*, 1993). Rather than using the InAs quantum dots, which luminescence at 1.1 eV, InGaAs dots are studied instead. A nominal indium composition of x=0.5 is used during the $In_xGa_{1-x}As$ quantum dot growth. These InGaAs dots emit at 1.3 eV, at an energy better matched with the sensitivity of the time resolved measurements. The time-resolved measurements will be presented in the following chapters. The second sample consisted of $In_xAl_{1-x}As$ quantum dots surrounded with $Al_{0.3}Ga_{0.7}As$ barrier (Leon *et al.*, 1994). With a nominal indium compostion of x=0.3, these dots are found to emit photons at 1.88 eV in the visible red spectral range. In this wavelength, the high sensitivity of GaAs PMT is used to study the ultra-narrow PL linewidth of the localized excitons from an ensemble of a few dots (Fafard *et al.*, 1996).

The $In_{0.5}Ga_{0.5}As$/GaAs quantum dots samples (MK11, MK14) are pseudomorphically grown by MBE, utilizing the coherent islanding effect of the InGaAs (Leonard *et al.*, 1993; Eaglesham *et al.*, 1990). The growth and the structure quality of the dots are described in Section 1.3. The sample structure, as shown in Figure 2.2, consists of a layer of quantum dots and a 6 nm $In_{0.17}Ga_{0.83}As$ reference quantum well, separated by a 100 nm GaAs barrier. The dots were covered by 30 nm of GaAs to provide the 3D confinement for optical studies. A reference sample (MK21) with only the InGaAs wetting layer is grown for the

purpose of identifying and comparing the optical properties of the quantum dots. The thickness of the wetting layer is 2 ML. The $In_{0.3}Al_{0.7}As/Al_{0.3}Ga_{0.7}As$ quantum dots are grown in a similar fashion as the $In_{0.5}Ga_{0.5}As/GaAs$ quantum dots (Leon *et al.*, 1994).

	30 nm GaAs
	InGaAs Quantum Dots
	100 nm GaAs
	6 nm $In_{0.17}Ga_{0.87}As$ Quantum Well
	GaAs substrate
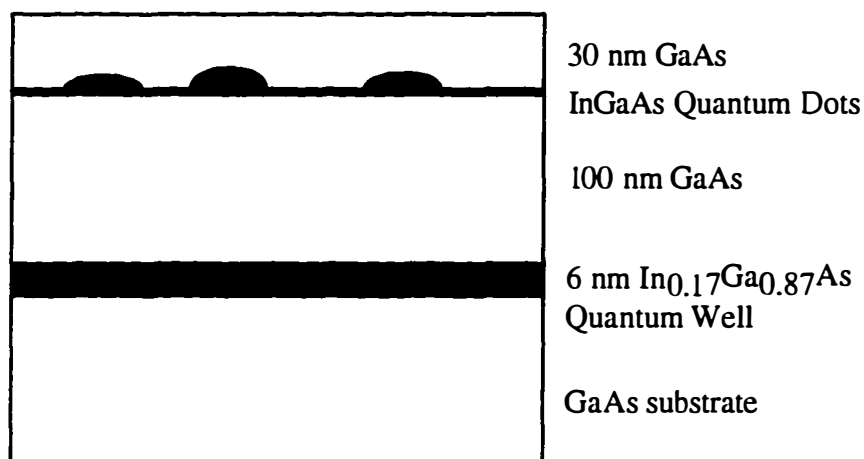
Figure 2.2 InGaAs/GaAs quantum dot sample structure (not drawn to scale). The line beneath the dots represents the wetting layer. For reference purpose, an identical wetting layer sample without the quantum dots were grown . These samples are grown by Devin Leonard using MBE.

Although the nominal indium composition of 50 percent is used during the growth of $In_{0.5}Ga_{0.5}As$ quantum dots, a larger number of indium atoms are incorporated in the dots. This change is caused by the complicated growth dynamics of strain layers (Synder *et al.*, 1993; Chang *et al.*, 1993). During the dot growth, the indium atoms segregate from the gallium atoms. A higher indium composition is found in the dots.

Besides the uncertainty in the indium composition, the actual amount of strain resulting from the coherent islanding process is also poorly determined. The resulting confinement potential becomes difficult to calculate without a clean picture of growth dynamics.

2.3 Photoluminescence from Quantum Dots

The low temperature (1.4 K) PL and PLE of the InGaAs quantum dots and the reference samples are shown in Figure 2.3. The self-organized quantum dots exhibit a broad luminescence peak at 1.293 eV. This peak assignment is confirmed by comparing the PL from the dot sample with the 1.44 eV emission from the wetting layer reference sample. The luminescence of the dot sample is shifted to a lower energy from that of wetting layer. This shift indicates that the new energy minima is associated only with the formation of the quantum dots.

A strong correlation exists between the broad linewidth (50 meV) of the quantum dot emissions and the large variation in the dot size distribution. The
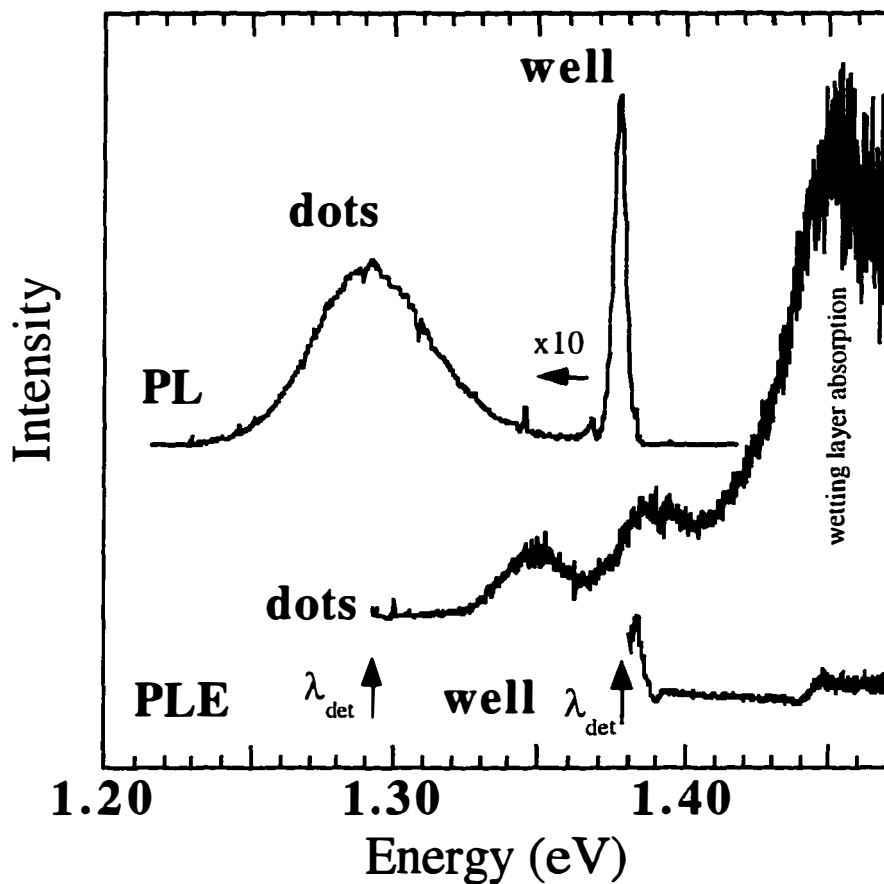
Figure 2.3 The photoluminescence (PL) and photoluminescence excitation (PLE) spectra of the $In_{0.5}Ga_{0.5}As/GaAs$ quantum dot sample (dots) and the $In_{0.17}Ga_{0.83}As$ quantum well sample (well). The full-width-at-half-max (FWHM) of the quantum dot peak is 50 meV. The PLE signal at the peak of the quantum dot PL is negligible. The quantum well absorption follows a step-function, as described by the 2D density of states (DOS). The 0D DOS of the quantum dots is indicated by the broadened delta function peaks. These measurements are performed with the help of Simon Fafard.

relationship between the dot size and the emission energy may be understood using a particle-in-a-box approximation. To a zeroth order, we approximate the quantum dot geometry using a flat, square box (see inset in Figure 2.4a) with an infinite potential barrier. Excluding excitonic effects, the PL emission energy is given by

$$E_{PL} = E_g + \frac{\pi^2 h^2}{2m_r}\left(\frac{n^2}{L^2} + \frac{l^2}{a^2} + \frac{p^2}{a^2}\right),$$
(2.1)

where m_r is the reduced mass of electron and hole, and L and a are the height and the width of the square box, respectively. The n, l and p are the quantum numbers associated with the particular energy states. The emission energy fluctuations resulting from the size variation is obtained by differentiating Equation 2.1 with respect to L and a:

$$\Delta E_{thickness} = -\frac{\pi^2 h^2}{m_r}\frac{\Delta L}{L^3}n^2$$

$$\Delta E_{width} = -\frac{\pi^2 h^2}{m_r}\frac{\Delta a}{a^3}\left(l^2 + p^2\right)$$
(2.2)

From Equation 2.2, the fluctuations in the energy levels are inversely proportional to the cube of the sizes. Therefore, the variation in the smallest dimension will have the largest contribution to the inhomogenous linewidth. Using Equation 2.2, for the ground state emission of the $In_{0.5}Ga_{0.5}As/GaAs$ quantum dots ($m_r = 0.026 \, m_o$, L = 7 nm, $\Delta L = 1$ nm, a = 20 nm, and $\Delta a = 5$ nm), the energy fluctuations due to the thickness variation is 60 meV, while the contribution from the lateral width variation is only 18 meV. Although the dot size variation is larger in the diameter than in the thickness (Figure 1.5), the variation in the dot thickness contributes

significantly to the emission energy fluctuations. Despite the over simplified assumptions employed, the estimated energy variation (60 meV) from this infinite, flat, and square potential yields a reasonable agreement with the measured PL linewidth of 50 meV.

2.4 Strain and Structure Effects on the Emission Energies

Equation 2.1 is a rather poor approximation of the PL emission energy. Besides the bold assumption of an infinite potential barrier, the complicated strain field inside the dot is ignored (Figure 1.6). A slightly better approximation of the emission energies can be obtained by considering the effect of a uniform and isotropic strain field inside the dot with a finite potential barrier. This approximation may provide us with the average values for the strain and the dot dimension. To use the exact solution of strain field requires a better understanding of the shape and the indium composition of these quantum dots, which is presently not available.

To obtain a uniform strain between the dot and the barrier, the strain within the quantum dot is given as the percentage of lattice mismatch between the barrier and the dot materials:

$$\varepsilon = \frac{a_{barrier} - a_{dot}}{a_{dot}}. \tag{2.3}$$

Since the lattice constant of In(Ga)As is larger than GaAs, the dot is under compressive strain. Following the strain theory prescribed by Pikus and Bir (1960), the bandgap of the strained dot material is written as,

$$E_{g,strained} = E_{g,bulk} + p \, m\sqrt{q^2 + r^2 + s^2}, \tag{2.4}$$

where p is the sum of hydrostatic bandshifts in the conduction band and the valence band, and $\sqrt{q^2 + r^2 + s^2}$ is the splitting energy between the heavy hole and the light hole. The p, q, r, and s are expressed in terms of the Pikus and Bir deformation potentials (a, b, and d) and the components of the strain tensor (ε_{ij}).

$$p = -a\left(\varepsilon_{xx} + \varepsilon_{yy} + \varepsilon_{zz}\right) = 3a\varepsilon$$

$$q = -b\left(\frac{1}{2}\left(\varepsilon_{xx} + \varepsilon_{yy}\right) - \varepsilon_{zz}\right) = 0$$

$$r = -\frac{\sqrt{3}}{2}b\left(\varepsilon_{xx} - \varepsilon_{yy}\right) + id\varepsilon_{xy} = 0 \qquad (2.5)$$

$$s = -id\left(\varepsilon_{xz} - i\varepsilon_{yz}\right) = 0$$

Under this extremely simplified assumption of an isotropic strain field inside the quantum dot, the shear components of strain tensor are zero. There is no energy splitting between the heavy hole and the light hole (q=r=s=0). In reality, the effect of the non-uniform strain will lead to a splitting of the heavy hole and the light hole. Our assumption can only be treated as a zeroth order approximation.

The parameters used for the calculation are obtained from the literature (Adachi et al., 1982; Madelung et al., 1991). The solution to the quantized energy level of a 3D finite potential box is reduced to three separated 1D finite potential square well problems. Numerical solutions are obtained by solving the Wave Equation across the barrier (Bastard, 1988). Luttinger and Kohn parameters are used to evaluate the effective masses of electron and holes (Luttinger and Kohn, 1955). The ratio of hydrostatic band shifts between the conduction band and the valence band are assumed to be 4 to 1 (Tan, 1992). The bulk conduction band offset is estimated to be 62 percent of the total band offset.
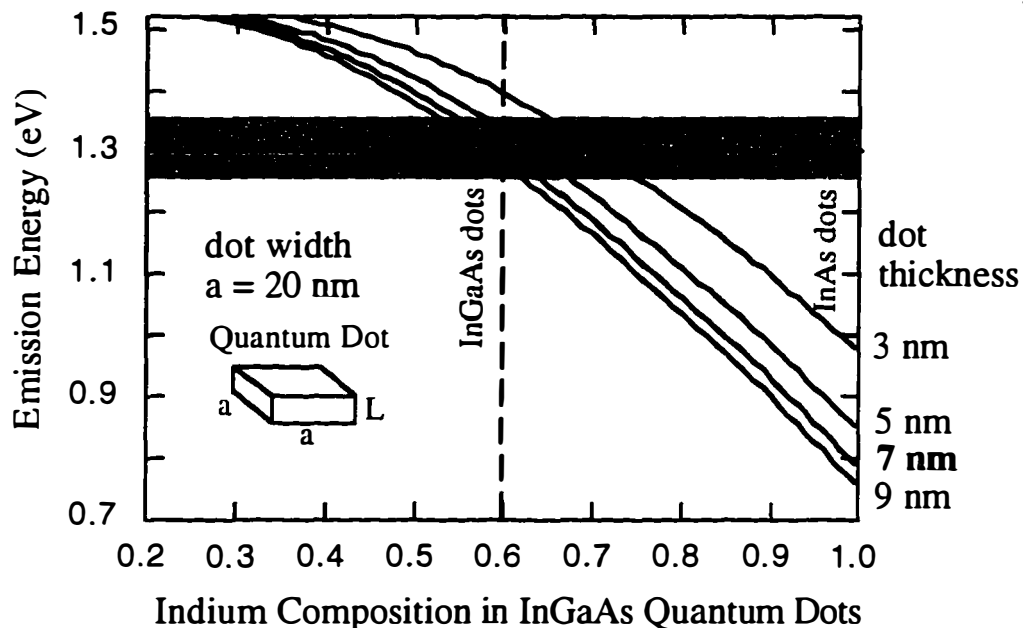
Figure 2.4a The effect of indium composition on the ground state emission energies for several dot thickness. A flat, square box potential is used for the model, and the effect of a uniform strain used for the calculation. Lateral width of 20 nm is assumed. The FWHM of the measured dot PL is indicated by the shaded region.

Using the average dot diameter of 20 nm measured from AFM (Figure 1.5), the effect of indium composition on the emission energy is plotted in Figure 2.4a. The full-width-at-half-max (FWHM) of the measured PL peak from Figure 2.3 is indicated in the shaded region on the vertical axis. Even though the nominal indium composition during the InGaAs dots growth is 0.5, a larger value of 0.6 is required to match the PL emission energies, assuming the average dot height of 7 nm. This discrepancy agrees with the results from the growth studies where the segregation of gallium and indium atoms occur during the InGaAs dot growth (Moison *et al.*,

1989; Leonard *et al.*, 1994). The resulting indium composition of the InGaAs dot

is higher than the nominal value used during the growth.
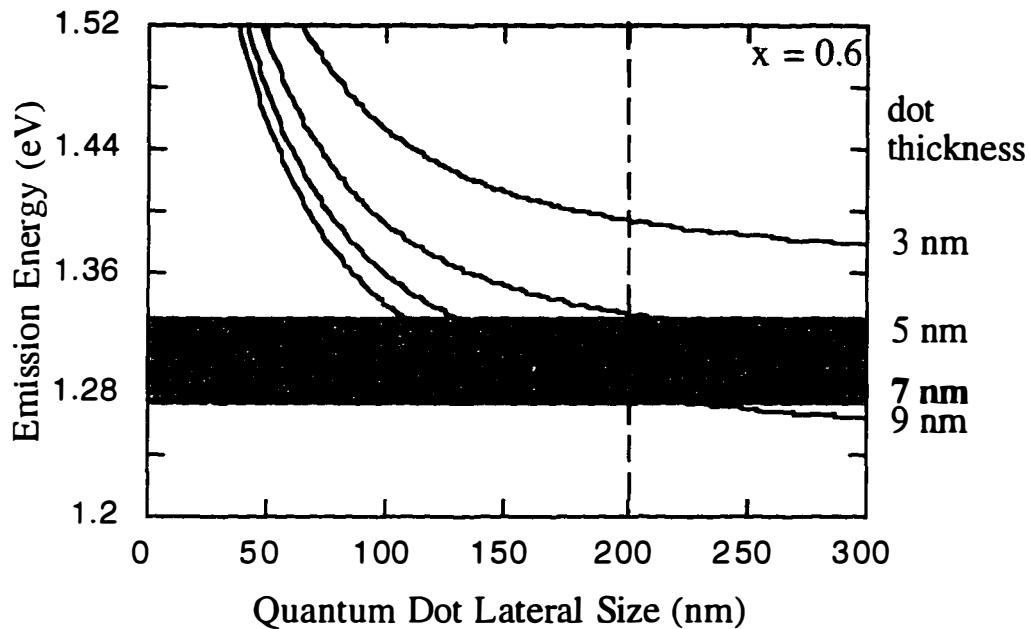
Figure 2.4b Ground state PL emission energies for dots with different width and thickness, for quantum dot with an indium composition of 0.6, indicated by the dashed line in Figure 2.4a. A good correlation between the dot sizes and emission energies can be observed. The FWHM of the measured dot PL is indicated by the shaded region.

For the InAs/GaAs quantum dots, a lower emission energy than the

measured value of 1.1 eV is predicted (Leonard *et al.*, 1994). The assumptions of

the box potential and the isotropic strain field can cause this difference. There are

other approximations that contribute to the inaccuracy of this model. The barrier

material is assumed to be rigid. In reality, the strain energy should be equally

distributed between the inside and the outside of the quantum dot (Love, 1944;

Grundmann *et al.*, 1995). We should expect a strain field in the surrounding GaAs barrier, as we observed from cross sectional TEM in Figure 1.6. The resulting confinement potential will depend strongly on the distribution of strain field in the barrier, unlike the simple flat square box that we have assumed. Furthermore, the splitting of the heavy hole and the light hole energies may arise due to the non-uniform strain field. Using a pyramid geometry, Grundmann *et al.* (1995) have shown that the light hole state is not confined due to the large biaxial strain in the dots.

Figure 2.4b plots the ground state PL emission energies of dots with different width and thickness. A quantum dot with an indium composition of 0.6, indicated by a dashed line in Figure 2.4a, is assumed. A good correlation between the dot sizes and the emission energies is observed. Also, the energy fluctuations resulting from the difference in the dot width (20 meV) is less than from the thickness (50 meV), as concluded from the infinite potential model in the previous section.

2.5 Photoluminescence Linewidth of the Quantum Dot

The broad dot PL peak is composed by an ensemble of extremely narrow peaks. Each peak is associated with a localized bound exciton in a different sized quantum dot (Marzin *et al.*, 1996; Farfard *et al.*, 1996). Figure 2.5 shows the PL spectra of approximately 600 $In_{0.3}Al_{0.7}As/Al_{0.3}Ga_{0.7}As$ quantum dots, isolated using an 1 μm x 1 μm etched mesa. The narrow lines (0.5 meV) of the localized excitons are reproducible in different scans, therefore discounting the factor of noise in the

measurement. At elevated temperatures where the thermal energy is much larger than the linewidth, the narrow linewidth characteristic of the emission remains unaltered. Since the homogenous PL linewidth at low temperatures is attributed to the acoustic phonon scattering (Feldmann *et al.*, 1988), the temperature independent linewidth indicates a significant reduction in the acoustic phonon scattering in the quantum dots. The issue of acoustic phonon scattering in quantum dots will be addressed in Section 4.9. The extremely narrow emission linewidth and the lack of thermal broadening at low temperature are clear evidences of localized bound excitons (Pankove, 1971) and the delta function density of states in these quantum dots.
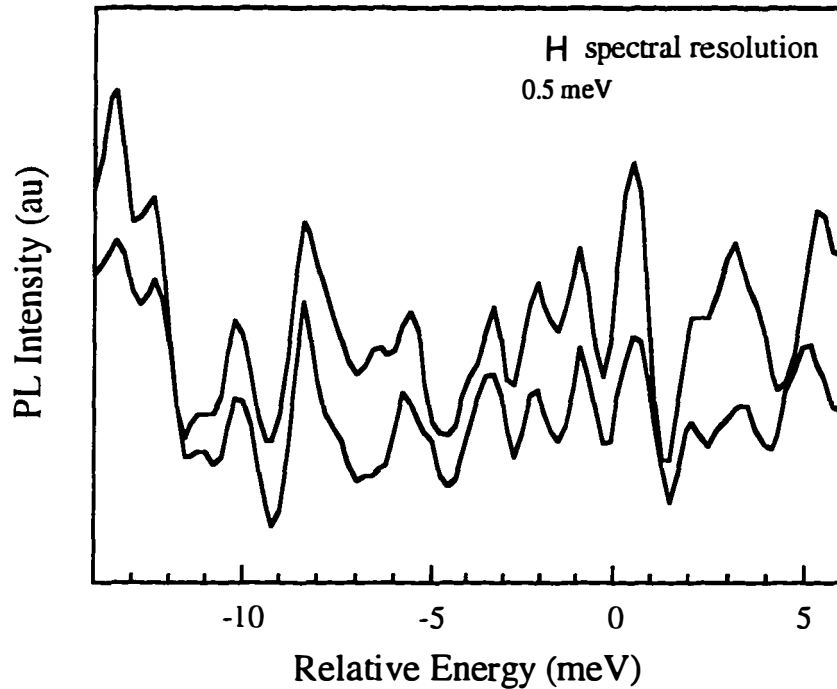
Figure 2.5 Photoluminescence spectra from an ensemble of approximately 600 dots, isolated using an 1 μm x 1 μm etched mesa. The narrow lines (0.5 meV) of the localized excitons can be reproduced in different scans, discounting the measurement noise (Fafard *et al.*, 1994).

2.6 Photoluminescence Excitation Spectra

In Figure 2.3, the relationship between the quantum dots PL and PLE peaks is distinctly different from the quantum well case. For the reference quantum well, the small Stoke shift of 4 meV between the PL and PLE peaks is attributed to the

monolayer fluctuations in the hetero-interfaces. At a high excitation intensity, this energy shift vanishes. The saturation of the localized energy minimum is associated with the monolayer fluctuations in the quantum well interfaces. For the quantum dots, a surprisingly large shift of 69 meV between PL and PLE peaks is observed. This implies there may be an unusual absorption characteristic for these quantum dots. Since this energy shift is independent of the excitation intensity, it cannot be explained by the usual Stoke shift involving a limited number of lower energy minimum (Yang *et al.*, 1993).

The non-overlapping PL and PLE spectra does not necessarily indicate the lack of quantum dot absorption. Rather, this particular PLE behavior is unique to the quantum dot structure. In the absorption measurement, the delta function nature of the density of states requires optical excitation into the extremely narrow ground state where the PLE detection and the PL emission is in resonance. The intensity of the weak ground state quantum dot PL is shadowed by the scattered laser light. Consequently, the ground state absorption of a quantum dot is difficult to detect using the PLE technique (Leonard, 1995; Fafard *et al.*, 1994). Although Ruhle *et al.* (1996) have successfully observed time-resolved PLE from the ground states of InP/InGaP quantum dots, no similar measurement has been reported for the InAs/GaAs dots.

Even though PLE is unable to provide us with information on the ground state absorption of the quantum dots, the strength and the shape of the excited state absorption are clearly observed at higher energies. Since the thickness (7nm) in the growth dimension can only support one quantized state, the notable peaks below the wetting layer absorption in the PLE spectra may be assigned to the

excited energy states introduced from the lateral quantum confinement. The existence of excited states in these quantum dots has also been cleanly verified using magneto-capacitance spectroscopy (Medeiros-Ribeiro *et al.*, 1995).

The evidence for the 0D nature of the quantum dots is found in the broadened delta function peak from the PLE spectra. The delta function peak is characteristically different from the step function lineshape usually observed in the quantum well (Figure 2.3 and 2.6). Rather than exhibiting narrow delta function peaks as the ground state PL, the absorption peaks for the excited states are broadened. These broadened states are attributed to the structural and composition variations among the quantum dots. Since the dots PL is composed by the emission from a large ensemble of individual dot each with a narrow PL linewidth, choosing a particular detection energy is essentially equivalent to selecting a subset of quantum dots with the same ground state emission energy. In this subset of dots with different dot shape and the indium composition, excited state energies can vary slightly.

Additionally, the excited states absorption peaks of the quantum dots shifted with the PLE detection energies, as shown in Figure 2.6. The energy between the ground state emission and the first excited resonance varied linearly from 51 to 63 meV as the PLE detection moved from the higher energy side of PL peak to the lower energy side, implying a larger shift for the larger dots (Fafard *et al.*, 1994; Leonard, 1994). One would expect larger dots to have smaller energy level spacing. This counter-intuitive nature of the energy shift is mediated by structure effect other than the geometry. Tsiper (1996) has suggested that such effect may be attributed to the effect of alloy disorder.

44
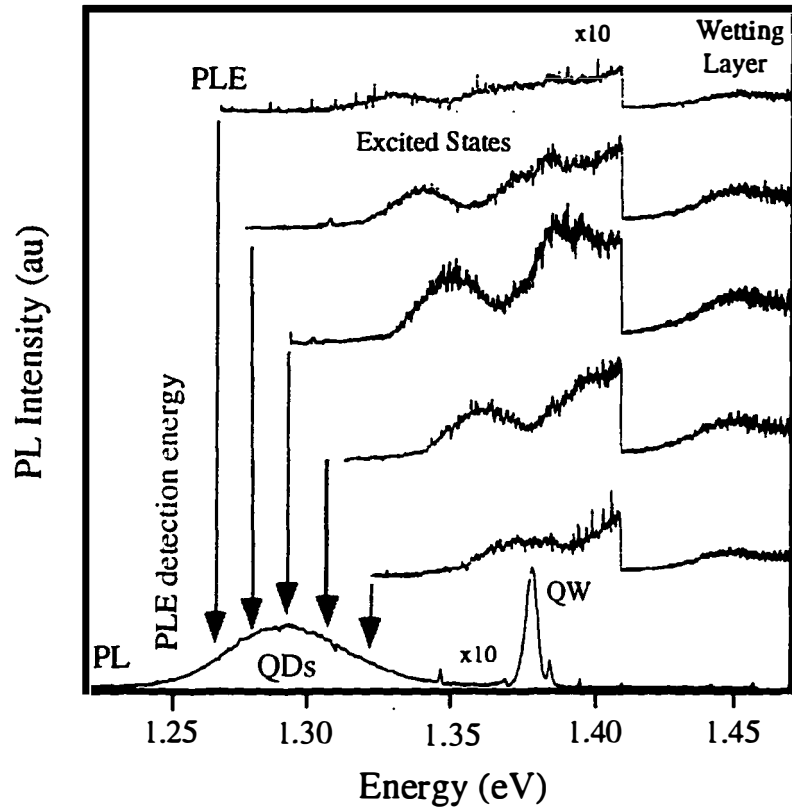
Figure 2.6 Photoluminescence excitation (PLE) spectra measured at various detection energies. The excited state's absorption peak of the quantum dots shifts with the selected dot sizes, determined by the PLE detection energy. (Fafard et al, 1994)

2.7 Excited States in Quantum Dots

In this section, the quantum box model presented in Section 2.4 is extended to address the energy positions of the excited states in the In(Ga)As/GaAs quantum dots. The effects of the non-uniform dot sizes on the excited state energies and lineshapes are investigated. Figure 2.7a plots the calculated transition energies of

the excited states vs. indium composition for the dot width of 20 nm and height of

7 nm. Both the heavy hole transitions and light hole transitions are present. Using

the Gaussian distributions of the dot sizes and heights obtained from AFM (Figure

1.5), the excited states absorption of the $In_{0.5}Ga_{0.5}As/GaAs$ quantum dots with the

ground state at 1.29 eV is plotted in Figure 2.7b. Effective masses of the electron

and the hole are approximated using Luttinger parameters for a strained quantum

well. The calculation shows an   excellent agreement with the measured PLE

(Figure 2.3).
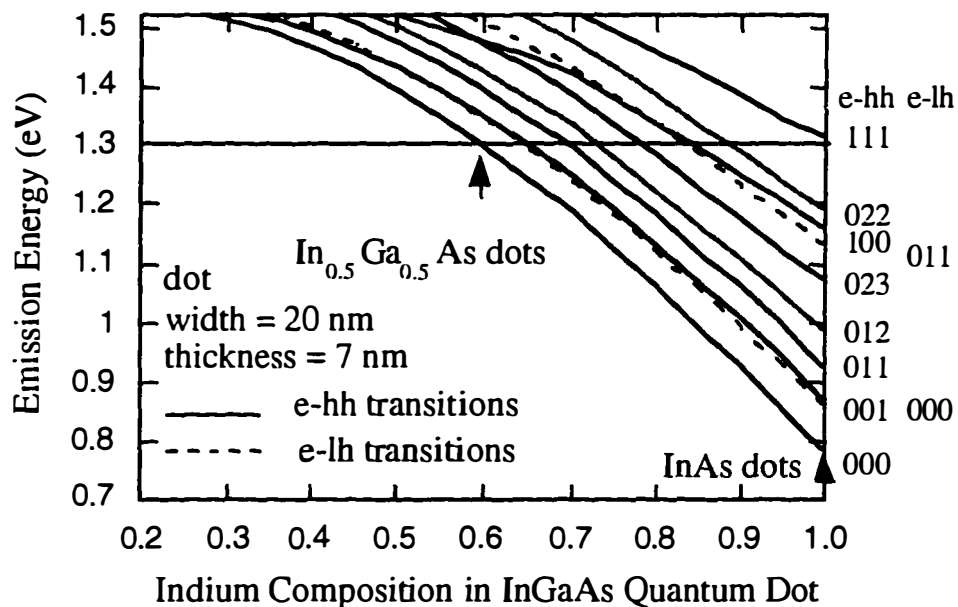
Figure 2.7a Transition energies of the excited states in quantum dot. Lateral width of 20 nm and height of 7 nm are assumed. Both the heavy hole and the light hole transitions are present. Only transitions with the same quantum numbers are considered.
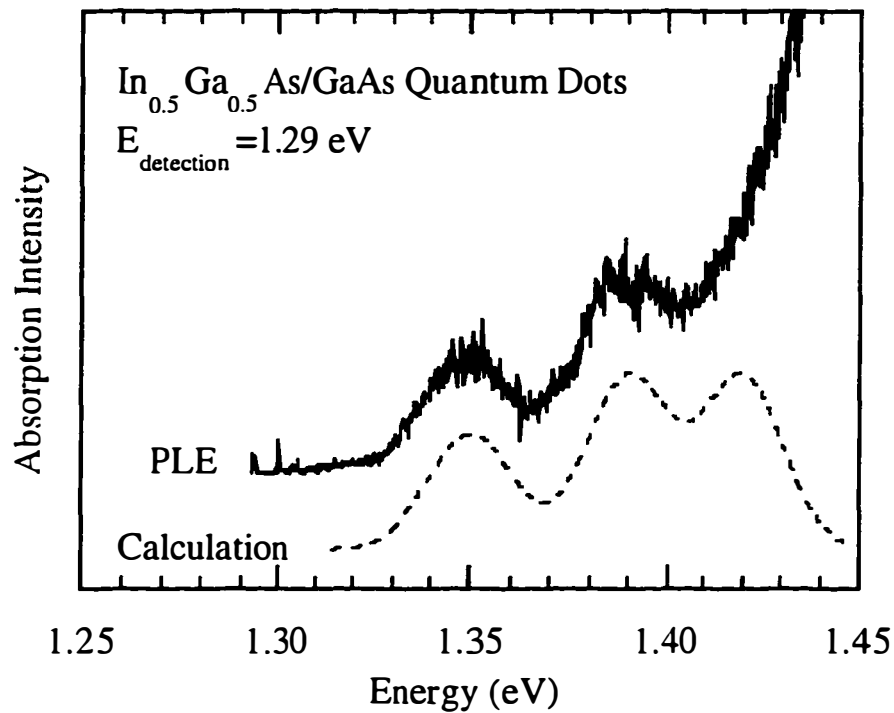
Figure 2.7b The calculated (dashed line) excited states absorption and the measured PLE (solid line) absorption spectra for the $In_{0.5}Ga_{0.5}As/GaAs$ quantum dot. Only the quantum dots with the ground state emission energy of 1.29 eV are considered in the calculation. Gaussian size distribution is used (Figure 1.5). The absorption of the wetting layer is not included in the calculation. The calculated energy positions show excellent agreements with the PLE spectrum.

2.8 Selective Excitation of Quantum Dot Photoluminescence

The large energy difference between the excited state absorption peaks and the ground state emission peak is utilized to selectively excite a subset of quantum dots with an identical excited state energy. Figure 2.8 shows the PL spectra from the selective excitation at various energies in the excited state . The excitation
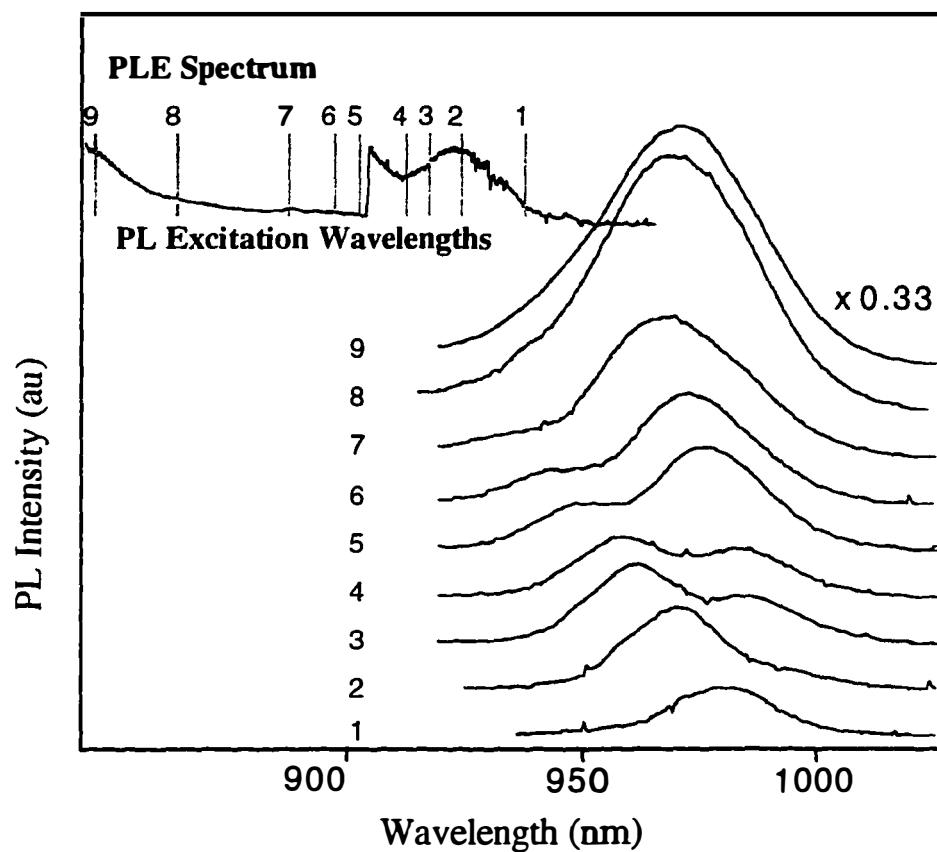
Figure 2.8 Photoluminescence (PL) spectra obtained using the selective excitation. Excitation energies are marked by the numbers in the PLE spectrum. Multiple resonance can be observed from the quantum dot PL spectra, indicating excitation in two subsets of dots (Fafard *et al.*, 1994).

energies are indicated in the corresponding PLE spectrum. As the exciting energy sweep through the excited states absorption peaks, interesting resonance is observed from the quantum dot PLs. At a low excitation energy, with only the first excited state presents (marked by 1 in Figure 2.8), a single PL peak is observed. As the excitation energy rises higher, the second excited states in the larger dots becomes resonant with the first excited states of the smaller dots, leading to multiple PL peaks in the PL spectrum, as indicated by traces 3, 4, 5, and 6. The overlap between the first and the second excited states agrees with the calculation in Figure 2.7b. As the excitation energy reaches the wetting layer, where all of the dots are populated, the excitation is no longer selective. The PL spectrum returns to what we observed for Figure 2.2. For the case of InAs/GaAs quantum dots, Schmidt *et al.* (1996) has observed multiple peaks from the excited states. This difference in the InGaAs/GaAs and InAs/GaAs dots may be attributed to the difference in the confinement energy of the material systems.

2.9 Radiative Efficiency of the Quantum Dots

Despite the observed energy spacing of 50 meV being larger than the LO phonon energy of 36 meV, a bright quantum dot PL is observed. An efficient energy relaxation mechanism clearly exists, contrary to the theoretical prediction of phonon-relaxation bottleneck (Bensity *et al.*, 1991). Although the peak intensity of the quantum dots PL is a factor 10 lower than the reference quantum well (Figure 2.3), their integrated PL intensities are comparable. If the non-radiative defects and

traps are the source of reduced PL efficiency, the intensity dependent PL could exhibit a threshold-like behavior (Fouquet *et al.*, 1985). At low temperature, the intensity dependence of the integrated PL emitted by the dots is linear from excitation power of 12 $\mu J/cm^2$ to 720 $\mu J/cm^2$. This implies that the defects and dislocations are neglible in our dot sample. Naturally, the quantum dots can only occupy a small area. Despite the small volume, their excellent efficiency confirms the quality of the dot structure observed from the TEM studies (Figure 1.6).

At higher temperatures, the radiative efficiency of the quantum dots remains constant. The temperature dependence of the $In_{0.5}Ga_{0.5}As/GaAs$ quantum dot PL is shown in Figure 2.9a. The PL emission persisted up to 180 K. The shift in the peak energies follows the normal temperature dependence of GaAs bandgap. Figure 2.9b plots the temperature dependence of the integrated PL efficiency for the reference quantum well and the quantum dots. The observed thermal quenching of the PL is caused by the dissociation of excitons into the electron-hole pairs. The thermally activated carriers can escape from the well or the dots via thermionic emission into the GaAs barrier or the wetting layer (Nakajima *et al.*, 1980; Bacher *et al.*, 1993; Lamkin *et al.*, 1990). The detailed analysis on the temperature dependent behavior will be presented in Chapter 4.

The thermal energy (kT) at the onset of the quenching may be used to approximate the exciton binding energy (Fafard *et al.* 1994). A binding energy of 12 meV is obtained for the quantum dot. This value is about twice that of the exciton binding energy for the quantum well (6 meV). The factor of 2 increase in

the binding energy supports an enhanced quantum confinement in the dot

structure (Vening *et al.*, 1993; Bryant, 1988; LeGeoff *et al.*, 1992).
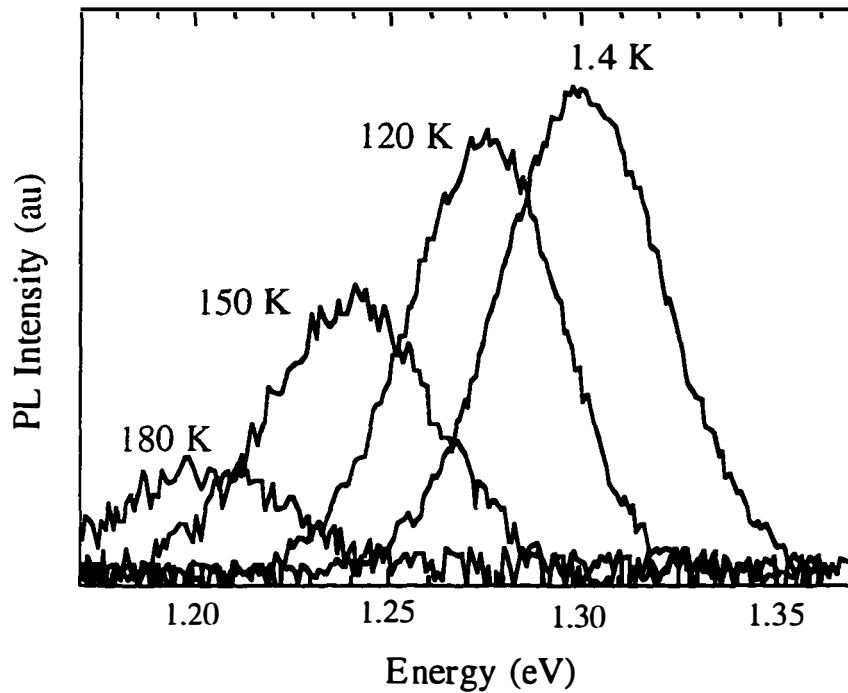
Figure 2.8a The temperature dependent PL of the self-organized quantum dots. The shift in the peak energies exhibit the normal temperature dependence of GaAs bandgap.
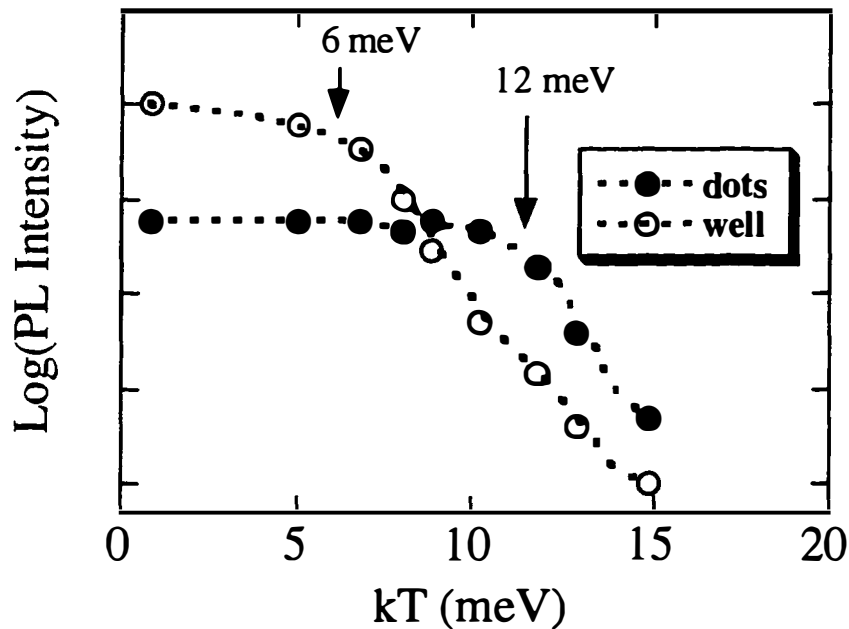
Figure 2.8b The temperature dependence of PL efficiency for the quantum dots and the reference quantum well. Even though the quantum dots cover only a fraction of the probed area, their integrated efficiency is comparable to that of the quantum well at low temperature, and can be almost two orders of magnitude larger at higher temperature. An energy of 6 meV for the onset of the thermal quenching in the quantum well, reminiscent of the exciton binding energy, and a value twice as large in the quantum dots can be extracted (Wang *et al.*, 1994; Fafard *et al.* 1994).

2.10 Summary

Using PL and PLE, we have observed the clear evidences of 0D density of the states in our quantum dot samples. The enhanced binding energy, the narrow PL linewidth and the delta function absorption line shape are all the signature characteristics of bound excitons in quantum dots.

A simple quantum box model including the effect of uniform strain yields a reasonable approximation of the energy positions for the ground state and the excited states. Despite the energy level spacing (50 meV) measured in PLE for the quantum dot being larger than the LO phonon energy (36 meV), an efficient PL is still observed, contrary to the theoretical prediction of the phonon-relaxation bottleneck (Benisty *et al.*, 1991). Efficient carrier relaxation channels from the excited states to the ground states of quantum dots are available.

The excellent optical properties of these quantum dots have led us to believe the extrinsic defects are negligible, and the intrinsic physical effects such as carrier relaxation are important but not well understood.

References

1. S. Adachi, *Journal of Applied Physics* **53**, no.12 8775-92 (Dec. 1982).

2. G. Bacher, H. Schweizer, J. Kovac, A. Forchel, H. Nickel, W. Schlapp, R. Losch, *Physical Review B-Condensed Matter* **43**, 11 9312-9315 (1991).

3. G. Bastard, *Wave Mechanics Applied to Semiconductor Heterostructures* (Les Editions de Physique, Halsted Press, Les Ulis Cedex, France-New York, N.Y, 1988).

4. H. Benisty, C. M. Sotomayortorres, C. Weisbuch, *Physical Review B-Condensed Matter* **44**, 19 10945-10948 (1991).

5. G. W. Bryant, *Physical Review B (Condensed Matter)* **37**, no.15 8763-72 (15 May 1988).

6. S. Z. Chang, T. C. Chang, S. C. Lee, *Journal of Applied Physics* **73**, 10 4916-4926 (1993).

7. C. J. Chou, G. F. Neumark, *Applied Physics Letters* **65**, 6 761-763 (1994).

8. S. W. Corzine, R. H. Yan, L. A. Coldren, *Applied Physics Letters* **57**, 26 2835-2837 (1990).

9. S. W. Corzine, L. A. Coldren, *Applied Physics Letters* **59**, 5 588-590 (1991).

10. D. J. Eaglesham, M. Cerullo, *Physical Review Letters* **64**, no.16 1943-6 (16 April 1990).

11. S. Fafard, R. Leon, D. Leonard, J. L. Merz, P. M. Petroff, *Physical Review B-Condensed Matter* **50**, 11 8086-8089 (1994).

12. S. Fafard, D. Leonard, J. L. Merz, P. M. Petroff, *Applied Physics Letters* **65**, 11 1388-1390 (1994).

13. S. Fafard, R. Leon, D. Leonard, J. L. Merz, P. M. Petroff, *Superlattices and Microstructures* **16**, 3 303-309 (1994).

14. S. Fafard, S. Raymond, G. Wang, R. Leon, D. Leonard, S. Charbonneau, J. L. Merz, P. M. Petroff, J. E. Bowers, *Surface Science* **362**, 1-3 778-782 (1996).

15. J. E. Fouquet, A. E. Siegman, R. D. Burnham, T. L. Paoli, *Applied Physics Letters* **46**, no.4 374-6 (15 Feb. 1985).

16. M. Grundmann, *et al.*, *Physical Review Letters* **74**, 20 4043-4046 (1995).

17. M. Grundmann, *et al.*, *Physica Status Solidi B-Basic Research* **188**, 1 249-258 (1995).

18. J. D. Lambkin, D. J. Dunstan, K. P. Homewood, L. K. Howard, M. T. Emeny, *Applied Physics Letters* **57**, no.19 1986-8 (5 Nov. 1990).

19. J. Lee, E. S. Koteles, M. O. Vassell, *Physical Review B (Condensed Matter)* **33**, no.8 5512-16 (15 April 1986).

20. S. LeGoff, B. Stebe, *Solid State Communications* **83**, 8 555-558 (1992).

21. P. Lelong, G. Bastard, *Solid State Communications* **98**, 9 819-823 (1996).

22. R. Leon, S. Fafard, D. Leonard, J. L. Merz, P. M. Petroff, *Applied Physics Letters* **67**, 4 521-523 (1995).

23. R. Leon, P. M. Petroff, D. Leonard, S. Fafard, *Science* **267**, 5206 1966-1968 (1995).

24. D. Leonard, M. Krishnamurthy, C. M. Reaves, S. P. Denbaars, P. M. Petroff, *Applied Physics Letters* **63**, 23 3203-3205 (1993).

25. D. Leonard, M. Krishnamurthy, S. Fafard, J. L. Merz, P. M. Petroff, *Journal Of Vacuum Science & Technology B* **12**, 2 1063-1066 (1994).

26. D. Leonard, K. Pond, P. M. Petroff, *Physical Review B-Condensed Matter* **50**, 16 11687-11692 (1994).

27. D. Leonard, S. Fafard, K. Pond, Y. H. Zhang, J. L. Merz, P. M. Petroff, *Journal of Vacuum Science & Technology b* **12**, 4 2516-2520 (1994).

28. A. E. H. Love, *A Treatise on the Mathematical Theory of Elasticity* (Dover, New York, 1944).

29. J. M. Luttinger, W. Kohn, *Physical Review* **97**, 10 869 (1955).

30. O. Madelung, *Semiconductors. Group IV Elements and III-V Compounds* (Springer-Verlag, Berlin-New York, 1991).

31.   J. Y. Marzin, J. M. Gerard, A. Izrael, D. Barrier, G. Bastard, *Physical Review Letters* **73**, 5 716-719 (1994).

32.   G. Medeiros-Ribeiro, D. Leonard, P. M. Petroff, *Applied Physics Letters* **66**, 14 1767-1769 (1995).

33.   Y. Nagamune, H. Watabe, M. Nishioka, Y. Arakawa, *Applied Physics Letters* **67**, 22 3257-3259 (1995).

34.   S. Nakajima, Y. Toyozawa, R. Abe, *The Physics of Elementary Excitations* (Springer-Verlag, Berlin-New York, 1980).

35.   J. I. Pankove, *Optical Processes in Semiconductors* (Prentice-Hall, Englewood Cliffs, N.J, 1971).

36.   G. E. Pikus, G. L. Bir, *Sov. Phys.-Solid State* **1**, 1502 (1960).

37.   G. E. Pikus, G. L. Bir, *Symmetry and Strain-Induced Effects in Semiconductors* (Wiley, New York, 1974).

38.   W. W. Ruhle, A. Kurtenbach, K. Eberl, *Nuovo Cimento Della Societa Italiana Di Fisica D-Condensed Matter Atomic Molecular And Chemical Physics Fluids Plasmas Biophysics* **17**, 11-1 1305-1313 (1995).

39.   K. H. Schmidt, G. Medeirosribeiro, M. Oestreich M, P. M. Petroff, and G. H. Dohler. *Physical Review B (Condensed Matter)* **54** 16 11346-11353 (1996).

40.   C. W. Snyder, J. F. Mansfield, B. G. Orr, *Physical Review B-Condensed Matter* **46**, 15 9551-9554 (1992).

41.   V. Srinivas, J. Hryniewicz, Y. J. Chen, C. E. C. Wood, *Physical Review B-Condensed Matter* **46**, 16 10193-10196 (1992).

42.   I.-H. Tan, Ph.D. Disseration, University of California, Santa Barbara (1992).

43.   Tsiper, E. V., *Physical Review B-Condensed Matter* **54**, 3 1959-1966 (1996).

44.   M. Vening, D. J. Dunstan, K. P. Homewood, *Physical Review B-Condensed Matter* **48**, 4 2412-2417 (1993).

45.   G. Wang, S. Fafard, D. Leonard, J. E. Bowers, J. L. Merz, P. M. Petroff, *Applied Physics Letters* **64**, 21 2815-2817 (1994).

56

46.   F. Yang, B. Henderson, K. P. Odonnell, *Physica B* **185**, 1-4 362-365 (1993).

Chapter Three

Time Dependence of Radiative Recombination in Quantum Dots

3.1 Introduction

Continuous wave measurements such as photoluminescence (PL) and photoluminescence excitation (PLE) spectroscopies can provide macroscopic information such as emission efficiency and absorption strength of the optoelectronic materials. These steady-state macroscopic properties are composed of many microscopic dynamic processes which are intrinsic to the semiconductor system. By monitoring the time-dependent response of an excited material system, a clear understanding of the microscopic scattering processes such as electron-hole recombination, electron-electron scattering, and electron-phonon scattering may be obtained.

Various techniques, each with different degrees of resolution and sensitivity, can be utilized to perform time-resolved spectroscopy measurements. Five of the most commonly employed methods are compared in Table 3.1. Depending on the dynamics and samples to be investigated, each method has its own advantages and difficulties. Time-correlated single photon counting (TCPC) system has an advantage of a large dynamic range (O'Conner, 1984). However, its time resolution is limited by the jitter of the detection electronics. The 200 ps resolution available from TCPC system can not cleanly resolve the sub-nanosecond recombination dynamics in the GaAs materials. Measurements with faster time

Characteristics	Fast Detector	Streak Camera	Time-Correlated Photon Counting	Non-Linear Up Conversion	Pump and Probe
Time Resolution	20 ps	1-10 ps	150 ps	0.1 ps	0.1 ps
Sensitivity	low	high	very high	medium	medium
Dynamic Range	low	medium	very high	medium	medium
Linearity	good	poor	good	good	good
Chapter Discussed	none	3,4	6	5	5

Table 3.1 Comparison of the time resolved photoluminescence (TRPL) measurement techniques. Different experiments are employed to study the various aspects of carrier dynamics in the self-organized quantum dots in this dissertation.

response are available. The resolution of the up-conversion and the pump-and-probe spectroscopies is limited only by the pulse width of laser system. Using a Ti:sapphire laser, a resolution as low as 100 fs is obtained. However, the time range of these measurements is limited by the travel length of the mechanical delay stage. The linearity of the signal becomes difficult to maintain when a few nanoseconds range is required. The femtosecond carrier dynamics in the self-organized quantum dots will be studied using pump-and-probe technique in Chapter 5, while the TCPC will be utilized in Chapter 6 to study the spatially indirect excitons in GaSb/GaAs quantum dots.

The desired picosecond resolution and nanosecond range are obtained using a streak camera. This chapter will focus on the time-resolved photoluminescence (TRPL) of the self-organized quantum dots measured using the streak camera. Published quantum dot radiative lifetimes will be compared with our measurements. The factors that affect the radiative lifetime of quantum structure will be discussed.

Section 3.2 will outline the details of the streak camera measurement. The TRPL of the self-organized quantum dots, the reference wetting layer, and the reference quantum well are presented in Section 3.3. The measured exciton lifetimes in the quantum dots is slower than the quantum well by a factor of about two. The quantum dot PL risetime is as fast as the quantum well, and a slower PL risetime is observed in the wetting layer reference sample. The objective of this chapter will focus on the understanding of these differences. In Section 3.4 and 3.5, the recombination dynamics of bulk and quantum well excitons are clarifed in the frame of excitonic polaritons. The recombination dynamics of the bound excitons in the quantum dots are explained in Section 3.6. The exciton lifetimes measured from various self-organized quantum dot materials are compared with other values reported in the literature. The large variations among them are attributed to the difference in the material and dimension. The effects of dot size and dot density on the carrier dynamics are investigated in Section 3.7 and 3.8. Since the wavefunction overlap is mediated by the size of the quantum dot, a large variation in the exciton lifetimes is observed from the spectrally resolved TRPL. In Section 3.9, the exciton density dependence of recombination dynamics are discussed. A distinct difference in the excitation intensity dependent lifetimes

between the quantum well and the quantum dot is observed. This difference is explained by the reduced exciton-exciton scattering in the quantum dots.

3.2 Time-Resolved Photoluminescence Measurements

For the time-resolved photoluminescence measurements, several pulsed lasers were used for the excitation source. Measurements performed prior to the summer of 1994 were done using 5 ps excitation pulses from a synchronously modelocked Styrl 9 dye laser. A frequency doubled Nd:YAG laser operated at 80 MHz was used as the pump source. During the summer of 1994, a passively modelocked Ti:sapphire laser pumped by a CW Ar^+ ion laser was installed to replace the dye laser system. This new solid state laser could produce 120 fs transform limited pulses with a tunable wavelength range from 750 nm to 910 nm, limited only by the bandwidth of the cavity mirrors. All pulsed laser systems used were manufactured by Coherent Inc.

During the streak camera measurement, the excitation pulse was focused onto the sample using a 10 cm focal length lens, producing a beam spot size of 50 μm on the sample. The intensity of the pulse was controlled using a variable neutral density filter. The sample was placed in a Janis flow cryostat and cooled with liquid helium. The photoluminescence was collected using a 2-inch diameter lens (f=6 cm), and the signal was spectrally resolved with a SPEX 0.75 meter spectrometer. A Hamamastu C1587 streak camera operated with a M1955 synchro-scan plug-in unit was used to detect the TRPL signal. The overall time resolution of the system was 10 ps. Although the streak camera could offer an excellent time resolution, the

non-linearity arising from the non-uniform sensitivity over the area of photocathode

required careful calibration and data correction.

The schematic of the streak camera measurement is presented in Figure 3.1.
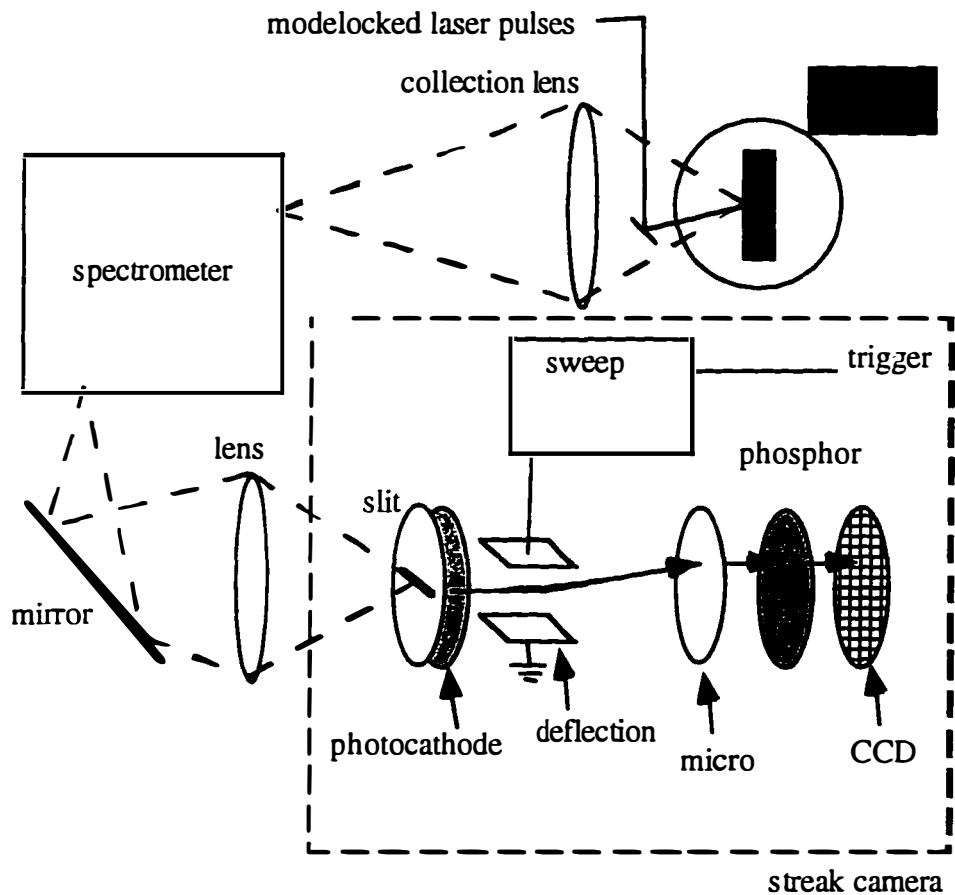
Figure 3.1 The schematic of streak camera measurement. When the photoluminescence photons are collected by streak camera, photo-electrons are generated from the photocathode. A synchronized sweeping voltage is ramped to deflect the photoelectrons onto the micro channel plate (MCP). Similar to the dynods in a photomultiplier tube, the function of MCP is to amplify the photoelectron intensity. The amplied signal is projected onto a phosphor screen and detected with a thermoelectric cooled CCD camera.

3.3 Exciton Lifetime in Self-Organized Quantum Dots

Various self-organized quantum dots samples were grown with different technologies and materials are studied using the time-resolved photoluminescence (TRPL). All samples exhibited similar physical properties as the InAs/GaAs quantum dots described in Section 1.3. Table 3.2 summarizes these samples and their properties.

The $In_{0.5}Ga_{0.5}As$ quantum dots samples studied here are identical to those described in Chapter 2. Based on their excellent photoluminescence properties, we believe that the intrinsic carrier dynamic is not obscured by defects and surface recombination.

Material System	Growth Method	PL Energy	TRPL Lifetime	Material Reference
$In_{0.5}Ga_{0.5}As/GaAs$	MBE	1.3 eV	850 ps	Leonard et al., 1993
InAs/GaAs	MBE	1.1 eV	1 ns	
$InAs/Al_{0.3}Ga_{0.7}As$	MBE	1.5 eV	700 ps	
$In_{0.5}Ga_{0.5}As/GaAs$	MOCVD	1.2 eV	600 ps	Oshinono et al., 1994
$In_{0.3}Al_{0.7}As/Al_{0.3}Ga_{0.7}As$	MBE	1.88 eV	450 ps	Leon et al., 1995
$In_{0.49}Ga_{0.51}P/InP$	MOCVD	1.7 eV	650 ps	Reaves et al., 1995
GaSb/GaAs	MBE	1.4 eV	30 ns	Sun et al., 1996

Table 3.2 Summary of self-organized quantum dots samples studied using TRPL. All samples were grown at UCSB, except the MOCVD $In_{0.5}Ga_{0.5}As/GaAs$ dots, which was obtained from Prof. Arakawa from University of Tokyo. Photoluminescence lifetimes were measured at low temperature (4 K).

In the data analysis, a simple three-level model described in Section 1.5 is used to analyze the temporal profiles. Although the capture process may involve intermediate states such as the wetting layer states or the excited states, the entire capture and relaxation process is modelled with a single time constant. The objective of this model is to consider the entirety of the carrier transport from the barrier to the ground state of the dots, rather than trying to separate the individual relaxation and capture mechanism. The carrier capture time from the excited state to the excitonic state and the radiative lifetime of exciton is modeled using two time constants. Since the integrated PL intensities are constant at low temperature, non-radiative processes such as thermionic emission are neglected. Analysis of the rate equations shows that the luminescence decay is described by (Bastard, 1988)

$$PL(t) \propto \frac{1}{\tau_{decay} - \tau_{capture}} \left(e^{-t/\tau_{decay}} - e^{-t/\tau_{capture}} \right) \quad . \qquad (3.1)$$

The measured temporal profiles are fitted to the convolution of Equation 3.1 with the system response.

One inherent difficulty can arise from Equation 3.1 that may confuse the interpretation of carrier dynamics. The assignment of the values τ_{decay} and $\tau_{capture}$ are ambiguous. Because of the factor $\left(\tau_{decay} - \tau_{capture} \right)$ in the denominator, the photoluminescence decay will always correspond to the slower of the two competing processes. However, in GaAs bulk and quantum well semiconductor material, intraband scattering is usually several orders of magnitude faster than

interband scattering (Shah, 1985). Therefore, the carrier relaxation time is fast when compared to the carrier lifetime, and the decay of the TRPL represents the carrier lifetime of the material. For the quantum dot material, we will employ the similar assumption that relaxation and capture of the carrier is fast when compared to the radiative decay process.

Figure 3.2 shows the low temperature TRPL of a 6 nm $In_{0.17}Ga_{0.83}As/GaAs$ quantum well, a 2 monolayer (ML) $In_{0.5}Ga_{0.5}As/GaAs$ quantum well, and $In_{0.5}Ga_{0.5}As/GaAs$ quantum dots. These samples are grown by MBE. The thickness of the 2 ML sample is similar to the wetting layer in the quantum dot sample. Using non-resonant excitation at the GaAs barrier (1.52 eV), the photoluminescence decays are measured at the PL peaks (Figure 2.3). At low excitation intensity (1 mW), the decay time of 336 ps and 882 ps are found for the reference quantum well and the quantum dots peaks, respectively. *In all samples, an increased decay time by a factor of more than 2 is observed for the quantum dot PL when compared to quantum well PL.* Similar observations of longer decay times from quantum wires structures are published in the literature. Using a similar InGaAs quantum dot sample, Raymond *et al.* (1996) have recently measured the ground state lifetime of 1 ns. For the strain-induced quantum wire, Tan *et al.* (1993) has observed carrier lifetimes of 420 ps for the quantum wires and 270 ps for the reference quantum well. Kono *et al.* (1992) has shown an increase in the carrier lifetime from 240 ps to 422 ps when the lateral dimension of the quantum wire is reduced from 30 nm to 10 nm. Weman *et al.* (1990) has measured a carrier lifetime of 380 ps for the serpentine superlattice quantum wire and 260 ps for a similar reference quantum well. These increases of the carrier lifetimes in the

lower dimensional quantum structures are not explained by the enhanced electron-hole wavefunction overlap in the quantum dots. Theoretically, a faster exciton lifetime is associated with an enhanced electron-hole wavefunction overlap (Hanamura, 1991).

One potential explanation for the increased luminescence decay time is the phonon bottleneck effect, where the carrier relaxation rate from the barrier into the quantum dots is reduced due to the restricted carrier-LO phonon scattering. However, the observed integrated PL efficiency of the quantum dots is comparable to the quantum well, as discussed in Section 2.9. The bright photoluminescence suggests that the phonon bottleneck effect is not significant in our sample structures.

The high indium content of the monolayer and dot samples suggests   that the observed slower exciton decay in the quantum dot and monolayer samples may be resulting from the interface scattering (Citrin, 1991). Citrin has suggested that excitons in quantum structures can be coupled coherently similar to an oscillating dipole array. This coherence is maintained within a certain volume. A clear correlation between the coherent volume of the quantum structures and the PL decay times is observed in Figure 3.2. With a larger lateral extension in the plane of the quantum well, the exciton in the 6 nm quantum well exhibits a faster decay time than the monolayer and the dot samples. The carriers in the monolayer sample have a slightly faster decay time (810 ps) than the quantum dot sample. Although the effect of the interface disorder may be important in the self-organized quantum dots, there is a sharp contrast between the slow TRPL risetime of the monolayer quantum well sample and the fast risetime of quantum dot sample, as observed in Figure 3.2.

The capture process in the ML sample involves the transport of excitons from the thinner region of the sample to the thicker region. If the capture process through the wetting layer was important in the quantum dot sample, then we should observe a similar slow rise in the TRPL. This implies that the radiative recombination dynamics in the quantum dot sample simply can not be presented in the picture of interface scattering.

In Figure 3.3, similar slow decays and fast rises are observed in the $In_{0.5}Ga_{0.5}As/GaAs$ quantum dots grown by MOCVD. The lifetime of 600 ps measured in the MOCVD dots further indicates that the observed carrier decay in the MBE sample does not result from growth related defects. The intrinsic lifetime of the self-organized quantum dot is independent of the growth method.

Table 3.2 summarizes the measured carrier lifetimes in various self-organized quantum dot samples. Altougth similar values are obtained for identical materials grown by different methods, the measured lifetimes are distinctly different for other material systems. The photoluminescence decay times for the MBE grown $In_{0.3}Al_{0.7}As/Al_{0.3}Ga_{0.7}As$ quantum dots and the MOCVD grown $InP/In_{0.49}Ga_{0.51}P$ quantum dots are 450 ps and 650 ns, respectively (Figure 3.3). Even though the material systems are different, these measured lifetimes are still slower when compared with quantum well samples of the same materials reported in the literature (Daiminger *et al.*, 1994; Fouquet *et al.*, 1990). These similarities further suggest that the observed increases in the radiative lifetimes are a fundamental difference between the quantum well and quantum dot structure.

In order to understand this increase of the radiative lifetime in the self-organized quantum dots, the radiative recombination processes in bulk and quantum well structures need to be clarified.
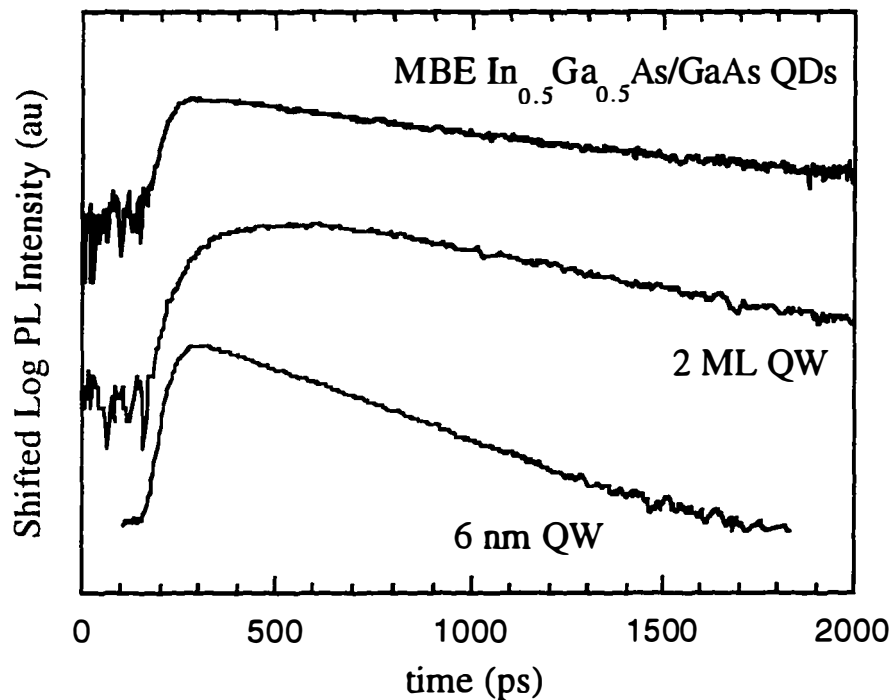
Figure 3.2 Low temperature time-resolved photoluminescence of a 6 nm $In_{0.17}Ga_{0.83}As$/GaAs quantum well (QW), a 2 monolayer (ML) $In_{0.5}Ga_{0.5}As$/GaAs quantum well, and $In_{0.5}Ga_{0.5}As$/GaAs quantum dots. The thickness of 2 ML sample is similar to the wetting layer in the quantum dot sample. Non-resonant excitation at GaAs barrier (1.52 eV) is used in the experiment.
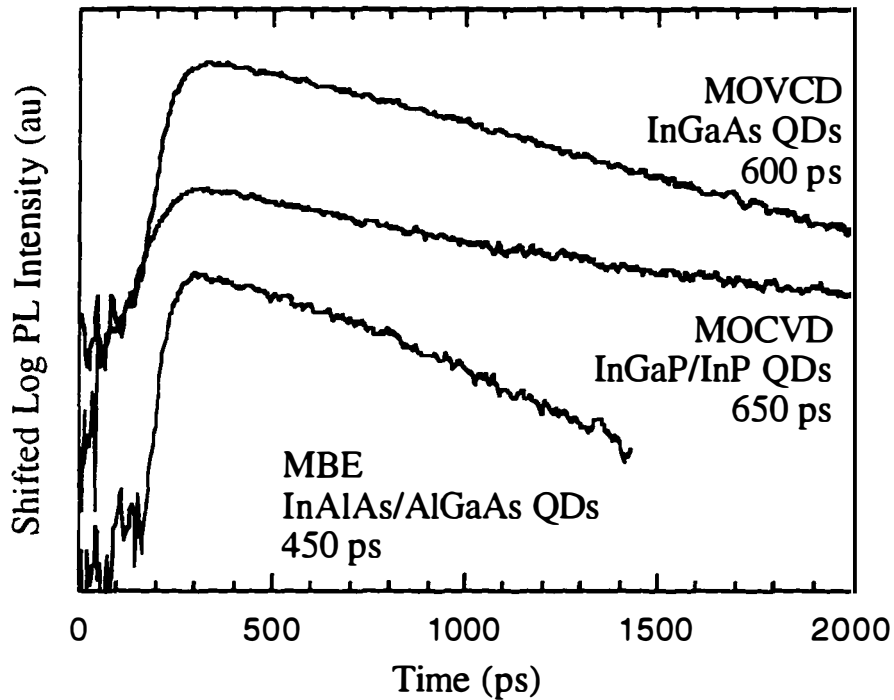
Figure 3.3 Low temperature time-resolved photoluminescence of the self-organized quantum dots grown with different materials and methods. References are listed in Table 3.2. Non-resonant excitations are used in the experiments. The excitation energies are listed in Table 3.3.

3.4 Radiative Recombination in Bulk Material

Radiative recombination occurs in a semiconductor when an excited electron in the conduction band relaxes to a hole state in the valence band, conserving energy by emitting a photon. Mediated by the Coulomb interaction between the

electron and hole, the radiative dynamics can exhibit either free carrier or excitonic properties. Free carrier process involves the recombination of non-interacting free electron and hole populations (Ridley, 1990). The macroscopic theory of free carrier luminescence is characterized by a bimolecular time decay (Pickin, 1989; Fouquet *et al.*, 1986),

$$\text{Bimolecular Decay} = \frac{Bn_o^2}{(1 + Bn_o t)^2},$$
(3.2)

where n_o is the injected carrier density, and B is the bimolecular recombination coefficient. Equation (3.2) describes a non-exponential time decay which is dependent on the density of carriers n_o. However, single exponential decays are observed for the quantum well and quantum dots samples (Figure 3.2), suggesting that the free carrier process is absent.

The excitonic process involves the recombination of an electron-hole pair bounded together as an exciton under Coulomb attraction. Excitons, rather than the free carriers, are usually dominant at low temperature, where the thermal energy (kT) of the lattice is less than the exciton binding energy. In contrast to the bimolecular process, the radiative lifetime of exciton is characterized by a single exponential decay (Fouquet, 1986), similar to the observed TRPL decays for the quantum well and dots.

Unlike the free electrons and holes, excitons in semiconductor are strongly coupled to the surrounding photon field. Under a strong dielectric coupling, the radiative dynamics of exciton are modified significantly. Hopfield (1958) has shown that the radiative decay of exciton is inhibited in bulk semiconductor due to the translational symmetry of the exciton wavefunction and the conservation of

Bulk Excitonic Polariton
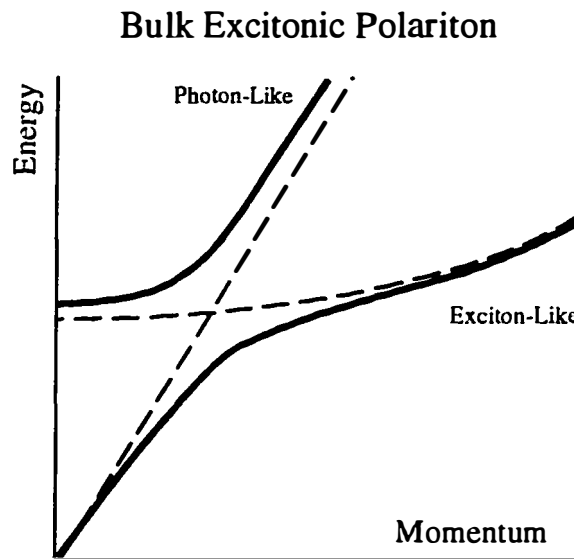
Figure 3.4a Excitonic polariton dispersion relation for bulk semiconductor material. The dashed curves are the un-coupled exciton and photon dispersion curves. In the excitonic polariton, the energy oscillates back and forth between the exciton and the photon modes. The radiative decay is inhibited due to the translational symmetry of the crystal. Radiative decay of bulk exciton-polariton occurs only at defects and interfaces, where the translation symmetry breaks.

crystal momentum. In the bulk semiconductor, the interaction of free excitons with photons does not lead to radiative decay for the excitons, but rather to stationary states called excitonic polaritons. In excitonic polaritons, the energy of the system oscillates back and forth between the excitons and the photons. Figure 3.4a plots the exciton-polariton dispersion relation, obtained by considering the Maxwell's Equations in a dielectric material. The observed radiative decay of exciton-polaritons is associated with phonons or translational-invariance breaking defects, impurities, or interfaces. Decay times of several nanoseconds have been reported for excitons in bulk GaAs and InP (Hwang, 1973; Keyes, 1994).

3.5 Carrier Dynamics in Quantum Well Structure

In quantum well structures, the dielectric coupling strength can be significantly modified. The translational invariance of the exciton wavefunction is broken due to the quantization of exciton momentum in the direction of confinement. Coupled to photon states outside the plane of the quantum well (indicated by the x in Figure 3.4b), excitonic polariton states with in-plane momentum below the crossing with the photon line become quasi-stationary. Efficient radiative decay is allowed (Figure 3.4b).

2D Excitonic Polariton
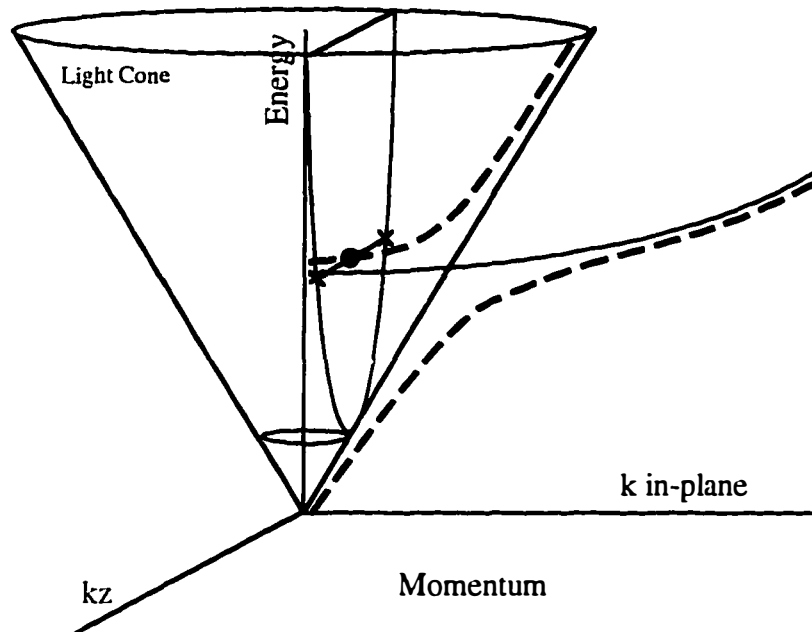
Figure 3.4b 2D quantum well exciton-polariton dispersion relation. The translational symmetry is removed due to the quantum confinement, resulting an ill-defined kz in the growth plane. Due to the ill defined momentum in the direction of the confinement, fhe exciton-polariton lying within the light cone can decay radiatively by coupling to photon states on the light cone. For the case of the quantum dots, the exciton dispersion become limited to very small k value due to the effect of the localization and 3D confinement. Since all exciton states are within the light cone, extremely fast decay should be expected (Hanamura, 1988).

The radiative lifetime of exciton in a quantum well is inversely proportional to the oscillator strength per unit area multiplied by the coherent area of the exciton (Hanamura, 1988; Bocklmann, 1993; Feldmann, 1988). The coherent volume is defined by the number of crystal unit cell over which the exciton wavefunction can interact coherently with the radiation field during the spontaneous emission process.

Theoretical analyses have predicted an extremely fast radiative decay time for the excitons in quantum well. A superradiant decay of 2.8 ps is derived from the theoretical work of Hanamura (1988). Using free excitons that are spatially coherent over the entire quantum well, Citrin (1993) and Andreani *et al.* (1992) have calculated the k=0 free exciton lifetime of 25 ps for an 10 nm GaAs/AlGaAs quantum well.

In spite of the careful theoretical analysis, the experimental reported lifetimes for excitons in quantum well are longer than the expected value. Decay times in the range of 60 ps to 1 ns are reported (Vinattier *et al.*, 1994; Bergman *et al.*, 1991; Ploog *et al.*, 1993; Martinez-Pastor *et al.*, 1993). This discrepancy is understood by arguing that the spatial coherence of the free excitons does not have an infinite extend. Instead, the coherent area is disrupted by the effects of rough quantum well interfaces and exciton-exciton scattering. A reduction in the oscillator strength of the radiative transition rate will lead to an increase in the radiative lifetime. For the quantum well with smooth interfaces, the effect of rapid acoustic phonon scattering of excitons will lead to a thermal distribution of excitons with non-zero center-of-mass momentum. Exciton states lying outside of the photon dispersion curve are non-radiative. Only the fraction of the thermalized states which are below the crossing with the photon line can decay radiatively. The resulted decay time coincides with the inverse of thermally averaged decay rate, which is larger than the theoretical k=0 value (Citrin, 1993; Andreani *et al.* 1992). The exciton lifetime of 336 ps observed for the InGaAs quantum well concurs with this picture.

For the case of the quantum dots, the exciton dispersion become limited to very small k value due to the effect of the localization and 3D confinement. The relationship between the exciton energy and momentum is essentially governed by the uncertainty principle. Since all exciton states are within the light cone, extremely fast decay should be expected (Hanamura, 1988). However, the exctonic-polariton picture isn't entirely the correct description for the radiative recombination process in the quantum dots. The effect of exciton localization must be closely considered.

3.6   Bound Exciton Recombination in Quantum Dots

Various reports of exciton lifetimes in different quantum dots materials are found in the literature (Table 3.3). Among this large variation of the reported values, three distinct dependences are observed. First, in contrast to the long decay observed for the InGaAs quantum dots, the reported values for the II-VI nanocrystals are as short as 30 ps. Second, for the III-V self-organized quantum dots with a similar size, the observed lifetimes decrease as the dot PL emission energy increases. Third, the dot PL decays are faster as the confinement dimensions become larger, approaching the values for the 2D quantum well.

These three observations in the reported quantum dot exciton lifetimes are essentially resulted from three related factors. Hanamura (1988) has shown that in the regime where the exciton Bohr radius and the confinement dimension is less than the emission wavelength, the radiative decay rate (Γ) of excitons is expressed as

$$\Gamma = \Gamma_o \bullet \left| \langle \chi_{electron} | \chi_{hole} \rangle \right|^2 \bullet \left(\frac{L}{a_B} \right)^n \qquad (3.3)$$

where n is 2 for quantum well structure and 3 for quantum dot structure.

The first term in Equation 3.3, Γ_o, is the oscillator strength per unit volume. Γ_o is an intrinsic property of semiconductor material. It is directly proportional to the bandgap energy of the semiconductor material (Bocklman, 1993; Citrin, 1991; Corzine, 1993). This factor contributes significantly to the decrease of the exciton lifetimes with the transition energy observed in Table 3.3. The reported PL lifetims is plotted vs. the emission energy in Figure 3.5a.

The second term, $\left| \langle \chi_{electron} | \chi_{hole} \rangle \right|^2$, is the square of the wavefunction overlap between the electron and the hole. Its value is affected by the quantum dot dimension, the confinement potential, and the effective masses of the electron and hole. Larger wavefunction overlap is obtained with a higher potential barrier and a smaller confinement dimension. However for the lighter mass particle, the effect of a small confinement dimension will push the wavefunction into the barrier, reducing the wavefunction overlap (Bastard, 1988). The wavefunction overlap does not depend strongly on the material system. Its effect is mainly observed through the variation in the lateral dot sizes.

Material System	Reference	Mean Size nm	Energy eV	Lifetime ps
InAs/GaAs	Mukai *et al.*	20	1.1	1000
InAs/GaAs	This Thesis[1]	20	1.1	1000
InAs/GaAs	Bogani *et al.*	25	1.28	700
$In_{0.5}Ga_{0.5}As/GaAs$	This Thesis	20	1.29	850
$InAs/Al_{0.3}Ga_{0.7}As$	This Thesis	20	1.5	700
$In_{0.3}Al_{0.7}As/Al_{0.3}Ga_{0.7}As$	This Thesis	20	1.88	450
$InP/In_{0.49}Ga_{0.51}P$	This Thesis	100	1.7	650
$InP/In_{0.49}Ga_{0.51}P$	Pistol *et al.*	45	1.75	1000
$InP/In_{0.48}Ga_{0.52}P$	Ruhle *et al.*	20	1.68	400
$In_{0.5}Ga_{0.5}As/GaAs$	Bocklemann *et al.*	450	1.71	280
$In_{0.1}Ga_{0.9}As/GaAs$	Watabe *et al.*	700	1.51	500
InGaAs/GaAs	Kono *et al.*	180	1.55	480
GaAs/AlGaAs	Zhang *et al.*	200	1.51	400
CdSe	Schulzgen *et al.*	2	2.1	30-200
CuCl	Masumoto *et al.*	3	3.2	76
CdSSe	Bugayev *et al.*	3	2.4	40-70

Table 3.3 Summary of the reported exciton lifetimes in various quantum dot samples. Only values measured at low temperature (<10 K) are included. Lifetimes are measured at PL peaks.

Excitation Intensity	Excitation Energy (eV)	Dot Density (cm^{-2})	Dot Growth Method
not reported	2.33	10^{10}	Atomic Layer Epiaxy
0.1 mW	1.55	10^{10}	MBE, by D. Leonard
1 mW	2.33	10^{10}	MBE
0.1 mW	1.55	10^{10}	MBE & MOCVD
0.1 mW	1.55	10^{10}	MBE, by G. Medeiro-Ribeiro
0.1 mW	2.33	10^{10}	similar result by Raymond *et al.*
0.1 mW	2.33	10^{10}	grown by Reaves *et al.*
0.5 mW	2.41	10^{10}	MOCVD
6 mW	1.68	10^{10}	MOCVD
0.002 mW	1.77	1 dot	thermal diffusion induced
0.1 mW	2.33	10^{7}	selective regrowth
3 mW	2.33	10^{8}	selective regrowth
0.023 mW	2.41	10^{8}	strain induced
16 $\mu J/cm^{2}$	3	n/a	
26 $\mu J/cm^{2}$	3.28	n/a	Nanocrystals
15 $\mu J/cm^{2}$	3.5	n/a	

Table 3.3 (Continue) All measurements reported are taken at low temperatures (1.4 - 20 K). [1] Lifetime of 1 ns is also measured by Raymond *et al.* (1996).
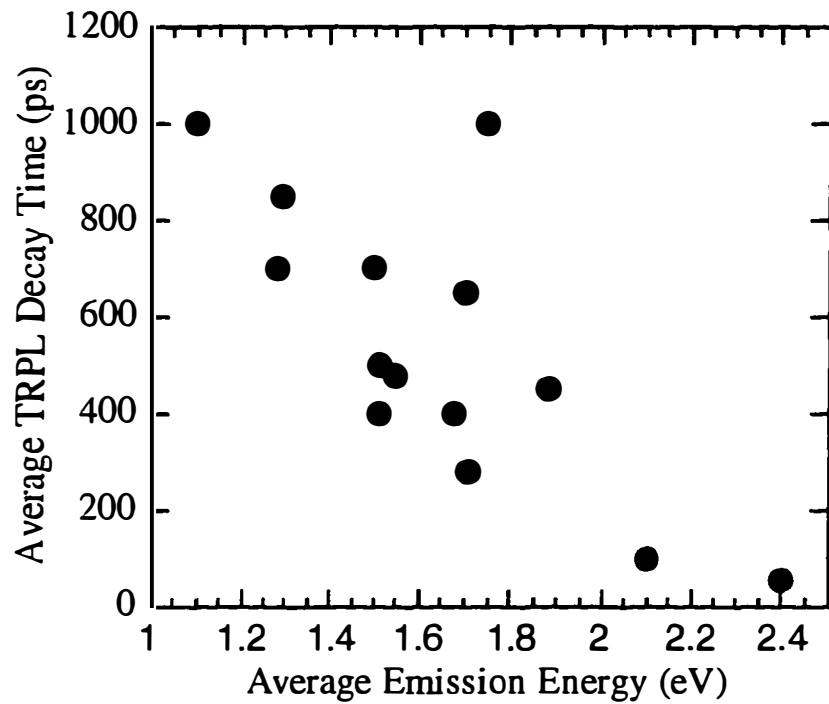
Figure 3.5a TRPL decay time vs. emission energy for various quantum dot materials listed in Table 3.3. A reduction in the exciton lifetimes are observed as the transition energy increases. This effect is attributed to the difference among the dot materials' oscillator strength.
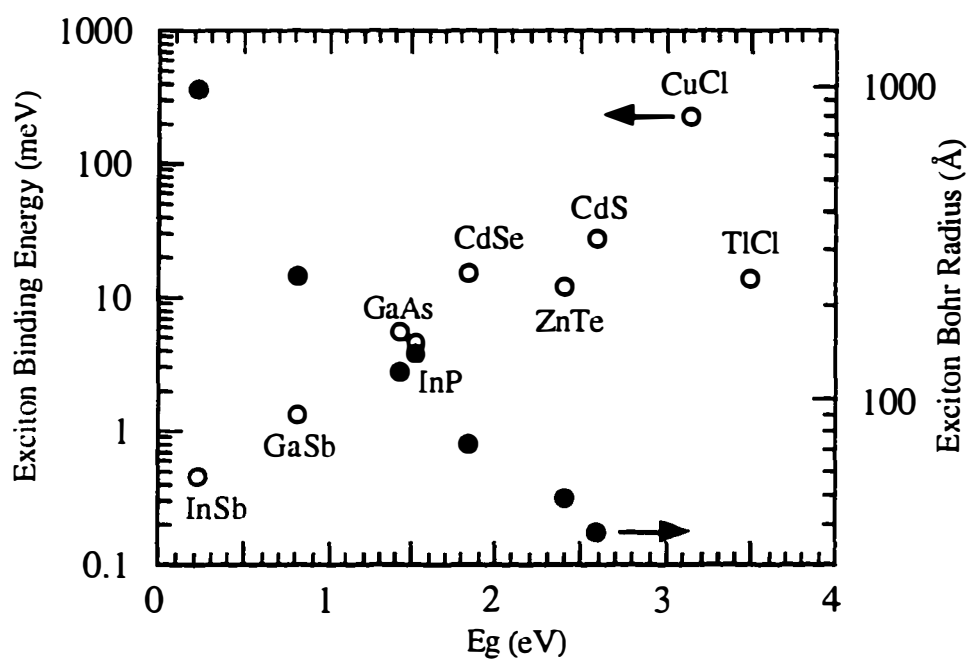
Figure 3.5b Exciton binding energy and Bohr radius vs. the bandgap energy in various bulk semiconductor materials.). A clear reduction of the exciton Bohr radius is observed for larger bandgap materials.

The last term, $(L/a_B)^n$ is the coherence factor, where a_B and L are the Bohr radius of the exciton and the dimension of the confinement potential, respectively. For a 2D quantum well or a large quantum box, L is essentially the coherence length of the exciton. Unlike the previous two terms where the dependence on the transition energy and confinement dimension are clear, the exact relationship between a_B and L is complicated. The exciton Bohr radius is dependent on both the bandgap energy and the confinement dimension. Figure 3.5b plots the dependence of bulk binding energy and radius on the bandgap energy for excitons in various semiconductor materials. The bulk exciton binding energies are obtained from literature (Pankove, 1971). A clear reduction of exciton Bohr radius is observed for larger bandgap materials. Furthermore, exciton binding energy and Bohr radius also vary with the degree of quantum confinement. The effective Bohr radius of 7 nm in a quantum well is reduced by a factor of 2 from the bulk value of 14 nm (Weisbuch and Vinter, 1991).

The relationship between a_B and L will determine if the radiative transition rate in a quantum dot is enhanced or reduced, when compared to a 2D quantum well of similar material. The radiative transition rate is enhanced when $a_B < L$. Since the crystal translational symmetry is removed in all directions, an exciton with an ill defined momentum can couple to all photon states. An efficient, superradiant luminescence can be expected (Brandt, 1992; Hanamura, 1988).

In the region $a_B > L$, the exciton is strongly localized. A localized exciton essentially disrupts the coherent nature of the exciton. The coherence area of the exciton is reduced to the area of a single quantum dot. The oscillator strength for the

bound exciton transition is given by the oscillator strength per unit volume multiplied by the volume covered by the wavefunction overlap of the electron and hole. Therefore, this reduction of the coherence area can lead to an increased exciton lifetime in the quantum dot. This effect is mainly responsible for the slow decay of excitons in self-organized quantum dots. Our observation concur with the reported dot PL lifetimes in the literature, as shown in Figure 3.5c.

However, the definition of the exciton is ambiguous in a quantum dot when $a_B > L$. The binding force between the electron and hole wavefunctions is no longer purely due to the Coulomb attraction. Enhancement of wavefunction overlap due to the effect of the lateral confinement potential becomes equally important as the reduction of the coherent area. This crossover between the reduction of the coherent area and the increase of the wavefunction overlap are observed in the spectral dependence of exciton lifetimes from a large size ensemble of the quantum dots.
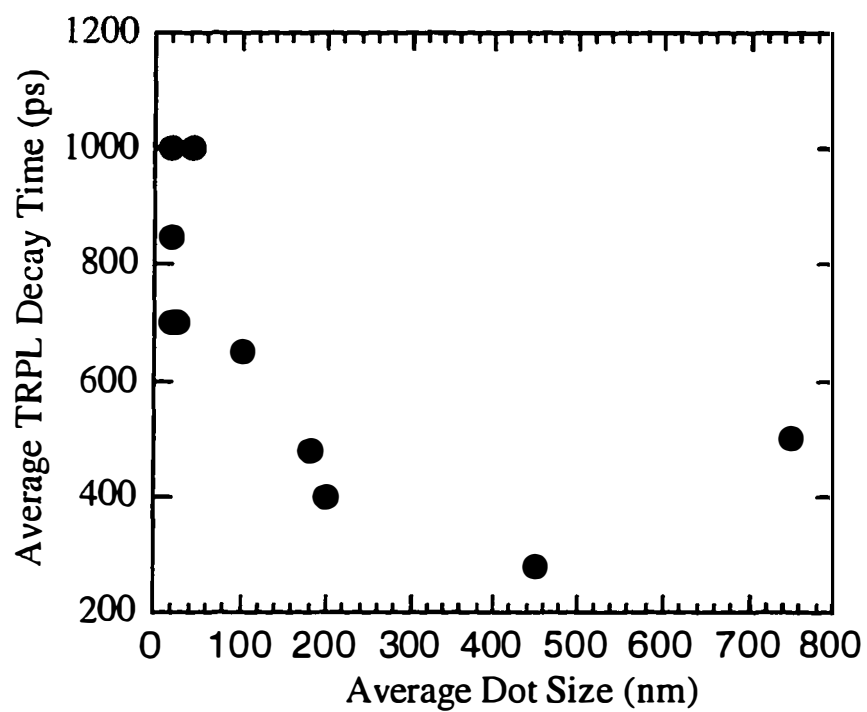
Figure 3.5c TRPL decay times vs. dot sizes. The increased PL lifetime for dot with smaller dimension is resulted from the effect of carrier localization.

3.7 Spectrally Resolved Recombination Dynamics

The effect of an enhanced electron and hole wavefunction overlap in the exciton is observed in the spectrally resolved TRPL of the $In_{0.5}Ga_{0.5}As/GaAs$ quantum dots as shown in Figure 3.6. The measured exciton lifetimes vary linearly from 650 ps to 1.5 ns as the streak camera detection wavelength is swept from the high energy side to the low energy side of the quantum dots PL spectra. The variation in the measured TRPL decay times indicates that the overlap of the electron and hole wavefunction of an exciton is enhanced by a factor of more than 2 for the thinner dots. The restricted internal motion of the electron and hole are clearly visible. Similar behavior is also observed in the MBE grown $In_{0.3}Al_{0.7}As/Al_{0.3}Ga_{0.7}As$ quantum dots (Fafard et al., 1996), the MOCVD grown $In_{0.5}Ga_{0.5}As/GaAs$ quantum dots (Wang et al., 1995), and the CdSe nanocrystals (Schulzgen et al., 1993). These spectral variations observed are a combination of the material's oscillator strength, the enhanced wavefunction overlap, and the reduction of the coherence area.

Raymond et al. (1996) and Mukai et al. (1996) have both obtained excited state TRPL using InGaAs quantum dots. Their PL spectra demonstrated excited state PL from multiple peaks. From the PL and PLE measurements, we observed a clear separation of ground state PL and the excited state absorption; therefore, the spectrally resolved TRPL presented here cannot be assigned to the excited state TRPL.

Wavelength (nm)

915   930   945   960   975   990

2 ns

Time Decay

0

LOG TRPL Intensity (au)

990 nm

975 nm

960 nm

945 nm

930 nm

0   400   800   1200

Time (ps)
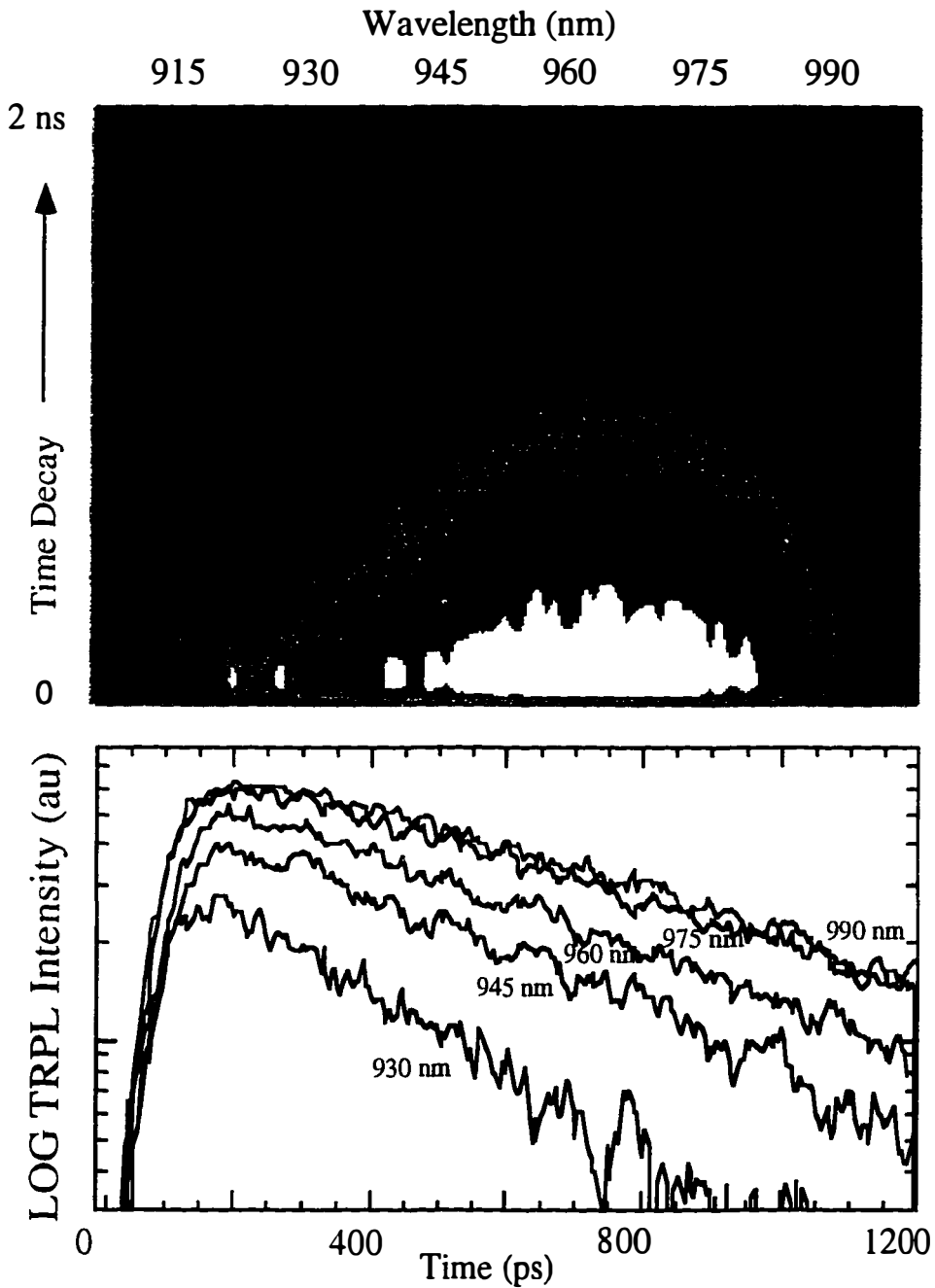
Figure 3.6 Spectrally resolved TRPL of the InGaAs/GaAs quantum dots. The measured exciton lifetimes vary linearly from 650 ps to 1.5 ns as the detection moves across the dot PL spectrum, indicating the exciton lifetime is a function of the dot size.

3.8 Dot Density Considerations

One may argue that the measured variation in the exciton lifetime vs. the dot size is the effect of exciton scattering and relaxation among the dots, since an inhomogenously broadened quantum well has a similar time-resolved spectral dependence. In order to clarify this point, the dependence of the exciton lifetime on dot density is investigated, using a variable dot density sample grown by Devin Leonard using MBE.

A sample with a gradual increase in the dot density is obtained by stopping the substrate rotation during the deposition of InGaAs. Since the indium effusion cell is positioned off center with respect to the substrate surface normal, a variation
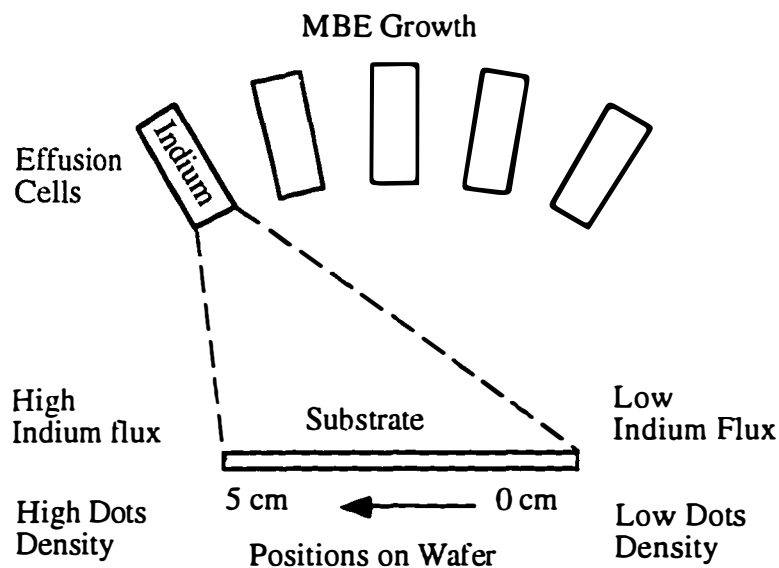
Figure 3.7a Schematic of MBE growth of self-organized quantum dots. Utilizing the difference in the indium flux across the substrate, a variation dot density sample can be achieved by stopping the substrate rotation during the deposition of InAs.

in the indium flux occurs across the sample (Figure 3.7a). The small difference in the indium flux can lead to a large variation in the dot density (Leonard *et al.*, 1994). This variation is observed from the intensity of the dot PL spectrum measured at various positions on the wafer. The spectrally resolved photoluminescence lifetimes are systematically measured at points where the dot density varies significantly (Figure 3.7b). No dependence of the exciton lifetimes on the dot density is detected, indicating that the dot density in the sample is below the critical density where carrier-carrier interaction between the adjacent dots is important.
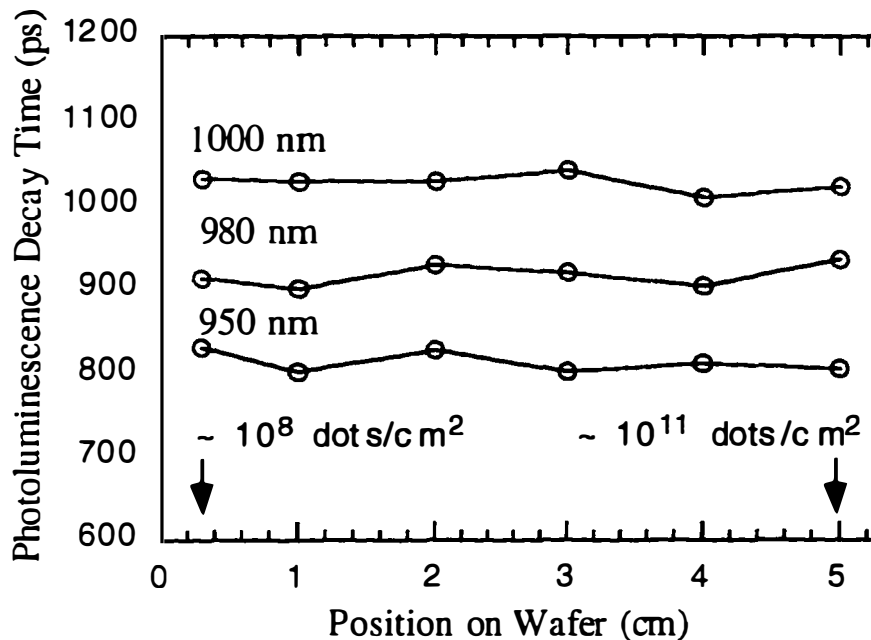
Figure 3.7b Spectrally resolved photoluminescence lifetime measured for various dot density across the wafer. No significant variation in the exciton lifetimes is detected as the dot density increases.The variation at difference wavelengths follows the same trend as Figure 3.5.
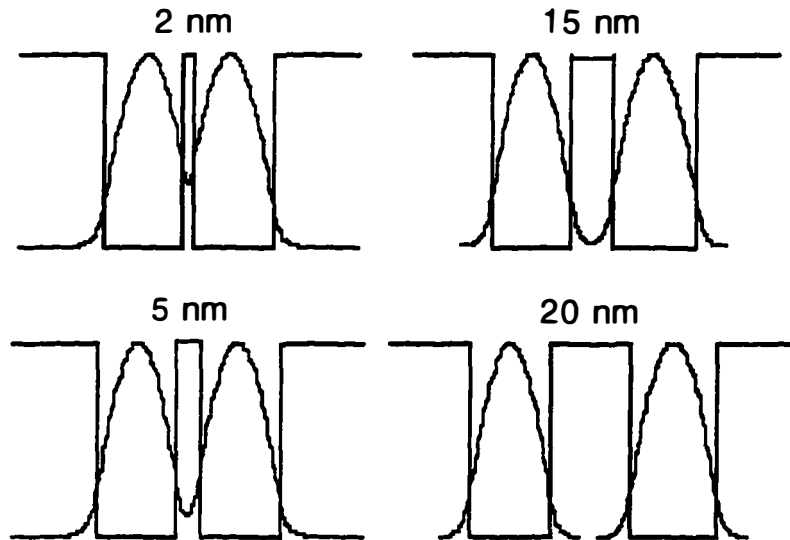
Figure 3.8 Wavefunction vs. the distance between square dots. Interdot carrier tunneling is important for dot distance less than 10 nm, if the width of dots are assumed to be 20 nm. The maximum dot density can be achieved without the carrier tunneling effect is approximately $10^{11}/cm^2$. The effect of the wetting layer transport and graded composition are ignored.

Carrier-carrier interaction among quantum dots will be important in quantum dot device where high dot density is required. Due to the small material volume, a larger number of quanutm dots are required for the fabrication of quantum dot laser (Mirin *et al.*, 1996; Bimberg *et al.*, 1996). The tunneling of carrier between dots will lead to dynamics similar to a quantum well with rough interfaces. The slow relaxation of carriers to the local energy minimum will produce a slow rise in the photoluminescence, as observed in Figure 3.3 for a 2 monolayer $In_{0.5}Ga_{0.5}As/GaAs$ quantum well. Figure 3.8 plots the wavefunction overlap as a function of the distance between dots. The effect of carrier tunneling will be important when the

barrier distance is less than 10 nm, if the width of dot are assumed to be 20 nm (Figure 1.5). To avoid significant carrier tunneling, the maximum dot density allowed is approximately $10^{11}/cm^2$.

3.9 Exciton-Exciton Scattering in Quantum Structures

Besides the tunnelling of the carriers between the adjacent dots, the carrier-carrier scattering within a single quantum dot can also affect the exciton dynamics. In a quantum well structure, the coherence among the excitons is strongly affected by the exciton-exciton interaction (Eccleston, 1991). The excitation intensity dependence of the exciton decays in a 6 nm $In_{0.17}Ga_{0.83}As/GaAs$ quantum well are shown in Figure 3.9a. Unlike the single exponential decay observed at a low pump intensity, the decay at high excitation intensity exhibits an initial slow decay. This slow decay observed at a large exciton density is the result of a reduced coherence area due to the Coulomb scattering among the excitons. This phase space filling effect can also be observed from the linear increase of the homogenous linewidth as the PL excitation intensity increases (Eccleston, 1991).

In the quantum dots, the exciton decays are a single exponential for all the excitation levels (Figure 3.9b). Unlike the quantum well case, the effect of exciton-exciton scattering is absent. The coherence area of the exciton in the quantum dot is determined solely from the area of the quantum dot rather than the exciton-exciton interaction. A similar effect is observed in the $In_{0.5}Ga_{0.5}As/GaAs$ quantum dots grown by MOCVD (Figure 3.9c) and in the $In_{0.3}Al_{0.7}As/Al_{0.3}Ga_{0.7}As$ quantum dots grown by MBE.

$6 \text{ nm } In_{0.17}Ga_{0.83}As$ Quantum Well
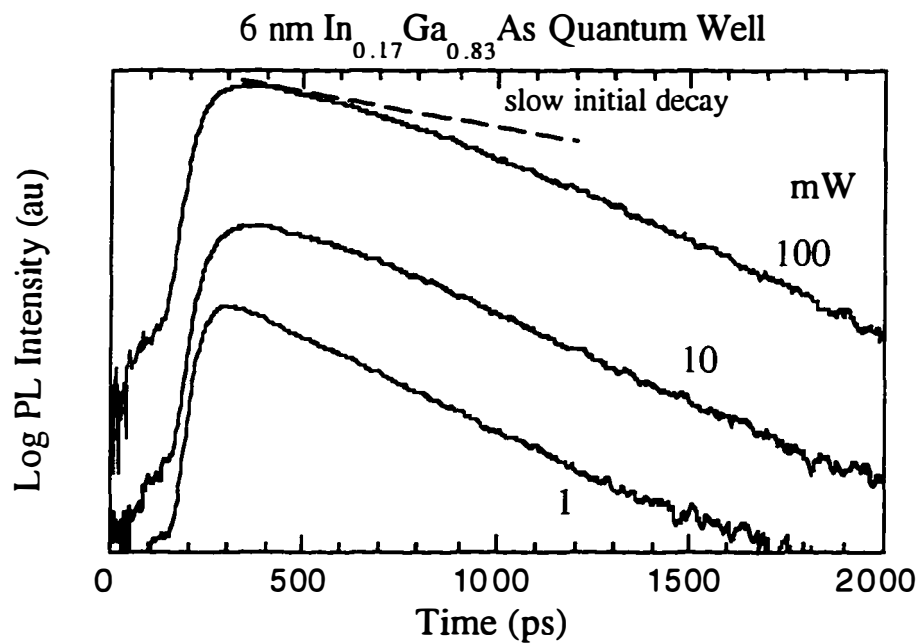
Figure 3.9a Intensity dependence of 6 nm quantum well TRPL. Slow initial decay can be observed at high pump intensity.

$In_{0.5}Ga_{0.5}As$ Quantum Dots (grown by MBE)
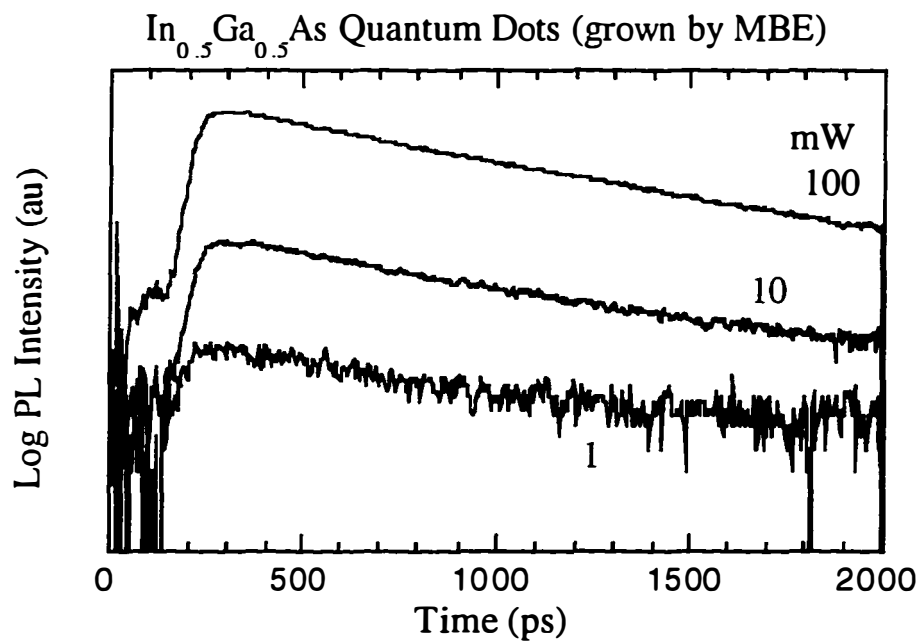
Figure 3.9b Intensity dependence of quantum dot TRPL. Single exponential decays are observed at all pump intensities.

Raymond *et al.* (1996) have measured excited state TRPL. They have observed an intensity dependent lifetimes, where the PL decay becomes slower at higher pump intensity. The difference between their measurements and the result presented here may be attributed to the effect of state filling, where the filled excited state can lead to a slow relaxation of the carrier and increase the lifetime of the ground state.

$In_{0.5}Ga_{0.5}As$ Quantum Dots (grown by MOCVD)
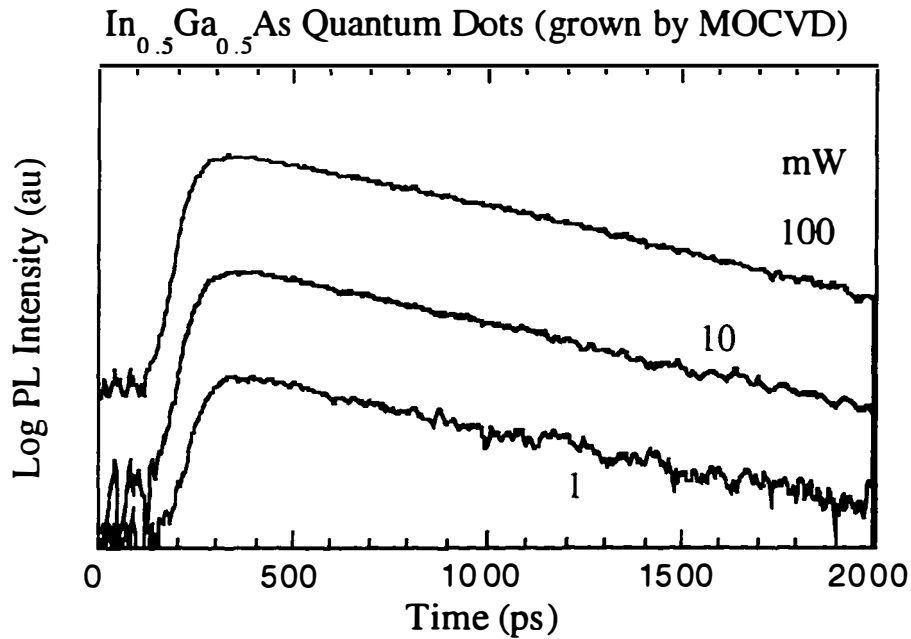
Figure 3.9c Intensity dependence TRPL of the quantum dots grown by MOCVD. The intensity dependence of the quantum dots grown by MBE and MOCVD are identical, indicating that the observed effect is an intrinsic property of the self-organized quantum dots.

3.7 Conclusions

From the TRPL of the excitons in quantum dots and quantum well, we understand that the oscillator strength of the exciton in the self-organized quantum dot is reduced due to a restricted coherence area. The reduction of the coherence area leads to an increase in the measured radiative lifetime. This increase in the radiative lifetime in the quantum dot material may have a significant effect on threshold of quantum dot laser. Since the threshold current of semiconductor laser is inversely proportional to the radiative lifetime of carriers, at least a factor of two reduction in the threshold current for quantum dot laser may be expected.

From the spectally resolved TRPL of the quantum dots, we also learned that the effect of a reduced coherence area may be countered by an enhanced wavefunction overlap. Lifetimes are reduced by a factor of two when the dots volume is reduced.

Our understandings of radiative recombination process in quantum dots can provide a unique ability to engineer special optoelectronic materials. If the physical dimension of the self-organized quantum dots can be controlled precisely during the growth, significant improvements over the performance of the today's optoeletronic devices will be achieved.

92
References

1. L. C. Andreani, F. Tassone, F. Bassani, *Solid State Communications* **77**, 9 641-645 (1991).

2. L. C. Andreani, *Physica Scripta* **T35**, Vt35 111-115 (1991).

3. L. C. Andreani, A. Dandrea, R. Delsole, *Physics Letters A* **168**, 5-6 451-459 (1992).

4. G. Bastard, *Wave Mechanics Applied to Semiconductor Heterostructures* (Les Editions de Physique, Halsted Press, Les Ulis Cedex, France-New York, N.Y, 1988).

5. J. P. Bergman, P. O. Holtz, B. Monemar, M. Sundaram, J. L. Merz, A. C. Gossard, *Physical Review B-Condensed Matter* **43**, 6 4765-4770 (1991).

6. D. Bimberg, *et al.*, *Physica Status Solidi B-Basic Research* **194**, 1 159-173 (1996).

7. U. Bockelmann, *Physical Review B-Condensed Matter* **48**, 23 17637-17640 (1993).

8. U. Bockelmann, P. Roussignol, A. Filoramo, W. Heller, G. Abstreiter, K. Brunner, G. Bohm, G. Weimann, *Physical Review Letters* **76**, 19 3622-3625 (1996).

9. F. Bogani, L. Carraresi, R. Mattolini, M. Colocci, A. Bosacchi, S. Franchi, *Nuovo Cimento Della Societa Italiana Di Fisica D-Condensed Matter Atomic Molecular And Chemical Physics Fluids Plasmas Biophysics* **17**, 11-1 1371-1375 (1995).

10. F. Bogani, L. Carraresi, R. Mattolini, M. Colocci, A. Bosacchi, S. Franchi, *Solid-State Electronics* **40**, Si 363-366 (1996).

11. O. Brandt, G. C. Larocca, A. Heberle, A. Ruiz, K. Ploog, *Physical Review B-Condensed Matter* **45**, 7 3803-3806 (1992).

12. A. Bugayev, H. Kalt, J. Kuhl, M. Rinker, *Applied Physics A-Solids and Surfaces* **53**, 1 75-80 (1991).

13. D. S. Citrin, *Solid State Communications* **84**, 3 281-284 (1992).

14. D. S. Citrin, *Physical Review B-Condensed Matter* **47**, 23 16069-16069 (1993).

15. F. Daiminger, A. F. Dite, E. Tournie, K. Ploog, A. Forchel, *Journal of Applied Physics* **76**, 1 618-620 (1994).

16. B. Deveaud, T. C. Damen, J. Shah, C. W. Tu, *Applied Physics Letters* **51**, no.11 828-30 (14 Sept. 1987).

17. B. Deveaud, J. Shah, T. C. Damen, W. T. Tsang, *Applied Physics Letters* **52**, no.22 1886-8 (30 May 1988).

18. R. Eccleston, R. Strobel, W. W. Ruhle, J. Kuhl, B. F. Feuerbacher, K. Ploog, *Physical Review B-Condensed Matter* **44**, 3 1395-1398 (1991).

19. J. Feldmann, G. Peter, E. O. Gobel, P. Dawson, K. Moore, C. Foxon, R. J. Elliott, *Physical Review Letters* **59**, no.20 2337-40 (16 Nov. 1987).

20. J. E. Fouquet, V. M. Robbins, S. J. Rosner, O. Blum, *Applied Physics Letters* **57**, no.15 1566-8 (8 Oct. 1990).

21. J. E. Fouquet, R. D. Burnham, *IEEE Journal of Quantum Electronics* **QE-22**, no.9 1799-810 (Sept. 1986).

22. E. Hanamura, *Physical Review B (Condensed Matter)* **38**, no.2 1228-34 (15 July 1988).

23. G. W. Hooft, W. A. J. A. van der Poel, L. W. Molenkamp, C. T. Foxon, *Physical Review B (Condensed Matter)* **35**, no.15 8281-4 (15 May 1987).

24. J. Hopfield, *Physical Review* **112**, 5 1555-1567 (1958).

25. C. J. Hwang, *Physical Review B (Solid State)* **8**, no.2 646-52 (15 July 1973).

26. Y. Kayanuma, *Physical Review B-Condensed Matter* **44**, 23 13085-13088 (1991).

27. B. M. Keyes, D. J. Dunlavy, R. K. Ahrenkiel, G. Shaw, G. P. Summers, N. Tzafaras, C. Lentz, *Journal of Applied Physics* **75**, 8 4249-4251 (1994).

28. M. Kohl, D. Heitmann, P. Grambow, K. Ploog, *Physical Review B (Condensed Matter)* **42**, no.5 2941-50 (15 Aug. 1990).

29. T. Kono, Y. Nagamune, M. Nishioka, Y. Arakawa, *Superlattices and Microstructures* **17**, 1 73-76 (1995).

94

30.   R. Leon, S. Fafard, D. Leonard, J. L. Merz, P. M. Petroff, *Applied Physics Letters* **67**, 4 521-523 (1995).

31.   D. Leonard, S. Fafard, K. Pond, Y. H. Zhang, J. L. Merz, P. M. Petroff, *Journal of Vacuum Science & Technology B* **12**, 4 2516-2520 (1994).

32.   D. Leonard, M. Krishnamurthy, S. Fafard, J. L. Merz, P. M. Petroff, *Journal of Vacuum Science & Technology B* **12**, 2 1063-1066 (1994).

33.   D. Leonard, K. Pond, P. M. Petroff, *Physical Review B-Condensed Matter* **50**, 16 11687-11692 (1994).

34.   D. Leonard, Ph.D. Dissertation: Self-Assembled Quantum Dots of $In_xGa_{1-x}As$ on GaAs, University of California, Santa Barbara, (1995).

35.   M. Lomascolo, M. Didio, D. Greco, L. Calcagnile, R. Cingolani, L. Vanzetti, L. Sorba, A. Franciosi, *Applied Physics Letters* **69**, 8 1145-1147 (1996).

36.   J. Martinezpastor, A. Vinattieri, L. Carraresi, M. Colocci, P. Roussignol, G. Weimann, *Physical Review B-Condensed Matter* **47**, 16 10456-10460 (1993).

37.   Y. Masumoto, S. Katayanagi, T. Mishina, *Physical Review B-Condensed Matter* **49**, 15 10782-10785 (1994).

38.   R. Mirin, A. Gossard, J. Bowers, *Electronics Letters* **32**, no.18 1732-4 (29 Aug. 1996).

39.   K. Mukai, N. Ohtsuka, H. Shoji, M. Sugawara, *Physical Review B-Condensed Matter* **54**, 8 R5243-R5246 (1996).

40.   D. V. O'Connor, D. Phillips, *Time-Correlated Single Photon Counting* (Academic Press, London-Orlando, 1984).

41.   D. Oberhauser, K. H. Pantke, J. M. Hvam, G. Weimann, C. Klingshirn, *Physical Review B-Condensed Matter* **47**, 11 6827-6830 (1993).

42.   J. Oshinowo, M. Nishioka, S. Ishida, Y. Arakawa, *Journal of Crystal Growth* **145**, 1-4 986-987 (1994).

43.   J. Oshinowo, M. Nishioka, S. Ishida, Y. Arakawa, *Japanese Journal of Applied Physics Part 2-Letters* **33**, 11b L1634-L1637 (1994).

44.   J. I. Pankove, *Optical Processes in Semiconductors* (Prentice-Hall, Englewood Cliffs, N.J. 1971).

45.   P. M. Petroff, G. Medeirosribeiro, *MRS Bulletin* **21**, 4 50-54 (1996).

46.   W. Pickin, J. P. R. David, *Applied Physics Letters* **56**, no.3 268-70 (15 Jan. 1990).

47.   M. E. Pistol, P. Castrillo, D. Hessman, S. Anand, N. Carlsson, W. Seifert, L. Samuelson, *Solid-State Electronics* **40**, Si 357-361 (1996).

48.   S. Raymond, S. Fafard S; P. J. Poole, A. Wojs, P. Hawrylak, S. Charbonneau, D. Leonard, R. Leon, P. M. Petroff, and J. L. Merz.*Physical Review B (Condensed Matter)* **54**, 16 11548-11554 (1996).

49.   S. Raymond, S. Fafard, S. Charbonneau, R. Leon, D. Leonard, P. M. Petroff, J. L. Merz, *Physical Review B-Condensed Matter* **52**, 24 17238-17242 (1995).

50.   C. M. Reaves, V. Bresslerhill, W. H. Weinberg, S. P. Denbaars, *Journal of Electronic Materials* **24**, 11 1605-1609 (1995).

51.   B. K. Ridley, *Physical Review B (Condensed Matter)* **41**, no.17 12190-6 (15 June 1990).

52.   W. W. Ruhle, A. Kurtenbach, K. Eberl, *Nuovo Cimento Della Societa Italiana Di Fisica D-Condensed Matter Atomic Molecular And Chemical Physics Fluids Plasmas Biophysics* **17**, 11-1 1305-1313 (1995).

53.   A. Schulzgen, J. Puls, F. Henneberger, V. Jungnickel, *Physica B* **185**, 1-4 571-574 (1993).

54.   J. Shah, A. Pinczuk, A. C. Gossard, W. Wiegmann, *Physica B & C* **134B+C**, no.1-3 174-8 (Nov. 1985).

55.   V. Srinivas, J. Hryniewicz, Y. J. Chen, C. Wood, *Physical Review B-Condensed Matter* **46**, 16 10193-10196 (1992).

56.   V. Srinivas, Y. J. Chen, C. Wood, *Physical Review B-Condensed Matter* **48**, 16 12300-12303 (1993).

57.   V. Srinivas, Y. J. Chen, C. Wood, *Solid State Communications* **89**, 7 611-614 (1994).

58.   C. K. Sun, G. Wang, J. E. Bowers, B. Brar, H. R. Blank, H. Kroemer, M. H. Pilkuhn, *Applied Physics Letters* **68**, 11 1543-1545 (1996).

59.   Y. Takahashi, S. Owa, S. S. Kano, K. Muraki, S. Fukatsu, Y. Shiraki, R. Ito, *Applied Physics Letters* **60**, 2 213-215 (1992).

59. I. H. Tan, Y. L. Chang, R. Mirin, E. Hu, J. Merz, T. Yasuda, Y. Segawa, *Applied Physics Letters* **62**, 12 1376-1378 (1993).

60. Y. Toda, M. Kourogi, M. Ohtsu, Y. Nagamune, Y. Arakawa, *Applied Physics Letters* **69**, 6 827-829 (1996).

61. S. L. Tyan, Y. C. Wang, C. C. Chang, J. H. Tung, M. T. Kuo, J. S. Hwang, *Chinese Journal of Physics* **33**, 6 699-706 (1995).

62. A. Vinattieri, J. Shah, T. C. Damen, D. S. Kim, L. N. Pfeiffer, M. Z. Maialle, L. J. Sham, *Physical Review B-Condensed Matter* **50**, 15 10868-10879 (1994).

63. G. Wang, S. Fafard, D. Leonard, J. E. Bowers, J. L. Merz, P. M. Petroff, *Applied Physics Letters* **64**, 21 2815-2817 (1994).

64. G. Wang, C.-K. Sun, D. Leonard, G. M. Riberio, J. E. Bowers, P. M. Petroff, J. Oshinowo, and Y. Arakawa, Postdeadline Paper, Quantum Optoelectronics Topical Meeting, Dana Point, CA, March 13-15 (1995).

65. H. Watabe, Y. Nagamune, F. Sogawa, Y. Arakawa, *Solid-State Electronics* **40**, Si 537-540 (1996).

66. C. Weisbuch, B. Vinter, *Quantum Semiconductor Structures : Fundamentals and Applications* (Academic Press, Boston, 1991).

67. H. Weman, C. I. Harris, J. P. Bergman, M. S. Miller, J. C. Yi, J. L. Merz, *Superlattices And Microstructures* **17**, 1 61-65 (1995).

68. Y. Zhang, M. D. Sturge, K. Kash, *Physical Review B-Condensed Matter* **51**, 19 13303-13314 (1995).

Chapter Four

Temperature Effects on
Radiative Recombination in Quantum Dots

4.1 Introduction

When the temperature of a semiconductor increases, the lattice expands and the oscillation of the atoms increases in frequency and amplitude. This dilation and the motion of the atoms not only leads to a change in the energy gap of the semiconductor but also enhances the scattering processes of carriers with the crystal lattice. In quantum structures, this increase of scattering between the carriers and lattice phonons can generate non-radiative decay paths and reduce the photoluminescence (PL) efficiency by removing carriers from the radiative state in the quantum structures. Consequently, this non-radiative recombination process can lead to a poor internal quantum efficiency in the potential quantum dot laser (Nagarajan, 1993; Bacher, 1991). In this chapter, the temperature effects on the radiative lifetime of exciton in the self-organized quantum dots are considered.

The effects of phonon absorption on the radiative recombination of exciton in quantum structures are separated into two regimes: $kT < \Delta E$ and $kT > \Delta E$. At low temperatures, where the thermal energy of the lattice (kT) is less than the confinement energy (ΔE), carrier-acoustic phonon scattering is dominant. Even though the acoustic phonon scattering may broaden the thermal distribution of carriers in k space, the energy change induced by the acoustic phonon scattering is

usually small compared to ΔE, which is not sufficient to remove the confined carriers from the quantum structure. Thus, the time-integrated PL efficiency is not affected by the acoustic phonon scattering process at low temperatures. However, the thermally broadened carrier distribution may lead to a decrease in k=0 exciton population and an increase in the averaged radiative lifetime (Feldmann *et al.*, 1988).

At higher temperatures, unlike the acoustic phonon scattering process, LO phonon scattering becomes important. When the thermal energy of the lattice is larger than the confinement energy, the scattering of LO phonons with carriers can efficiently excite the carriers from the quantized state in the dot to the continuum states on the barrier (Bacher *et al.*, 1993). Due to this non-radiative scattering process, a significant decrease in PL efficiency can occur.

In this chapter, the temperature effects on the radiative recombination in the self-organized quantum dots resulting from these two scattering processes are studied. The thermionic emission due to the absorption of LO phonons is found to be important at high temperatures, and the restricted carrier-acoustic phonon scattering is reflected in the constant radiative decay time at low temperatures.

The distinguishable effects of the thermionic emission process on the time-integrated PL efficiency and the time-resolved PL (TRPL) decay times are investigated separately. In Section 4.2 and 4.3, based on the thermionic emission theory, a model for the temperature dependence of PL efficiency is developed. The analysis from the PL model is compared with the experimentally measured PL lineshapes and energies at various temperatures. Excellent agreement is obtained

between the measured and the calculated PL spectra. In Section 4.4 and 4.5, the confinement energies and the carrier capture times inferred from the measured temperature dependence of PL efficiency are analyzed.

In Section 4.6, the temperature dependence of the TRPL decay times from the self-organized quantum dots is presented. In Section 4.7, the separation of the non-radiative and the radiative contributions from the measured TRPL decays indicates that a strong reduction of TRPL decay times occurs at the onset of thermionic emission process studied in the previous sections. Good agreement is obtained betweent the measured non-radiative decay times and the thermionic emission model. In Section 4.8, the dot size dependence of the thermionic emission rate is studied using temperature and spectral dependent TRPL. A larger confinement energy is found for the larger dots. Finally, Section 4.9 will focus on the effects resulted from the acoustic phonon scattering process at low temperatures. The temperature dependence of the intrinsic radiative lifetime in different quantum structures are derived and compared to the published results in the literature. For quantum dots, the intrinsic radiative lifetimes are found to be temperature independent. This is a distinct signature of 0D materials.

4.2 Temperature Dependence of Photoluminescence Model

There are two factors that contribute to the temperature variation in the photoluminescence process. The first factor is the temperature dependence of the bandgap energy in the dot and the barrier materials. Changes in the bandgap energy can lead to shifts in the PL emission energy. The temperature dependence of bandgap energy is well known and has been extensively researched (Van Vechten

and Malloy, 1990; Madelung, 1991). Figure 4.1 compares the measured and calculated PL peak energies for a 6 nm $In_{0.17}Ga_{0.83}As$/GaAs quantum well and $In_{0.5}Ga_{0.5}As$/GaAs quantum dots. The temperature dependent PL peak energy is calculated using the model identical to Section 2.4. The PL emission energies measured in both quantum structures follow closely with the temperature dependence of GaAs bandgap at low temperatures. At higher temperatures, the emission energies of the quantum dots are slightly lower than the calculated value. The lower dot PL peak energies may be attributed to the re-trapping of the thermally emitted carriers at higher temperatures.

The second factor that contributes to the temperature effects is the temperature dependence of the radiative and the non-radiative scattering processes. An increase in the non-radiative scattering rate can severely decrease the PL efficiency. Although non-radiative processes can also arise from traps, defects, and dislocations, only the thermionic emission of carriers due to the LO phonon scattering is considered here.
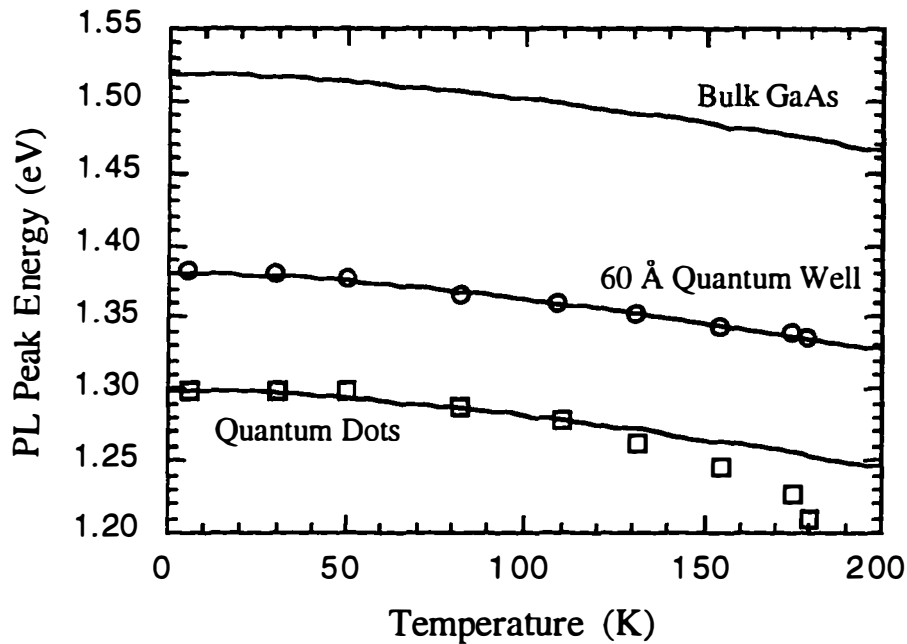
Figure 4.1 Calculated and measured PL emission peaks for a 6 nm $In_{0.17}Ga_{0.83}As$/GaAs quantum well and $In_{0.5}Ga_{0.5}As$/GaAs quantum dots. The calculation is based on the published temperature dependent bandgap of (In)GaAs. The effect of strain is included. The lower dot PL peak energies may be attributed to the re-trapping of the thermally emitted carriers at higher temperatures. Effect of strain is included in the calculation.

The microscopic principle behind the thermionic emission of carrier is closely associated to the carrier capture process. The photoluminescence efficiency of the quantum dots is determined from a balance between the capture and the thermal emission of the carriers. Both processes are the results of carrier-LO phonon scattering. In the capture process, carriers lose energy to the lattice by emitting LO phonons. While in the thermionic emission process, the opposite situation occurs. At thermal equilibrium, the relationship between the scattering times of these two processes may be estimated using a detailed balance argument

(Sze, 1981). Assuming a Maxwell-Boltzman distribution for the carriers in the quantum structure, the ratio of the capture and emission times may be expressed as

$$\frac{\tau_{emission}}{\tau_{capture}} = e^{\Delta E / kT} \qquad (4.1)$$

where $\tau_{emission}$ and $\tau_{capture}$ are the thermionic emission time from the dot to the barrier and the capture time from the barrier to the dot, respectively.

The assumption of Equation 4.1 is incorporated in the rate equation model presented in Section 1.5. The steady state solution of the photoluminescence intensity is obtained by setting the rate equations to zero. For quantum dots with an uniform size distribution, the temperature dependent PL efficiency of the ground state spectral line is

$$PL(T, E) = I_o \left(1 + \frac{\tau_{decay}}{\tau_{capture}} e^{\frac{[E_b(T) - E]}{kT}} \right)^{-1} \qquad , \qquad (4.2)$$

where $E_b(T)$ is the temperature dependence of the barrier bandgap energy. For the self-orgainzed quantum dots with a broadened Gaussian size distribution, the PL spectrum is obtained by convolving Equation 4.2 with the dot size distribution.

$$PL(T, E) = I_o e^{-4 \ln(2) \left(\frac{(E - E_o)}{\Gamma} \right)^2} \left(1 + \frac{\tau_{decay}}{\tau_{capture}} e^{\frac{(E_b - E)}{kT}} \right)^{-1} . \qquad (4.3)$$

where Γ is the full-width-at-half-max (FWHM) of the dot PL at low temperatures, and E_o is the peak energy of the dot distribution..

4.3 Effect of Thermionic Emission on Photoluminescence Spectra

The measured and the calculated (Equation 4.3) temperature dependent PL are shown in Figure 4.2. The radiative decay time of 1 ns (Chapter 3) and the capture time of 0.5 ps (Chapter 5) are used in the calculation. A good qualitative agreement is obtained between the observed spectra and the thermionic emission model. At a higher temperature, a reduction of PL efficiency is observed; however, the PL peak is shifted to a lower energy from the calculated value. Unlike bulk material where the PL intensity is reduced at higher temperature due to the activation of the non-radiative traps, the reduction of the PL efficiency in the quantum dot is attributed to the thermionic emission process. The shift of PL peak to the lower energy may be attributed to the trapping of the thermionically emitted carriers by the lower energy quantum dots. A similar observation is reported for the case of adjacent quantum wells (Bacher *et al*, 1991; Fafard *et al.,* 1995), where an enhanced efficiency is found for quantum well with a larger confinement energy. The thermal redistribution of the carriers among the quantum dots can lead to a significant effect on the optical gain. This particular effect on the quantum dot laser will be addressed in Chapter 7.
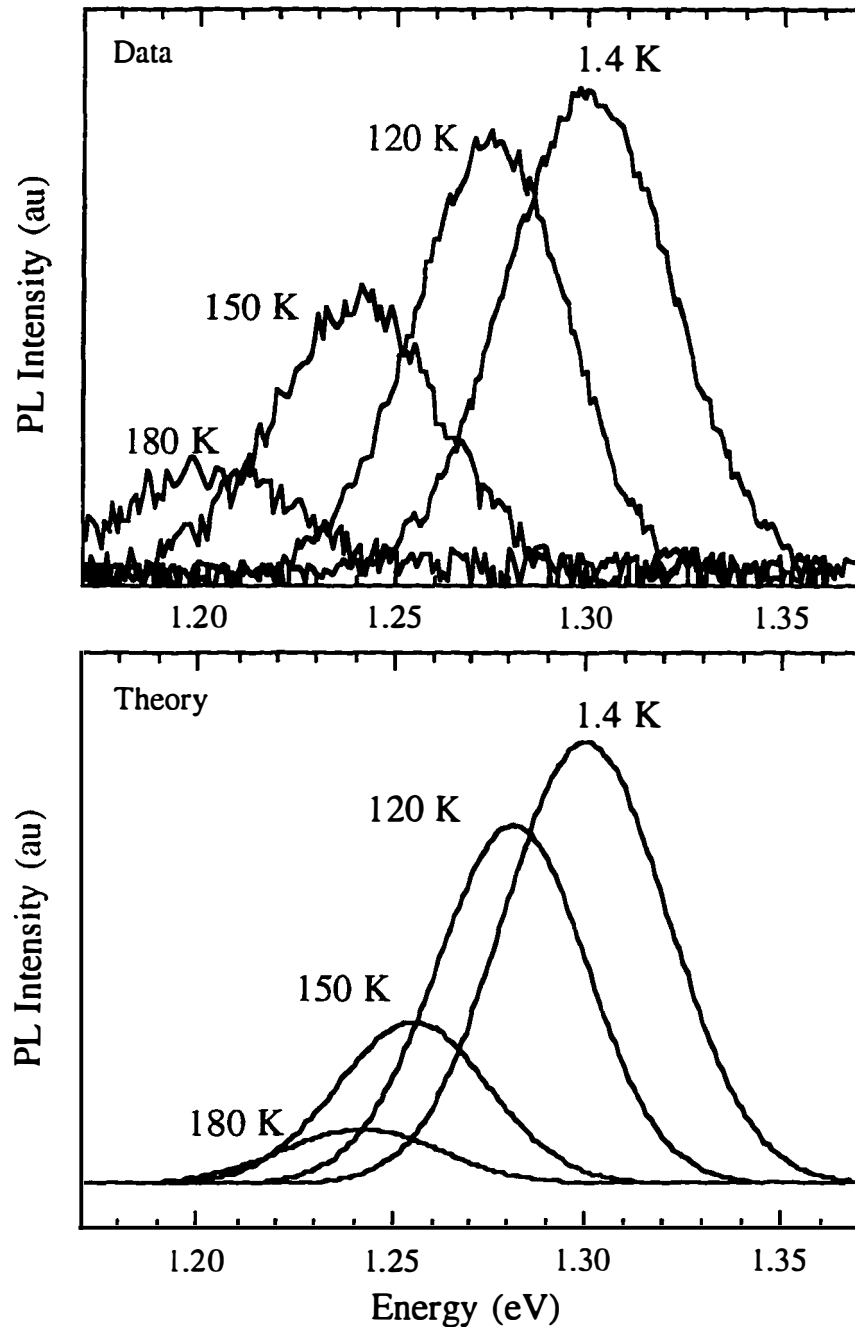
Figure 4.2 The calculated (Equation 4.3) and measured temperature dependence of PL for $In_{0.5}Ga_{0.5}As/GaAs$ quantum dots. The reduction of the PL efficiency at high temperature is attributed to the thermionic emission process. The radiative decay time of 1 ns (Chapter 3) and the capture time of 0.5 ps (Chapter 5) are used in the calculation.

4.4 Temperature Dependence of Photoluminescence Efficiency

From Equation 4.2, two parameters may be obtained from the measured temperature dependent PL efficiency. First, the characteristic confinement energy is estimated from the slope in the Arrhenius plot of PL intensity. Second, an approximate value of carrier capture time may be inferred from the ratio $\tau_{decay}/\tau_{capture}$.

Figure 4.3a shows the Arrhenius plot of the measured temperature dependent PL efficiency for various self-organized quantum dots samples. The 6 nm $In_{0.17}Ga_{0.83}As$ quantum well is included for the reference purpose. A confinement energy of 120 meV is obtained for the quantum well. This value is in close agreement with the theoretically calculated value of 140 meV (Corzine, 1993) and experimentally published results (Bacher *et al.*, 1991), suggesting that the thermionic emission of carriers is responsible for the thermal quenching of luminescence observed.

In Figure 4.3b, the measured confinement energies vs. the difference between the emission energy of the dots and the barrier materials are plotted for various self-organized quantum dots. For the InGaAs/GaAs and AlInAs/AlGaAs quantum dots with the smaller confinement energies, the measured values match closely with the expected values. For the InAs/AlAs and InAs/AlGaAs quantum dots with a larger dot to barrier energy difference, lower confinement energies are measured. This reduction of the confinement potential may be caused by the presence of wetting layer or non-radiative interface defects.
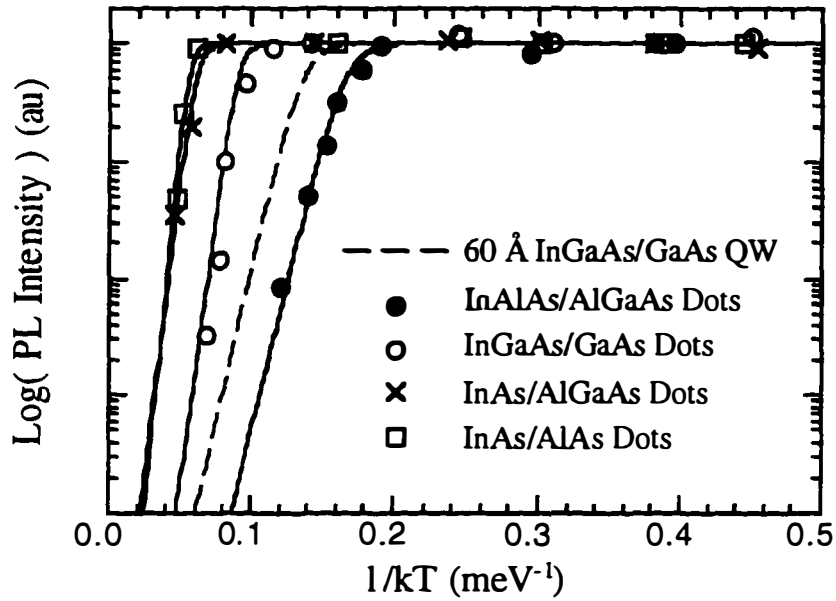
Figure 4.3a Temperature dependence of PL efficiency for various self-organized quantum dots (Fafard *et al.*, 1995).
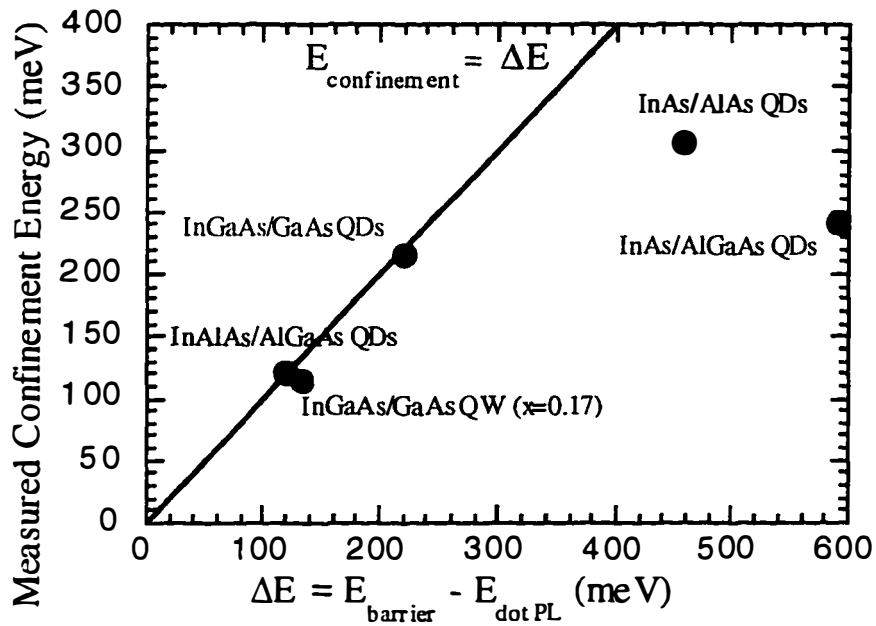

Figure 4.3b Estimated confinement energies ($\Delta E_c + \Delta E_v$) from Figure 4.2a vs. the energy difference between the barrier and the dot materials. The solid line is the expected values. The theory breaks down at large values of confinement energies.

Besides the variation of the confinement energy in the different materials, the confinement energy is also influenced by the size of the quantum dot. Figure 4.4a plots the temperature dependence of PL efficiency at several dot emission energies. Relative energies are used to adjust for the temperature dependence of bandgap energy shift. The measured PL efficiencies at various temperatures show good agreements with Equation 4.2. The extracted confinement energies vs. dot PL energies are shown in Figure 4.4b.

A confinement energy of 193 meV is obtained at the peak of the $In_{0.5}Ga_{0.5}As$/GaAs quantum dot PL. This value is in close agreement with the 220 meV obtained from the capacitance spectroscopy (Leonard, 1994; Mederiros-Riberiro *et al.*, 1995). A clear dependence of the confinement energies on the dot size is observed. A larger confinement energy is obtained at a lower PL energy, suggesting deeper confinement potentials for the larger and thicker dots within the size distribution. This observation concurs with our understanding of quantum structure, where a deeper confinement should be expected as the volume of the quantum dots increase (Bastard, 1991).
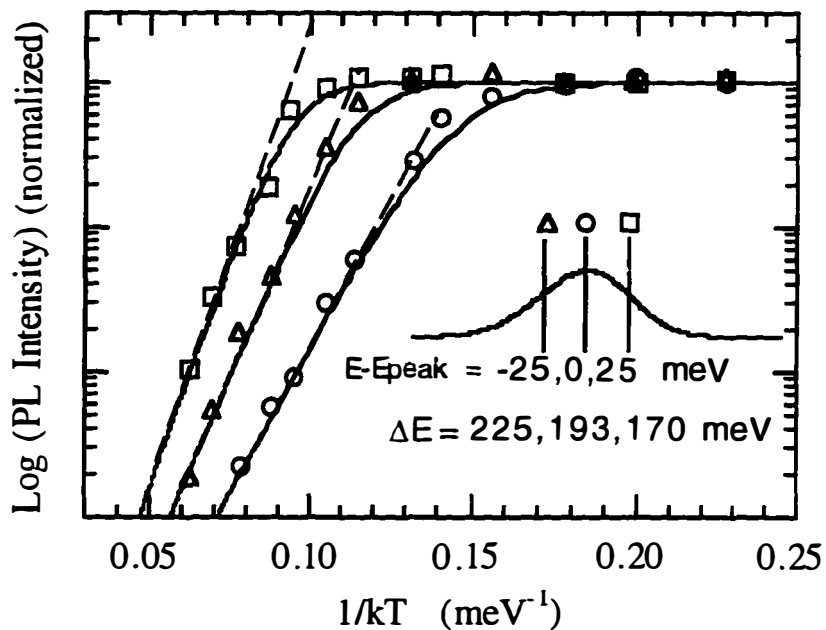
Figure 4.4a Temperature dependence of the InGaAs/GaAs quantum dot PL efficiencies at different dot emission energies.
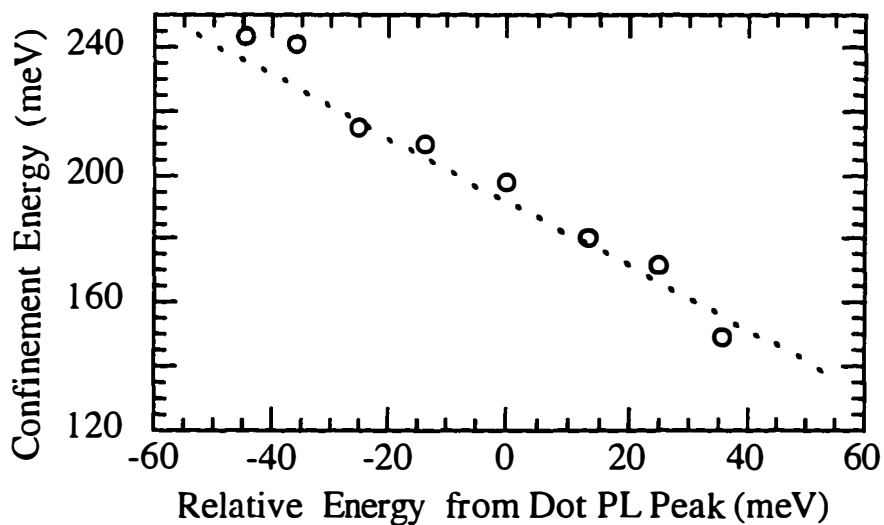

Figure 4.4b Extracted confinement energies vs dot PL energies. A deeper confinement potential is observed for the larger dots.

4.5 Estimation of Carrier Capture Time in Quantum Dots

The ratio $\tau_{decay}/\tau_{capture}$ in Equation 4.2 can be used to infer the carrier capture time in the quantum dot structure. Carrier capture times between 10 fs and 1 ps are obtained from various curve fits. Quantum dot exciton lifetimes measured in Chapter 3 are used for τ_{decay}. This result is similar to the values measured for the quantum well, despite the large difference between the two quantum structures. Blom *et al.* (1991) has found capture times as short as 0.5 ps. The rapid carrier capture time indicates an efficient relaxation of carriers exists in these quantum dots, suggesting the phonon relaxation bottleneck (Benisty *et al.*, 1991) may be negligible. By measuring the excited state TRPL, the carrier relaxation from the excited state and ground state of the dots has been studied by Raymond *et al.* (1996) and Mukai *et al.* (1996). They have found that the effect of state filling is significant. A more in-depth discussion on the energy relaxation processes in the self-organized quantum dots is presented in Chapter 5.

4.6 Temperature Dependent Photoluminescence Lifetime

In the previous sections, the results from the steady state measurements of the temperature dependent PL have provided valid evidence to support the thermionic emission theory (Equation 4.1). In the following sections, a different approach is employed. The temperature dependent TRPL is utilized to directly study the temperature effects on the radiative and the non-radiative lifetimes. The streak camera measurement described in Chapter 3 is used to measure the TRPL of the

$In_{0.5}Ga_{0.5}As/GaAs$ quantum dots at various temperatures. A heater and a temperature controller are employed to ensure the stability of the sample temperature. To avoid carrier scattering due to Auger processes, the carrier density is limited to 1.4×10^{12} cm^{-2} in all measurements.

The temperature dependent photoluminescence decay times of the self-organized quantum dots and the reference quantum well are shown in Figure 4.5.
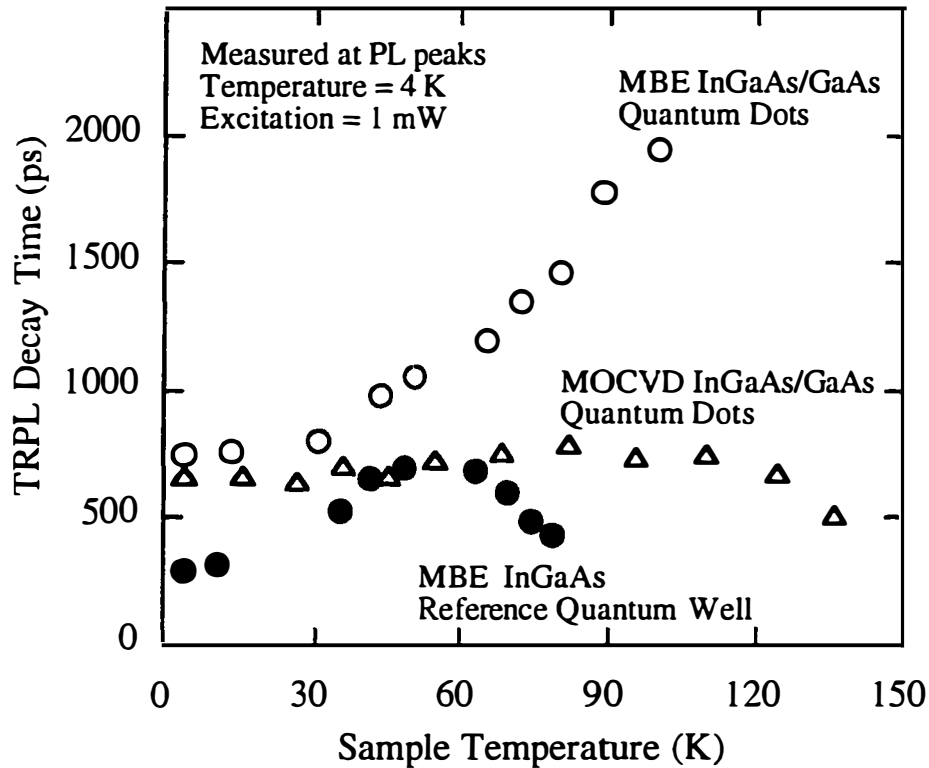

Figure 4.5 Temperature dependence of the quantum dot and quantum well carrier lifetimes. The increase of the decay times in the MBE quantum dots results from the trapping of the thermionically emitted carriers from the adjacent quantum well on the same sample. The measurements are taken at PL peaks. The spectral dependence of lifetimes are discussed in Section 3.7.

At low temperatures, the PL decay times of the 6 nm reference quantum well increase linearly with sample temperatures. This linear temperature dependence is a typical characteristic of free excitons in quantum well (Nakajima *et al.*, 1980; Gurioli, 1991). However, the similar linear dependence is not present for the quantum dot cases. At temperatures below 30 K, a constant temperature dependence is observed for the MBE InGaAs quantum dot PL decay times. A similar observation is also found in the MOCVD InGaAs dot sample for temperature as high as 100 K. This particular temperature dependence of radiative lifetime is intrinsic to the quantum dot structure, which will be clarified in Section 4.9.

At higher temperatures, where the reduction in the PL decay times are observed for both the 6 nm $In_{0.17}Ga_{0.83}As/GaAs$ quantum well and the MOCVD $In_{0.5}Ga_{0.5}As/GaAs$ quantum dots, the $In_{0.5}Ga_{0.5}As/GaAs$ MBE quantum dot sample exhibits increased decay times. This increase at higher temperatures is attributed to the re-capturing of thermionically emitted carriers from the adjacent quantum well. For the MOCVD quantum dot sample without the reference quantum well, the reduction of PL decay times is attributed to the activation of the thermionic emission process.

The temperature dependence of the thermionic emission time may be extracted from the measured TRPL decay times. In a high quality quantum dot sample where dislocations and defects are absent (Chapter 2), the non-radiative decay is attributed to the thermionic emission. From the rate equations presented in

Section 1.4, the measured PL decay rate is simply the sum of radiative decay rate and thermionic emission rate.

$$\frac{1}{\tau_{measured}(T)} = \frac{1}{\tau_{radative}(T)} + \frac{1}{\tau_{thermionic}(T)} \qquad (4.4)$$

Since the quantum efficiency $\eta(T)$ of PL is proportional to the ratio of the radiative lifetime and the measured decay time, the radiative and the non-radiative contributions in the measured decay times may be separated by measuring the temperature dependence of PL and TRPL.

$$PL(T) \propto \frac{\tau_{measured}(T)}{\tau_{radiative}(T)} = \eta(T) \qquad (4.5)$$

Combine Equation (4.4) and (4.5), the temperature dependence of the radiative lifetime and the thermionic emission time are obtained,

$$\tau_{radiative}(T) = \frac{\tau_{measured}(T)}{\eta(T)}$$

$$\tau_{thermionic}(T) = \frac{\tau_{measured}(T)}{1 - \eta(T)} \qquad (4.6)$$

Following Equation (4.6), Figure 4.6a and 4.6b show the temperature dependence of the radiative and the non-radiative decay rates for the 6 nm $In_{0.17}Ga_{0.83}As/GaAs$ quantum well and the $In_{0.5}Ga_{0.5}As/GaAs$ quantum dot samples.
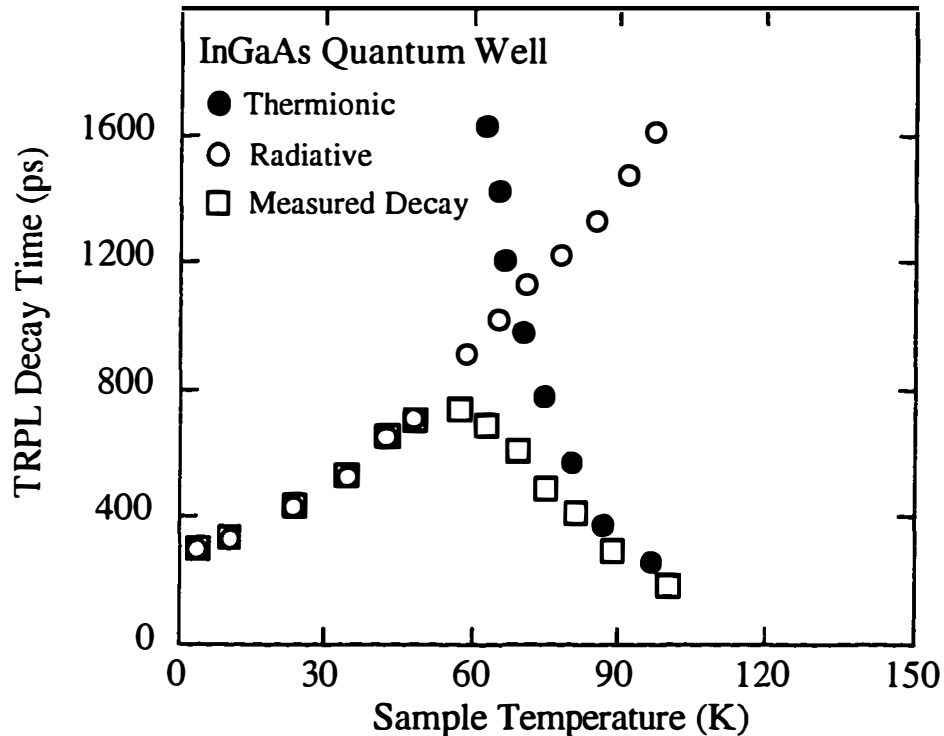
Figure 4.6a Separation of the radiative and the thermionic contribution of the recombination for the 6 nm $In_{0.17}Ga_{0.83}As/GaAs$ quantum well. The measurements are taken at PL peaks. By comparing the temperature dependent non-radiative decay time with the thermionic emission theory (Figure 4.7), a confinement barrier of 120 meV is obtained. This result is in close agreement with the band offset calculated by Corzine (1994) and measured by Bacher *et al.* (1991), indicating the reduction of PL decay time is mainly attributed to the thermionic emission process rather than defect related non-radiative recombination.

4.7 Temperature Dependence of the Thermionic Emission Process

From the comparison with the temperature dependence of PL intensity as shown in Figure 4.4a, the non-radiative recombination in Figure 4.6 a and b are found to be dominant at temperatures where an efficient thermal emission into the barrier is observed. Figure 4.7 compares the extracted non-radiative lifetimes with

Equation 4.1, using the values of confinement energies obtained from Figure 4.3

and 4.4.
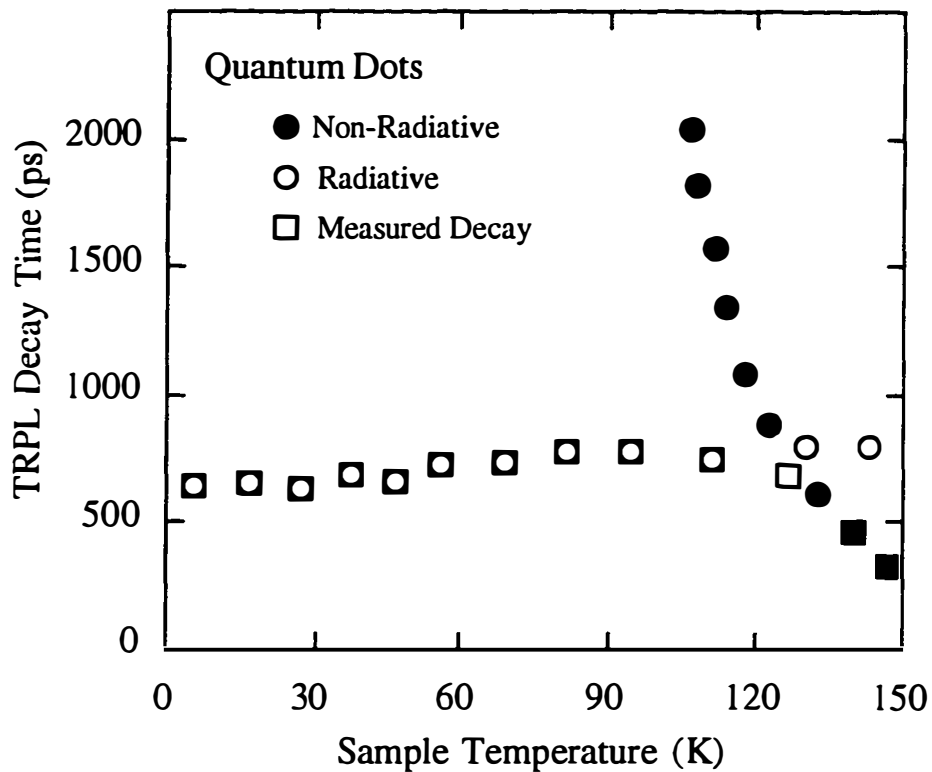
Figure 4.6b Separation of the radiative and the non-radiative
contribution of the recombination for the MOCVD grown
InGaAs/GaAs quantum dots. The measurements are taken at PL
peaks.

In both the quantum well and the quantum dot cases, the measured values

from TRPL are slightly less than the result obtained from the temperature dependent

PL efficiency. There are several possible explanations can attribute to this

discrepancy. Non-radiative recombination processes other than the thermionic

emission may exist in the material. The presence of other non-radiative

recombination processes can effectively lower the confinement potential, removing carriers from the quantum dots before the activation of the thermionic emission process. Furthermore, the reduction of confinement potential due to the non-radiative recombination may be masked by the continuous-wave PL measurements. Under a steady state excitation, the non-radiative traps and centers may be saturated.

The small disagreement between the two values can also be attributed to the measurement technique. The capturing of the thermionically emitted carriers by the lower energy quantum dots can effectively shift the PL peak energy and increase the carrier lifetime. Additionally, the published theoretical analysis has shown that a thermionic emission theory similar to Equation 4.1 can break down in the quantum limit. The reduction of carrier-LO phonon scattering can increase the carrier escape time for quantum well with dimension less than 5 nm (Tsai *et al.*, 1994).
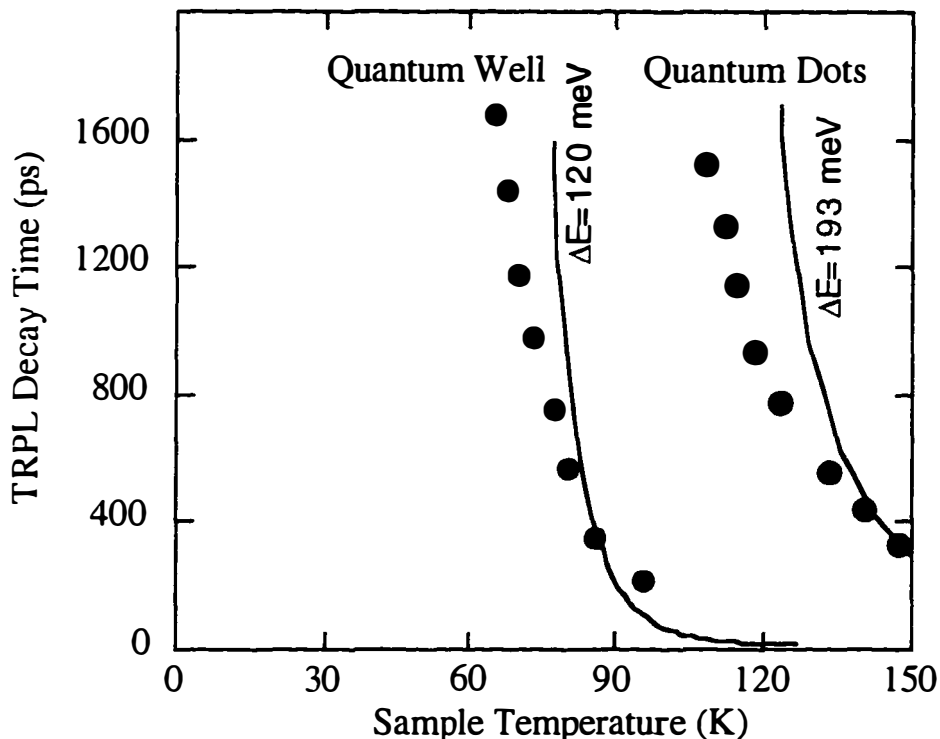
Figure 4.7 Measured non-radiative lifetimes at various temperatures (solid dots). Solid lines are the results obtained from the temperature dependent PL efficiency (Figure 4.3 and 4.4). A good agreement is obtained between the two separated measurements. The quantum dots are grown by MOCVD.

4.8 Dot Size Dependence of Thermionic Emission Rate

Since the broad linewidth of the quantum dot luminescence reflects the non-uniform size distribution, a correlated variation should also be observed in the confinement energy and the associated thermionic emission rate. Figure 4.8a plots the spectral dependence of the measured lifetimes for the $In_{0.5}Ga_{0.5}As/GaAs$ quantum dots at 1.4 K and 100 K.

Since the measured PL efficiency is constant at low temperatures (Figure 2.8b), the measured decay time at 1.4 K may be assigned to the radiative lifetime,

and the thermionic emission lifetimes at 100 K are obtained using Equation 4.4.

The radiative lifetime at 100 K is approximated by the low temperature value

(Section 4.9). Figure 4.8b shows the extracted thermionic emission times for dots

with different emission energies. A clear spectral dependence on the dot size is

observed. A longer thermionic emission time is observed for dots with a lower PL

energy, inferring a greater confinement potential for the larger and thicker dots

within the size distribution. This observation concurs with the conclusions in

Section 4.4. A similar spectral behavior is also observed from the

$Al_{0.3}In_{0.7}As/Al_{0.3}Ga_{0.7}As$ quantum dot sample.
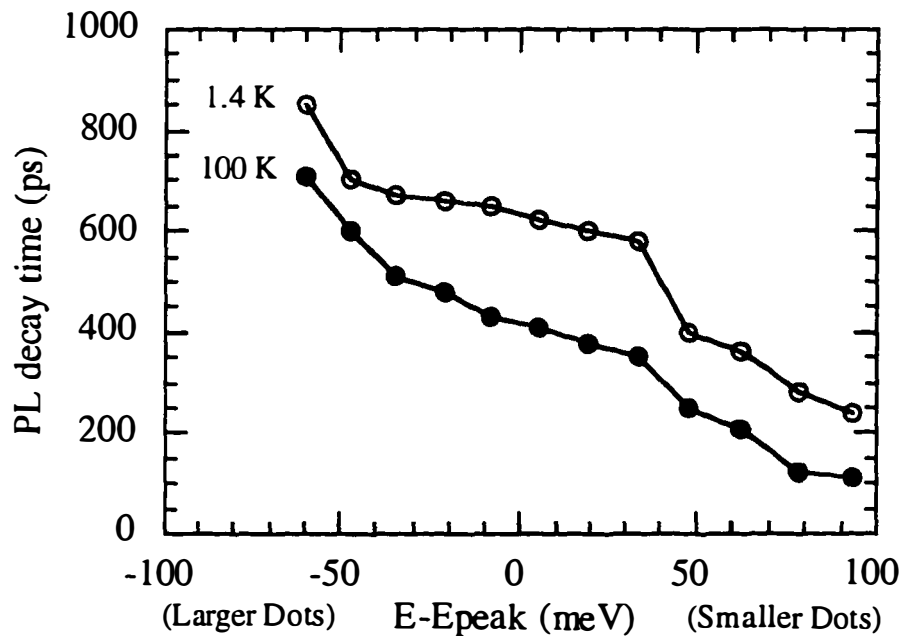
Figure 4.8a Spectral dependence of the measured lifetimes for the
$In_{0.5}Ga_{0.5}As/GaAs$ quantum dots at 1.4 K and 100 K. The increased
PL lifetime at lower energy does not result from the effect of carrier
diffusion (Section 3.7 and 3.)

$$\frac{1}{\tau_{em}} = \frac{1}{\tau_{1.4K}} - \frac{1}{\tau_{100K}}$$
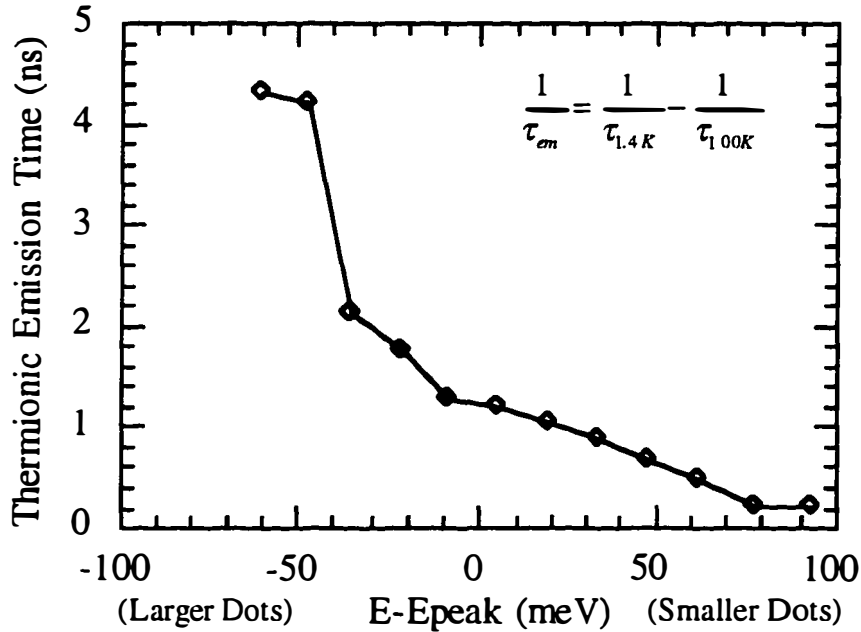
Figure 4.8b The extracted thermionic emission times for dots with different emission energies. The radiative lifetime at 100 K is approximated by the low temperature value (Section 4.9). A longer thermionic emission time is observed for dots with a lower PL energy, inferring a greater confinement potential for the larger and thicker dots within the size distribution

4.9 Temperature Dependence of the Radiative Lifetime

In Figure 4.6, the temperature dependence of the PL decays for the quantum dots is distinctly different from the quantum well case at low temperatures. The exciton lifetimes of the quantum wells exhibit a linear temperature dependence, while a flat temperature dependence for the quantum dots is observed. This variation in the temperature dependence is a fundamental difference between the 2D and 0D quantum structures.

In the quantum well case, the linear temperature dependence is explained in the frame of exciton-acoustic phonon scattering. For a free exciton in the quantum well, Feldmann *et al.* (1988) and Bockelmann *et al.* (1992, 1993) have shown that

the radiative lifetime of exciton is inversely proportional to the exciton population at k=0, where the electron-hole pair has zero center-of-the-mass momentum. At finite temperatures, the enhanced acoustic phonon scattering will produce an increased thermal broadening of the free exciton distribution in the momentum space and a reduced exciton population at k=0. Since the emitted photons can not carry away any excess exciton momentum due to momentum conservation, only excitons with center-of-mass wavevector less than the photon wavevector are allowed to recombine radiatively. Therefore, the experimentally observed radiative lifetime is essentially an averaged lifetime over the thermally broadened exciton distribution. The thermally averaged decay time can be expressed by

$$\tau(T) = \tau_o \times r(T)^{-1}. \tag{4.4}$$

where $r(T)$ is the fraction of the excitons within the radiative states, and τ_o is the intrinsic radiative lifetime of the k=0 exciton. The intrinsic radiative lifetime is independent of temperature. Its value is determined by the oscillator strength of the material, the overlap of electron and hole wavefunctions, and the coherence area of the exciton (Chapter 3). Assuming a Maxwell-Boltzmann carrier distribution, $r(T)$ can be expressed as (Feldmann $et\ al.$ 1988)

$$r(T) = \frac{\int_o^\Delta \rho(E)e^{-E/kT}dE}{\int_o^\infty \rho(E)e^{-E/kT}dE}, \tag{4.5}$$

where Δ is the maximum energy which the exciton can decay radiatively, and $\rho(E)$ is the exciton density of states in the quantum structure. For $kT < \Delta$, $r(T)$ is unity,

Quantum Structure	Density of States, $\rho(E)$	Radiative Lifetime $kT > \Delta$	Experimental Evidence
Bulk	$\dfrac{1}{2\pi^2}\left(\dfrac{2m_r}{h^2}\right)^{3/2}\sqrt{E}$	$3\sqrt{\pi}\left(\dfrac{kT}{\Delta}\right)^{3/2}\tau_{o,3D}$	Hooft *et al.*, 1987 Keyes *et al.*, 1994
Well	$\dfrac{m_r}{\pi h^2}$	$\dfrac{kT}{\Delta}\tau_{o,2D}$	Gurioli *et al.*, 1991 Bacher *et al.*, 1993
Wire	$\dfrac{\sqrt{2m_r}}{\pi h}\dfrac{1}{\sqrt{E}}$	$\sqrt{\dfrac{\pi kT}{4\Delta}}\tau_{o,1D}$	Akiyama *et al.*, 1994 Kono *et al.*, 1995
Dot	$\delta(E)$	$\tau_{o,0D}$	Wang *et al.*, 1994 Zhang *et al.*, 1995

Table 4.2 Temperature dependence of radiative lifetimes for 3D, 2D, 1D and 0D structures. Analytical expressions are obtained for $kT > \Delta$. Radiative lifetime is given by the intrinsic radiative lifetime $\tau_{o,nD}$ for $kT < \Delta$.

and the radiative lifetime is simply τ_o. For the case $kT > \Delta$, the analytical expressions for the temperature dependent radiative lifetimes are obtained. Table 4.2 summarizes the temperature dependence of radiative lifetime for bulk (3D), quantum well (2D), quantum wire (1D), and quantum dot (0D) structures. The derived temperature dependence of radiative lifetime follows $(T)^{n/2}$, where n is the dimensionality of quantum structure. This derivation agrees well with the observed carrier lifetime in the $In_{0.17}Ga_{0.83}As/GaAs$ quantum well and the $In_{0.5}Ga_{0.5}As/GaAs$

quantum dots. For the localized excitons in the quantum dots, thermal broadening has little effect on the exciton distribution in the k space. The radiative lifetime of excitons should exhibit a constant temperature dependence, as our observation indicates.

4.10 Summary

The temperature effects on the radiative recombination in the quantum dots are studied. Various self-organized quantum dot samples are compared. Thermionic emission is found to be responsible for the thermal quenching of PL intensity at high temperatures. From the thermionic emission theory, the confinement energies for the self-organized quantum dots are obtained from the temperature dependent PL and TRPL measurements. The measured confinement energies agree with the results from the capacitance spectroscopy (Leonard, 1995).

The intrinsic radiative lifetime in the quantum dot material is found to be independent of temperature. This is a desirable characteristic for potential optoelectronic applications. However, to extend this advantage to higher temperatures, a larger confinement energy is required to reduce the effect of the thermionic emission.

The confinement energy in the quantum dot material presents an interesting design problem. On one hand, quantum dots need to be sufficiently small to allow observation of the desired delta function density of states. On the other hand, the confinement potential from the quantized energy state to the barrier needs to be large enough to attain a better radiative efficiency. Careful engineering considerations in this area are needed to achieve efficient quantum dot lasers.

122
References

1. H. Akiyama, H. Sakaki, *Materials Science And Engineering B-Solid State Materials For Advanced Technology*, **35** 1-3:284-287 (1995).

2. P. A. Andrekson, R. F. Kazarinov, N. A. Olsson, T. Tanbunek, R. A. Logan, *IEEE Journal of Quantum Electronics* **30**, 2 219-221 (1994).

3. G. Bacher, H. Schweizer, J. Kovac, A. Forchel, H. Nickel, W. Schlapp, R. Losch, *Physical Review B-Condensed Matter* **43**, 11 9312-9315 (1991).

4. G. Bacher, C. Hartmann, H. Schweizer, T. Held, G. Mahler, H. Nickel, *Physical Review B-Condensed Matter* **47**, 15 9545-9555 (1993).

5. G. Bastard, *Wave Mechanics Applied to Semiconductor Heterostructures* (Halsted Press, New York, 1988).

6. H. Benisty, C. M. Sotomayor-Torres, C. Weisbuch, *Physical Review B (Condensed Matter)* **44**, no.19 10945-8 (15 Nov. 1991).

7. U. Bockelmann, *Physical Review B-Condensed Matter* **48**, 23 17637-17640 (1993).

8. U. Bockelmann, K. Brunner, G. Abstreiter, *Solid-State Electronics* **37**, 4-6 1109-1112 (1994).

9. S. W. Corzine, Ph.D. Dissertation: Design of Vertical-Cavity Surface-Emitting Lasers with Strained and Unstrained Quantum Well Active Regions, University of California, Santa Barbara, (1993).

10. S. Ehret, H. Schneider, E. C. Larkins, J. D. Ralston, *Journal of Applied Physics* **77**, 6 2537-2543 (1995).

11. S. Fafard, S. Raymond, G. Wang, R. Leon, D. Leonard, S. Charbonneau, J. L. Merz, P. M. Petroff, J. E. Bowers, *Surface Science* **362**, 1-3 778-782 (1996).

12. J. Feldmann, G. Peter, E. O. Gobel, P. Dawson, K. Moore, C. Foxon, R. J. Elliott, *Physical Review Letters* **59**, no.20 2337-40 (16 Nov. 1987).

13. M. Gurioli, A. Vinattieri, M. Colocci, C. Deparis, J. Massies, G. Neu, A. Bosacchi, S. Franchi, *Physical Review B-Condensed Matter* **44**, 7 3115-3124 (1991).

14. G. W. Hooft, W. A. J. A. van der Poel, L. W. Molenkamp, C. T. Foxon, *Physical Review B (Condensed Matter)* **35**, no.15 8281-4 (15 May 1987).

15. G. Karunasiri, *Journal of Applied Physics* **79**, 10 8121-8123 (1996).

16. B. M. Keyes, D. J. Dunlavy, R. K. Ahrenkiel, G. Shaw, G. P. Summers, N. Tzafaras, C. Lentz, *Journal of Applied Physics* **75**, 8 4249-4251 (1994).

17. T. Kono, Y. Nagamune, M. Nishioka, Y. Arakawa, *Superlattices and Microstructures* **17**, 1 73-76 (1995).

18. J. D. Lambkin, D. J. Dunstan, K. P. Homewood, L. K. Howard, M. T. Emeny, *Applied Physics Letters* **57**, 19 1986-1988 (1990).

19. J. Lee, E. S. Koteles, M. O. Vassell, *Physical Review B (Condensed Matter)* **33**, no.8 5512-16 (15 April 1986).

20. D. B. Leonard, Ph.D. Dissertation: Self-Assembled Quantum Dots of $In_xGa_{1-x}As$ on GaAs, University of California, Santa Barbara, (1995).

21. O. Madelung, *Semiconductors. Group IV Elements and III-V Compounds* (Springer-Verlag, Berlin-New York, 1991).

22. J. Martinez-Pastor, A. Vinattieri, L. Carraresi, M. Colocci, P. Roussignol, G. Weimann, *Physical Review B-Condensed Matter* **47**, 16 10456-10460 (1993).

23. G. Medeiros-Ribeiro, D. Leonard, P. M. Petroff, *Applied Physics Letters* **66**, 14 1767-1769 (1995).

24. P. Michler, A. Hangleiter, A. Moritz, V. Harle, F. Scholz, *Physical Review B-Condensed Matter* **47**, 3 1671-1674 (1993).

25. S. Nakajima, Y. Toyozawa, R. Abe, *The Physics of Elementary Excitations* (Springer-Verlag, Berlin-New York, 1980).

26. G. Salardi, B. Pellegrini, T. Di Leo, *Solid-State Electronics* **22**, no.4 435-41 (April 1979).

27. H. Schneider, K. von Klitzing, *Physical Review B (Condensed Matter)* **38**, no.9 6160-5 (15 Sept. 1988).

28. S. M. Sze, *Physics of Semiconductor Devices 2nd Edition* (John Wiley & Sons, Inc., New York, 1981).

124

29. C. Y. Tsai, L. F. Eastman, Y. H. Lo, C. Y. Tsai, *Applied Physics Letters* **65**, 4 469-471 (1994).

30. J. A. Van Vechten, K. J. Malloy, *Journal of Physics-Condensed Matter* **2**, 2 281-293 (1990).

31. M. Vening, D. J. Dunstan, K. P. Homewood, *Physical Review B-Condensed Matter* **48**, 4 2412-2417 (1993).

32. P. Viktorovitch, G. Kamarinos, *Solid-State Electronics* **19**, no.12 1041-2 (Dec. 1976).

33. G. Wang, S. Fafard, D. Leonard, J. E. Bowers, J. L. Merz, P. M. Petroff, *Applied Physics Letters* **64**, 21 2815-2817 (1994).

34. Y. Zhang, M. D. Sturge, K. Kash, *Physical Review B-Condensed Matter* **51**, 19 13303-13314 (1995).

Chapter Five

Carrier Capture and Relaxation Processes in Quantum Dots

5.1 Introduction

For a quantum structure to emit light efficiently, a fast relaxation of electrons and holes must occur. The transport of the carriers from the continuum states in the barrier into the ground state can govern the intrinsic modulation bandwidth of quantum optoelectronic devices (Nagarajan *et al.*; 1992; J. Wang *et al.*, 1996). Evidence of finite carrier relaxation time has been observed in quantum well lasers and amplifiers (Hultgren *et al.*, 1992; Hall *et al.*, 1992). For quantum well lasers, the relaxation broadening of gain spectra can reduce the peak gain and smear the desirable sharp density of states at the band edge (Asada, 1989). Dynamical effects such as spectral hole burning and carrier heating due to finite carrier relaxation time are the probable causes of the gain compression effect in the semiconductor quantum well lasers (Defonzo and Gomatam, 1990; Uskov *et al.*, 1990; Willatzen, 1991).

The objective of this chapter is to investigate experimentally the carrier capture and relaxation processes in the self-organized quantum dots. The general principles of the energy relaxation processes in semiconductors are introduced in Section 5.2, 5.3, and 5.4. The theory of the phonon-relaxation bottleneck (Benisty *et al.* 1991) is explained in Section 5.3. The measurement setup and samples are described in Section 5.5 and 5.6. Section 5.7 will focus on the effect of the two-

photon absorption process in the barrier material that is surrounding the quantum dot. The low temperature absorption transients are analyzed in Section 5.8 and 5.9. A fast carrier capture and relaxation time is observed. In Section 5.10, our result is compared to the published theoretical values. The conclusion from our study indicate that the effect of phonon-relaxation bottleneck is not significant in the self-organized quantum dots, suggesting that other carrier relaxation mechanisms are important.

5.2 Energy Relaxation Processes in Semiconductor

Two types of scattering processes are important in semiconductors: carrier-carrier scattering and carrier-phonon scattering. Carrier-carrier scattering is derived from the Coulomb interaction. Although carriers can exchange energy and momentum among themselves, the average energy of the entire carrier distribution is constant due to the energy conserving nature of the elastic scattering process. The relaxation of one carrier requires the excitation of another carrier to a higher energy state. This ineffective energy relaxation process is also limited between carriers with small momentum difference since the scattering cross section of the Coulomb potential is proportional to $1/\Delta k^2$ (Goodnick, 1988). Consequently, the energy exchanged between the carriers is relatively small compared to the average energy of the entire carrier distribution.

The energy relaxation process in semiconductors occurs primarily through carrier-phonon scattering. Unlike the energy conserving nature of carrier-carrier interaction, carrier-phonon scattering processes are dissipative. The entire carrier

distribution can relax by transferring the excess energy to the surrounding crystal lattice. Carriers at a higher energy can relax by emitting either acoustic or optical phonons. A phonon is a mode of vibration in the crystal lattice. An acoustic phonon is associated with the low frequency vibration in the lattice. Since the acoustic phonon energy is proportional to the magnitude of the wavevector, the emission of an acoustic phonon by the carrier can only correspond to a small energy change. For the efficient carrier relaxation, a large number of the acoustic phonon scattering events must be required.

An efficient carrier relaxation can occur by the emission of polar optical phonons. An optical phonon is associated with the larger energy and the higher frequency vibration mode of the crystal lattice. Its phonon energy is independent of the wavevector. In GaAs materials, carriers can relax 36 meV by the emission of a single polar longitudinal optical (LO) phonon. Due to the large LO phonon energy, fewer scattering events are required in the carrier relaxation process.

In reality, all three scattering events can occur simultaneously in semiconductor. Their scattering rate is determined not only by the scattering cross section of the physical processes but also the number of the final states that are available.

5.3 Energy Relaxation in Bulk and Quantum Well

For an efficient carrier relaxation to occur, empty states must exist at one LO phonon energy away from the initial state. This condition is easily satisfied in bulk and quantum well materials (Figure 5.1a), where the density of states vary continuously between the barrier states and the ground state (Figure 1.1). Fast

relaxation rates of carriers are usually observed in bulk and quantum well materials. Alexandrou *et al.* (1995) has found that electrons thermalize in bulk GaAs within 200 fs. For GaAs/AlGaAs quantum well material, similar observations have been reported by Knox *et al.* (1986). The fast energy relaxation time in these materials is attributed to the efficient LO phonon emission process. Singh *et al.* (1989) and Hess *et al.* (1988) have compared the calculated acoustic phonon and optical phonon scattering rates. They have reported that the acoustic scattering rate is typically an order of magnitude smaller than the LO phonon scattering rate in bulk GaAs crystals.

5.4 Energy Relaxation in Quantum Dots

Unlike energy relaxation in quantum well and bulk materials, the situation is vastly different in quantum dots. Because of the delta function density of states, the distribution of the energy levels is discrete in the quantum dots. In order for the carrier at a higher energy level to emit a LO phonon, the energy level spacing must differ by one phonon energy (Figure 5.1b), a condition that does not naturally occur in quantum dots. Mis-matched energy levels will lead to a significant reduction in the carrier-LO phonon scattering rate. Under the assumption that carrier-phonon scattering is the dominant energy relaxation process, a large increase in the carrier relaxation time may be expected in quantum dot material when compared to quantum well material. Sub-picosecond carrier relaxation time has been reported for quantum well material by Knox *et al.* (1985). The theoretical prediction of carrier relaxation time in quantum dot materials can be as slow as several nanoseconds (Bocklemann *et al.,* 1992). The resulting poor

photoluminescence efficiency is predicted by the theory of phonon-relaxation
bottleneck (Benisty *et al.*, 1991; Bocklemann *et al.*, 1992). Benisty *et al.* have
shown that the PL efficiency in the quantum dot material can be reduced by three
orders of magnitude when compared to quantum well.

In spite of the predictions of the phonon-relaxation bottleneck, the efficient
photoluminescence from the self-organized quantum dots exhibits a clear
contradiction. Many theoretical studies have attempted to explain the efficient carrier
relaxation observed in these quantum dot structures. Efros *et al.* (1995) have
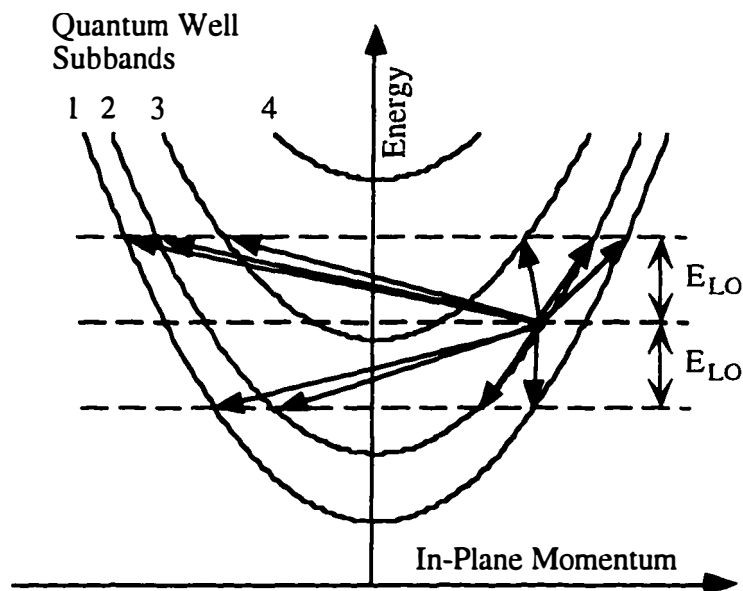
Figure 5.1a Optical phonon scattering processes in quantum well.
Final states for the scattering processes always available. Only 2-
particle scattering process is considered here. Manybody
renormalization from Coulomb interation between electron and hole
may effectively modify the above picture by sharing part of phonon
energy to the electron and the hole (Efros *et al.*, 1995).

Fast   Slow
Relaxation   Relaxation

Quantum Dot   2 $-\!\!\!\!-\!\!\!\!-$ 2 $-\!\!\!\!-\!\!\!\!-$
Energy Levels E_{LO} E_{LO}
                 1 $-\!\!\!\!-\!\!\!\!-$

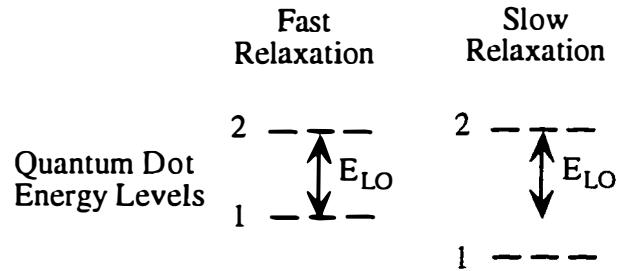   1 $-\!\!\!-\!\!\!-$

Figure 5.1b Optical phonon scattering process in quantum dots. Efficient carrier relaxation occurs only if the energy spacing is equal to multiples of LO phonon energy.

recently suggested that the effect of the phonon-bottleneck may be removed due to the role of Auger-like processes. Bockelman and Egeler (1992) have also found that efficient carrier capturing processes may occur through Auger related scattering process for quantum dots with the lateral dimension less than 40 nm. Sercel (1995) has suggested that multiple phonons assisted tunneling through deep levels may be responsible for the efficient photoluminescence observed in the InGaAs quantum dots. Recently, Knipp *et al.* (1996) has proposed that the efficient scattering of electrons from acoustic phonons can occur via a "ripple mechanism", where the relaxation of the carrier takes place when the wavefunction is perturbed due to the acoustic phonon induced movement in the dot interface. They have found that the scattering due to the ripple mechanism dominates from the deformation potential for dot sizes less than 50 nm.

These theoretical studies have proposed many open questions regarding the energy relaxation processes in quantum dots. Using resonance excitation experiments under steady state conditions, Heitz *et al.* (1996) and Schmidt *et al.*

(1996) have provided evidence that carrier relaxation is governed by the multiple phonon scattering processes. The scattering of LO phonons due to the extended wavefunctions in the quantum dot structure and the broadening of acoustic phonons can lead to a fast carrier capture and an efficient exciton relaxation. However, the direct measurements of these fast relaxation processes have been lacking. Past time-resolved investigations have only considered the radiative decay rates in the quantum dots. Carrier relaxation times are indirectly inferred from the lifetime measurements of the excited state TRPL (Mukai *et al.*, 1996; Raymond *et al.*, 1995). It is the objective of this chapter to study experimentally the sub-picosecond carrier relaxation processes in the self-organized quantum dots.

5.5 Experimental Considerations

To achieve the sub-picosecond time resolution necessary for the observation of the fast carrier relaxation, a measurement technique other than the streak camera must be employed. As the result of the availability of femtosecond laser pulses, femtosecond spectroscopy techniques are developed where the time resolution as low as 100 fs is obtained. There are two complementary techniques available to study the ultrafast dynamics in the quantum dots. The sum frequency up-conversion experiment (Shah, 1988 and 1996) is used to time-resolve the photoluminescence dynamics, and the pump-and-probe experiment (Knox, 1988) is used to study the absorption dynamics.

The up-conversion technique utilizes the nonlinearity induced by the laser pulse as a gate for the luminescence. Using a nonlinear crystal, the photoluminescence decay is mixed with a time delayed laser pulse to generate the

sum frequency signal. Because the mixing process only takes place during the presence of the laser pulse, time resolution comparable to the laser pulse width is achieved, provided the phase matching conditions in the non-linear crystal are satisfied. However, the success of using this technique to time-resolve the quantum dot photoluminescence dynamics has been limited. Due to the low conversion efficiency of the nonlinear process (<1%), an extremely bright PL signal is required. A single layer of InGaAs quantum dots may have an integrated PL comparable to the quantum well, but the spectrally separated dot PL intensity is still too weak to generate an efficient sum frequency signal above the noise level of photomutiplier tube. Similar measurements in quantum well structures usually employ 10 or more identical quantum wells. A multiple layer quantum dot sample with a bright PL comparable to the multiple quantum well samples are required.

Instead of focusing on the dynamics of photoluminescence, pump-and-probe spectroscopy is used to study the ultrafast absorption dynamics in the quantum dots. The pump-and-probe experiment utilizes the Pauli exclusion principle that the absorption of the material is proportional to the number of empty states available. As the initial carriers generated by the pump pulse recombine, the time dependent change in the absorption of the subsequent probe pulses will reflect the carrier dynamics in the material. A schematic diagram of the pump-and-probe spectroscopy experiment is shown in Figure 5.2.

An 80 MHz, tunable, and passive modelocked Ti:sapphire laser pumped with an Ar^+ laser is used to generate the 120 fs pump and probe pulses. To remove the effect of sample heating, a pulse picker is used to reduce the repetition rate of the laser pulses to 1 MHz. The laser pulses are split into the pump and the probe

133

pulses. Time resolved absorption dynamics are obtained by varying the linear time-delay between the pump and the probe pulses using a Klinger stepping motor delay stage. A 5 cm graded index lens is use to focus the pump and probe pulses onto the sample in a non-collinear configuration. To avoid the detection of the pump pulses, cross polarizations are used between the pump and probe pulses. The residual pump pulses are filtered using a polarizing beam splitter cube, and the transmitted probe pulses are detected using a silicon photodiode.
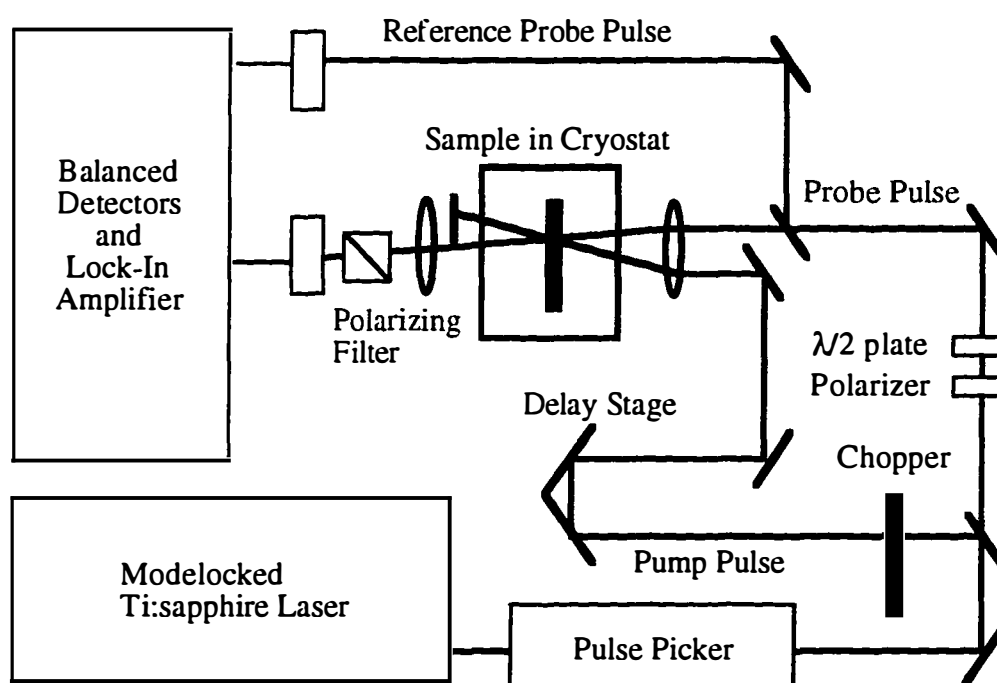
Figure 5.2 The schematic of the pump-and-probe experiment.

The weak absorption associated with the small volume of the quantum dots requires us to design a detection scheme with an extremely high signal to noise ratio. The pump induced change in the transmission of the probe pulses though the quantum dot sample is detected using a balanced optical bridge circuit to reduce the laser noise. The detected signal is amplified using both a pre-amplifier and a digital lock-in amplifier.

5.6 InAs/AlGaAs Quantum Dot Sample

For the transmission studies, a thin film quantum dot sample and a reference sample are prepared. The samples are mounted onto a 3 mil thick transparent fused silica glass slide using cryogenic epoxy. The GaAs substrate and the GaAs cap layer are removed using standard wafer lapping and wet etching techniques. The thin film is held on a liquid helium cold finger cryostat during the experiments.

The quantum dot sample structure is shown in the Figure 5.3a. An $Al_{0.3}Ga_{0.7}As$ separate confinement structure is used to increase the confinement energy of the InAs quantum dots. Unlike the InAs/GaAs, the energy levels in the InAs/$Al_{0.3}Ga_{0.7}As$ quantum dots are near 800 nm, at wavelengths matched to the ultrafast laser system. The spectrum of the pump and the probe pulses is indicated in Figure 5.3b.

To extinguish any possible effects due to the different growth conditions, a reference sample with only the wetting layer is obtained from the same wafer as the dot sample. The wafer is grown by suspending the substrate rotation during the deposition of InAs monolayers. A variable dot density is achieved (see Figure 3.7a). The obtained wetting layer reference sample has the identical growth

condition, but without the quantum dots. The low temperature photoluminescence

of the InAs/$Al_{0.3}Ga_{0.7}As$ quantum dots is shown in Figure 5.3b.
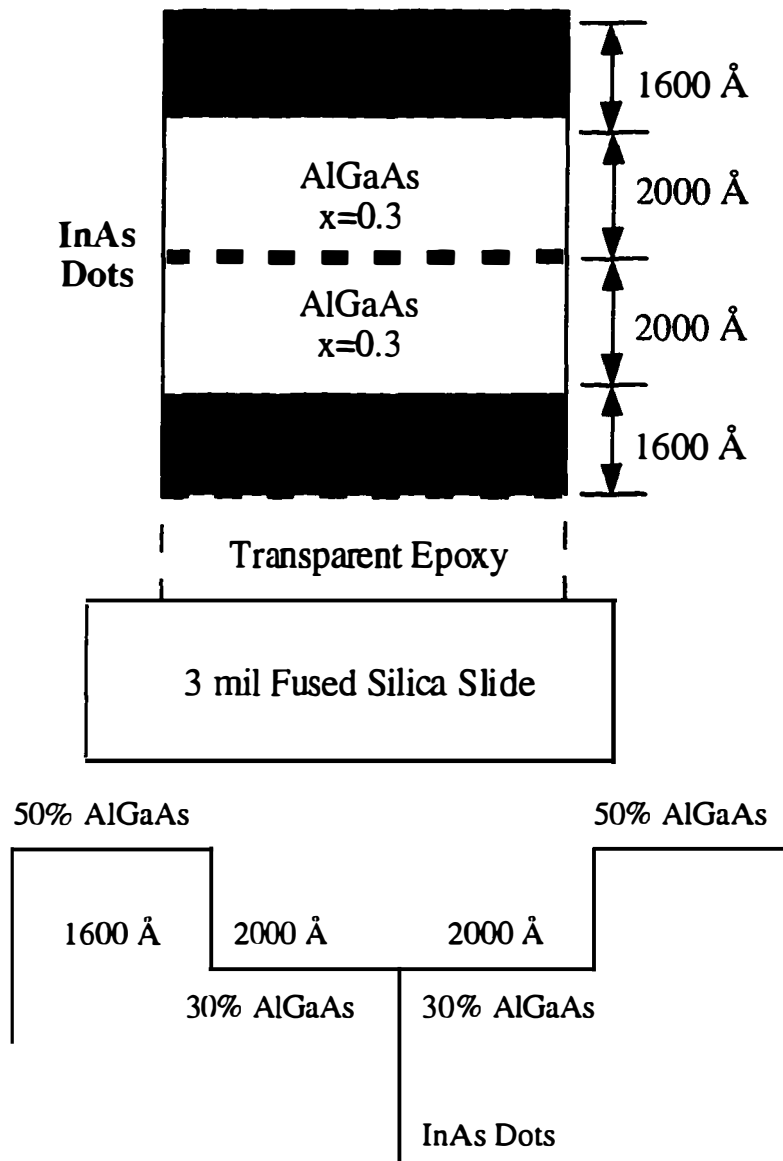
Figure 5.3a Prepared sample structure for the pump and probe experiment. Figure is not drawn to scale.
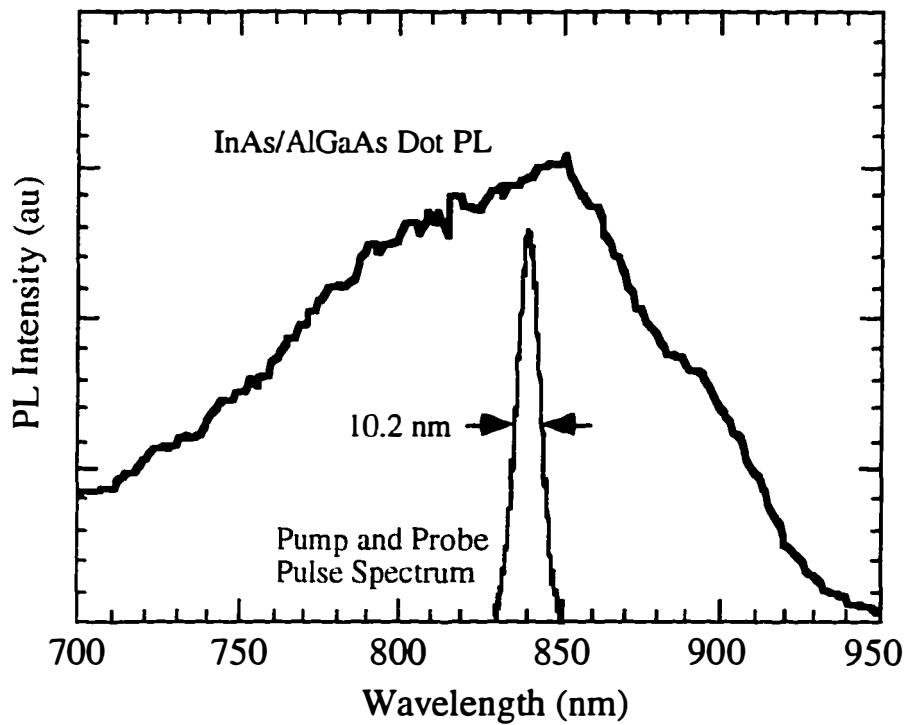
Figure 5.3b Photoluminescence spectra of InAs/$Al_{0.3}Ga_{0.7}As$ quantum dots. The spectral position of the pump and probe pulses is indicated.

5.7 Two-Photon Absorption in the AlGaAs Barrier

Figure 5.4 shows the low temperature (10 K) pump induced probe transmission changes of the InAs/$Al_{0.3}Ga_{0.7}As$ quantum dot sample and the wetting layer reference sample. Several pump excitation intensities are used. A fast two-photon absorption signal is observed when the pump and probe pulse overlap at

zero time delay. The strength of this signal depends linearly on the pump intensity as shown in Figure 5.5.
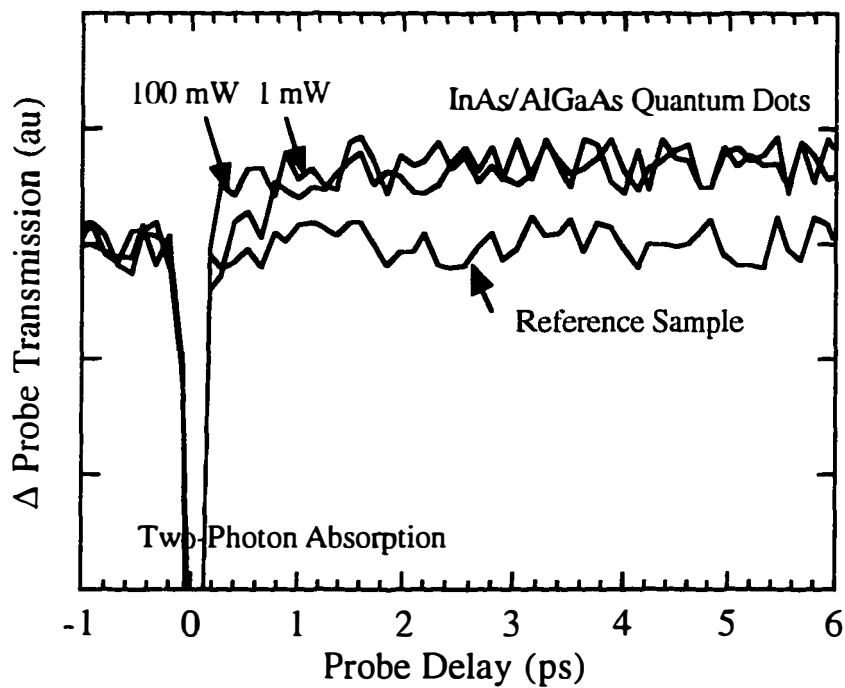
Figure 5.4 Low temperature pump induced probe transmission changes of the InAs/AlGaAs quantum dots and the reference sample. Pump intensity = 1 mW and probe intensity = 0.1 mW.

This observation is in contrast with the normal understanding of two-photon absorption process where the population of the generated carrier is proportional to

138

the square of the photon number. To explain this un-intuitive observation, the

dynamics of the pump-and-probe measurement need to be understood. The rate of
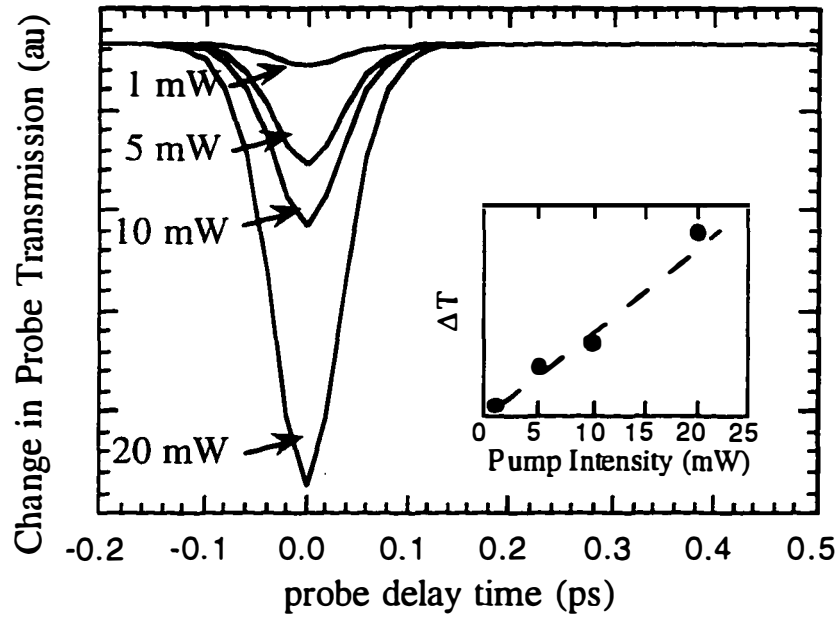
Figure 5.5 Two-photon absorption transient vs. intensity of pump pulse. A linear dependence is observed.

carriers absorbed by the sample due to the two-photon absorption of the pump and

the probe pulses can be expressed as

$$\frac{d}{dt}N_{TPA} = v_g \beta \left(I_{pump}(t) + I_{probe}(t + \Delta t) \right)^2$$

(5.1)

where v_g is the group velocity of the light and β is the two photon absorption coefficient. Δt is the time delay between the pump and probe pulses. When the effect of the pump modulation is applied to Equation 5.1, the induced changes in the carrier population is

$$\frac{d}{dt}\Delta N_{TPA} = \frac{d}{dt}\Delta N_{TPA}\bigg|_{\substack{pump\\on}} - \frac{d}{dt}\Delta N_{TPA}\bigg|_{\substack{pump\\off}}$$
$$= v_g\beta\left(I_{pump}^{2}(t) + 2I_{pump}(t)I_{probe}(t+\Delta t)\right)$$

(5.2)

The intensity reduction in the transmitted probe pulses due to the two-photon absorption is derived from the second term in Equation (5.2).

$$\Delta I_{probe} = -2\hbar\omega v_g\beta I_{pump}(t)I_{probe}(t+\Delta t)$$

(5.3)

Thus, contrary to one's intuition, the measured changes in the probe transmission does not depend on the square of the pump pulse intensity. The observed linear dependence of the two-photon absorption of the probe pulses on the pump intensity is not surprising afterall.

The strong two-photon absorption signal is unlikely due to the quantum dots because their small absorptive volumes. Since the identical behavior is observed in the reference sample where no quantum dot is present, the two-photons absorption process is assigned to the surrounding AlGaAs barrier. A similar two-photon absorption from the AlGaAs waveguide is also found by Zaitsev *et al.* (1997).

5.8 Transient Absorption at Low Temperatures

In Figure 5.4, for all pump intensities, the pump induced change in the probe transmission becomes saturated after 2 ps. Besides the fast transient associated with the two-photon absorption, a fast rise is observed at a high pump intensity. The instantaneous rise of the absorption is the evidence of the states filling effect in the quantum dots. A slower risetime is observed for the lower pump intensity.

$$t = 0 \qquad\qquad t > 0$$

$$N_{TPA}$$

$$\tau_{relax}$$

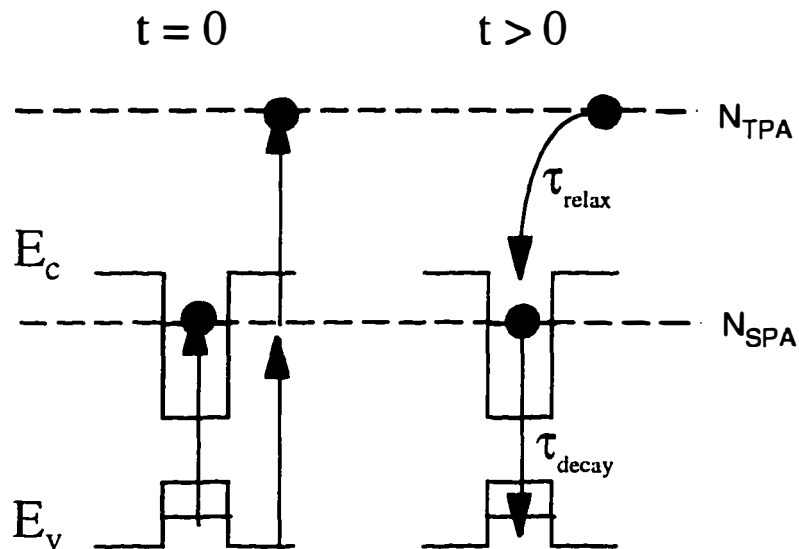$$E_c$$

$$N_{SPA}$$

$$\tau_{decay}$$

$$E_v$$

Figure 5.6   Schematic model of the pump-and-probe dynamics in the quantum dots. Initial carriers are generated by two-photon and single-photon absorption processes. At t > 0, the relaxation of carrier generated from the two-photon absorption will increase the carrier density in the dots.

The simple state filling effect can not explain this non-instantaneous behavior. The slow rise in the transmission of the probe pulses indicates the number of the carriers in the quantum dots is increasing slowly. Since this occurs without the presence of the pump pulses, single photon absorption process can not be responsible. The only other source of carriers besides the single photon absorption is from the two-photon absorption process. At a low pump intensity where not all the states in the quantum dots are filled by the direct absorption, the empty states will be filled slowly by the carriers relaxing from the surrounding AlGaAs barrier (Figure 5.6).

Since the absorption of the probe pulses is directly proportional to the number of empty states available, the measured change in the transmission of the probe pulses is a direct reflection on the carrier population N_{Dots} in the quantum dots. A set of rate equations is developed to model the effect of single-photon absorption (SPA) and two-photon absorption (TPA) on the carrier dynamics in the quantum dots,

$$
\frac{d}{dt}N_{TPA} = v_g\beta\left(I_{pump}(t) + I_{probe}(t+\Delta t)\right)^2 - \frac{N_{TPA}}{\tau_{relaxation}}
$$

$$
\frac{d}{dt}N_{Dots} = v_g\alpha\left(I_{pump}(t) + I_{probe}(t+\Delta t)\right) + \frac{N_{TPA}}{\tau_{relaxation}} - \frac{N_{Dots}}{\tau_{radiative}}
$$

$$(5.4)$$

where α is the carrier density dependent absorption coefficient for the single photon process. The density dependence of α can be approximately expressed as

$$
\begin{aligned}
\alpha &= \alpha_o\left(1 - \frac{N_{Dots}}{\sigma A}\right) & N_{Dots} &< \sigma A \\
&= 0 & N_{Dots} &>= \sigma A
\end{aligned}
$$

$$(5.5)$$

where σ is the dot density and A is the area of the probe pulse. Equation 5.5 is required to properly model the absorption saturation observed in Figure 5.4.

In Equation 5.4, the carriers are depleted from the quantum dots states only through radiative recombination. The carrier population generated from the TPA and SPA processes are coupled together by the carrier relaxation time from the higher energy state to the quantum dot state. Thus, by analyzing the slow risetime in the low pump intensity case, a measurement of energy relaxation time is obtained.

Figure 5.7 plots the solutions of Equation 5.4 vs. the time delay Δt between the pump and the probe pulses. Parameters used in the simulation are listed in Table 5.1. A carrier relaxation time of 0.5 ± 0.06 ps is obtained.
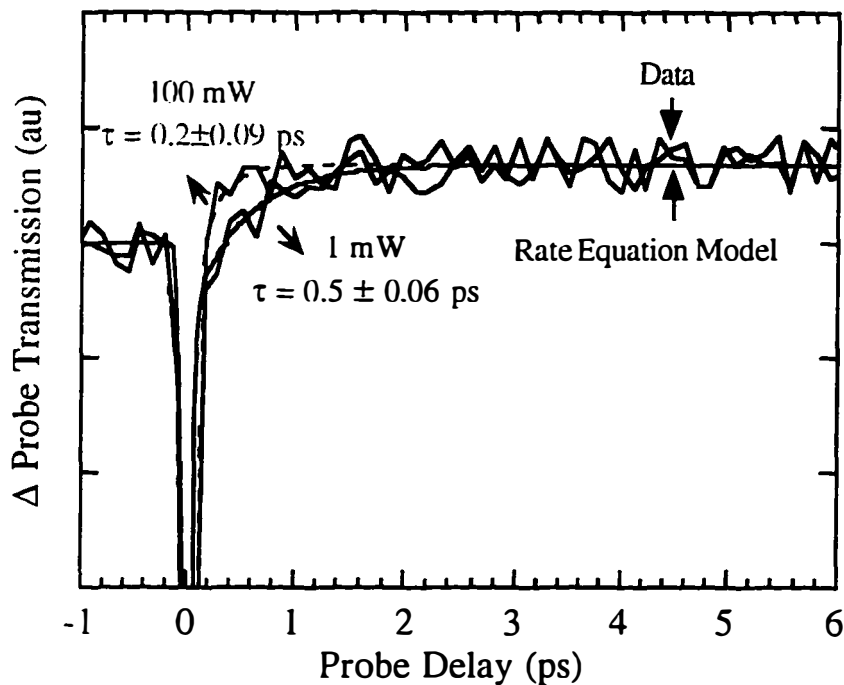
Figure 5.7 Comparison of the measured change in the probe transmission with the fit to the rate equation model. A carrier relaxation time of 0.2±0.09 and 0.5±0.06 ps is obtained from the curve fit for the excitation intensities of 100 mW and 1 mW, respectively.

5.9 Temperature Dependent Effects

As the sample temperature increases, the absorption response remains a fast rise for the case of high pump intensities. This indicates the instantaneous absorption process is independent of temperature. However, at a low pump intensity where the effect of the two-photon absorption is dominant, the risetime becomes longer as the sample temperature rises (Figure 5.6). A retarded carrier

relaxation occurs at higher temperatures. This slow relaxation is understood in a similar picture as the radiative decay process in the quantum dots. At high temperatures, the increased phonon scattering will increase the motion of the carriers on the AlGaAs barrier. Only carriers with zero momentum are allowed to relax into the quantum dots.

A	area of probe beam spot	$1\ \mu m^2$
σ	dot density	$10^{11}\ cm^{-2}$
β	two-photon absorption coefficient	$6 \times 10^{-22}\ m^{-2}$
v_g	group velocity	$8.3 \times 10^7\ m/s$
n	index of refraction	3.62
$\tau_{radiative}$	radiative lifetime	700 ps
$\tau_{relaxation}$	carrier relaxation time	0.5 ± 0.06 ps

Table 5.1 Parameters used in the rate equation analysis (Figure 5.7).
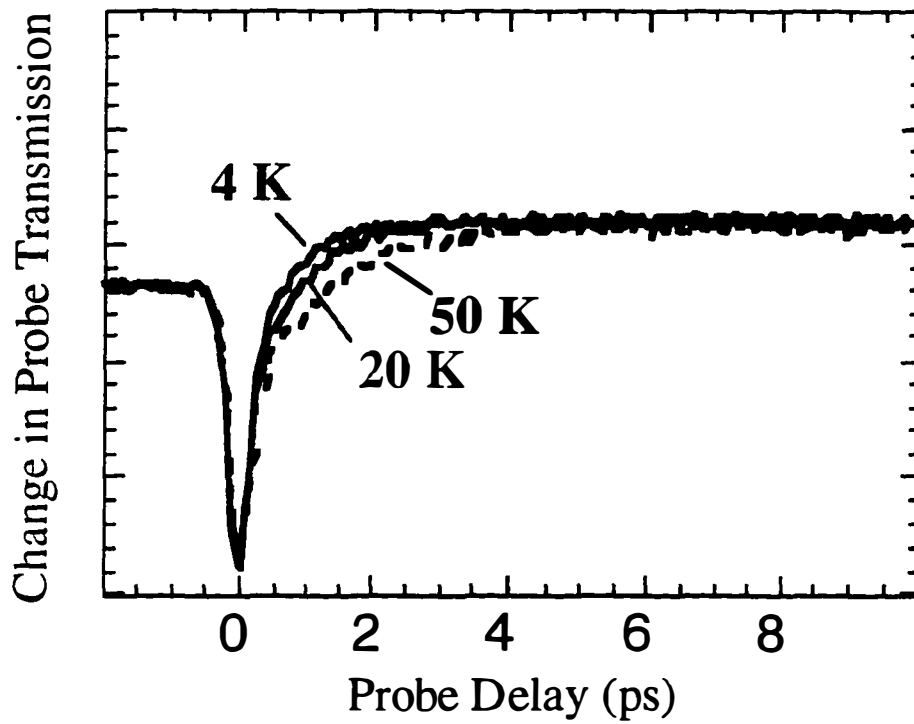
Figure 5.8 Probe transmission transient vs. sample temperatures. Slower risetimes are observed at higher temperatures. The risetime vs. temperature is plotted in Figure 5.9.
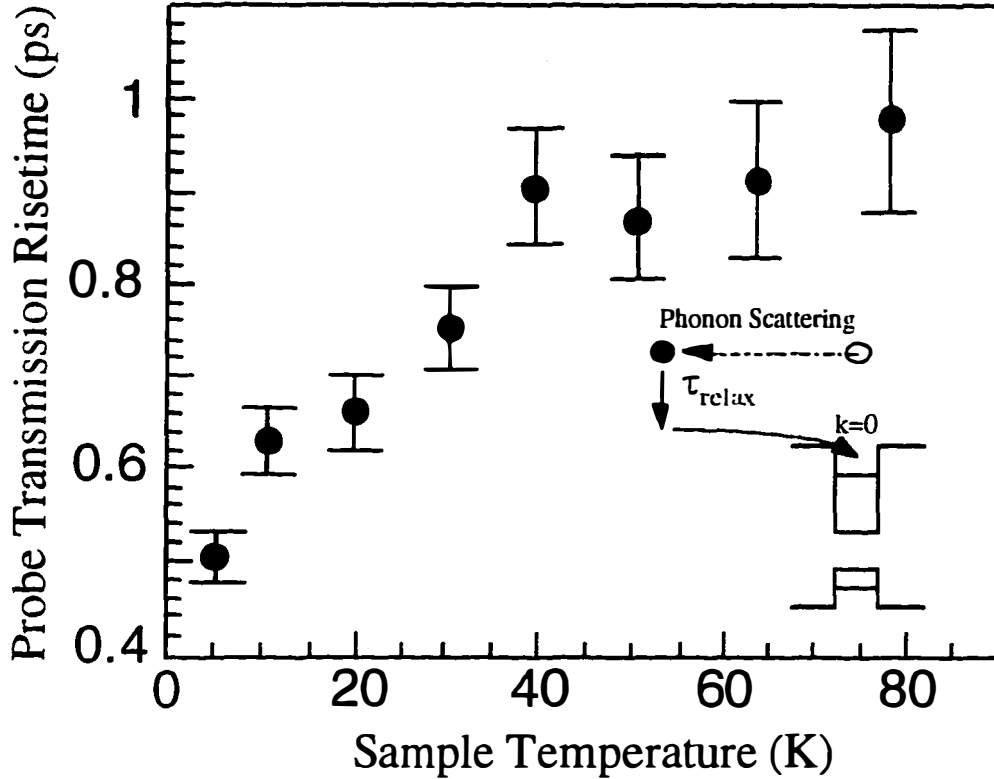
Figure 5.9 Probe transmission risetime vs. sample temperature. The increase in the risetime of the probe pulse absorption at higher temperatures is attributed to the enhanced carrier-acoustic phonon interaction.

5.10 Does Phonon Bottleneck Exist ?

The phonon bottleneck theory of Benisty *et al.* (1991) is solely based on the reduction of LO-phonon scattering rate in quantum structures (Figure 5.1b). A reduced PL efficiency is predicted for the quantum dots. Figure 5.10a compares the integrated PL efficiency of InGaAs/GaAs quantum dots with the theoretical prediction of Benisty *et al.* (1991). Since only the relative scale is used in their theory, the dot PL efficiency is normalized to the reference quantum well PL. Our

result show that the PL efficiency of the quantum dots are similar to that of quantum well, indicating that other relaxation processes besides carrier-LO phonon scattering are important.
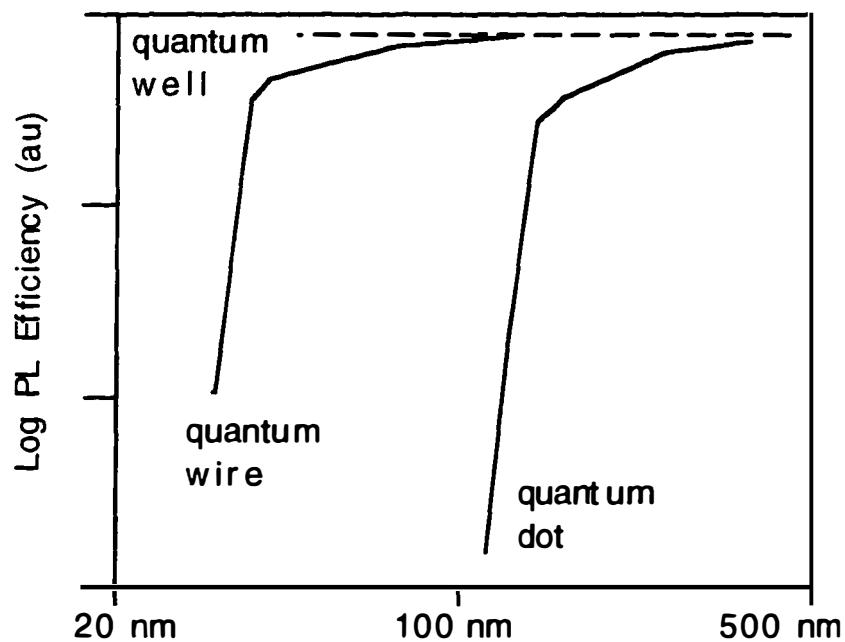
Figure 5.10a Theoretical prediction of phonon bottleneck from Benisty *et al.* (1991). A reduction of PL efficiency is predicted for quantum dot structures. The PL efficiency is comparable for the quantum dot and quantum well in our measurements, indicating that the carrier relaxation in the quantum dot is not dominant by the effect of phonon bottleneck and other relaxation processes are important.

Other theoretical calculations of carrier relaxation time in quantum dots have been developed based on Auger related Coulomb scattering (Bockelmann and Egeler, 1992; Efros *et al.*, 1995), deep level tunnelling (Sercel, 1995), ripple effect due to carrier-acoustic phonon scattering (Knipps, 1996). Figure 5.10b compare the measured carrier relaxation time with the theoretical calculation of Bockelmann

148

et al. (1992). Our measurements show a good agreement with the scattering rate

calculated using Auger-like processes, indicating that Coulomb scattering may be

the dominant carrier relaxation process. Similar calculations have also been carried

out by Efros *et al.* (1995). Manybody renormalization of Coulomb scattering

process in quantum dots can induce a rapid transfer of the electron energy to the

hole energy in the valence band. Under this scattering mechanism, the electron

thermalization time can be as fast as 2 ps in CdSe nanocrystal (Efros *et al.*, 1995).

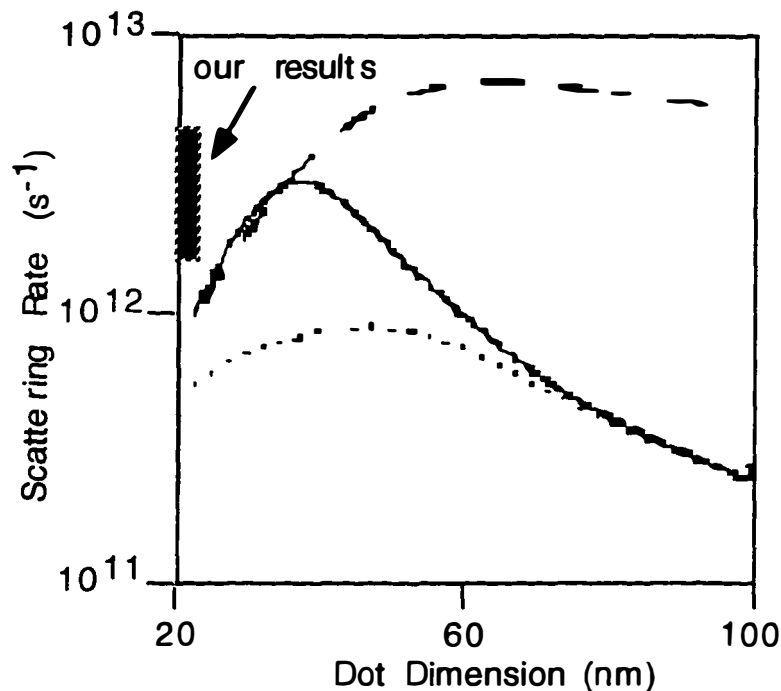Figure 5.10b Theoretical calculation of carrier scattering rate in quantum dots using Auger-like Coulomb scattering processes (Bocklemann and Egeler, 1992). Various screening mechanism is compared in the calculation. The carrier relaxation rates measured in this chapter is in a good agreement with the calculation, indicating that Auger-like processes may be the dominant carrier relaxation in quantum dots.

5.11 Summary

The study of absorption dynamics in the quantum dots is complicated by the intrinsic small volume of the dots. The extremely high sensitivity is required to observe the transient signal above the noise level. Due to the small absorption in the dots, two-photon absorption strongly affects the carrier dynamics in our measurements. The relaxation of carriers from the two-photon absorption is analyzed using a rate equation model. Comparing the published theoretical results for quantum dot (Bockelmann and Egeler, 1992), a fast carrier relaxation time of 0.5 ± 0.06 ps is found in the $InAs/Al_{0.5}Ga_{0.5}As$ quantum dots. This relaxation time is as fast as the electron thermalization time in quantum wells measured by Knox *et al.* (1985). Due to a simple momentum conservation requirement, the effect of phonon scattering will retard the carrier capture process at higher temperatures.

Even though the relaxation time measured in the InAs/AlGaAs quantum dots contradicts the theoretical prediction of phonon bottleneck (Benisty *et al.*, 1991), the bottleneck effect may still be important in other dot structures and materials. The fast relaxation time may be attributed to the Auger-like scattering processes in quantum dots (Bockelmann and Egeler, 1992; Efros *et al.*, 1995). Higher quality samples with multiple layers of quantum dots are needed to clarify further the relaxation mechanism in self-organized quantum dots.

150
References

1. A. Alexandrou, V. Berger, D. Hulin, *Physical Review B-Condensed Matter* **52**, 7 4654-4657 (1995).

2. M. Asada, *IEEE Journal of Quantum Electronics* **25**, 9 2019-2026 (1989).

3. H. Benisty, C. M. Sotomayor-Torres, C. Weisbuch, *Physical Review B (Condensed Matter)* **44**, no.19 10945-8 (15 Nov. 1991).

4. P. W. M. Blom, C. Smit, J. E. M. Haverkort, J. H. Wolter, *Physical Review B-Condensed Matter* **47**, 4 2072-2081 (1993).

5. P. W. M. Blom, J. Claes, J. E. M. Haverkort, J. H. Wolter, *Optical and Quantum Electronics* **26**, 7 S667-S677 (1994).

6. U. Bockelmann, T. Egeler, *Physical Review B-Condensed Matter* **46**, 23 15574-15577 (1992).

7. U. Bockelmann, *Physical Review B-Condensed Matter* **48**, 23 17637-17640 (1993).

8. U. Bockelmann, K. Brunner, G. Abstreiter, *Solid-State Electronics* **37**, 4-6 1109-1112 (1994).

9. F. Bogani, L. Carraresi, R. Mattolini, M. Colocci, A. Bosacchi, S. Franchi, *Nuovo Cimento Della Societa Italiana Di Fisica D-Condensed Matter Atomic Molecular And Chemical Physics Fluids Plasmas Biophysics* **17**, 11-1 1371-1375 (1995).

10. F. Bogani, L. Carraresi, R. Mattolini, M. Colocci, A. Bosacchi, S. Franchi, *Solid-State Electronics* **40**, Si 363-366 (1996).

11. U. Cebulla, G. Bacher, A. Forchel, D. Schmitz, H. Jurgensen, M. Razeghi, *Applied Physics Letters* **55**, 10 933-935 (1989).

12. A. P. Defonzo, B. Gomatam, *Applied Physics Letters* **56**, 7 611-613 (1990).

13. A. L. Efros, V. A. Kharchenko, M. Rosen, *Solid State Communications* **93**, 4 281-284 (1995).

14. J. M. Gerard, J. Y. Marzin, G. Zimmermann, A. Ponchet, O. Cabrol, D. Barrier, B. Jusserand, B. Sermage, *Solid-State Electronics* **40**, Si 807-814 (1996).

15. B. N. Gomatam, A. P. Defonzo, *IEEE Journal of Quantum Electronics* **26**, 10 1689-1704 (1990).

16. S. M. Goodnick, P. Lugli, *Physical Review B (Condensed Matter)* **37**, no.5 2578-88 (15 Feb. 1988).

17. K. L. Hall, G. Lenz, E. P. Ippen, U. Koren, G. Raybon, *Applied Physics Letters* **61**, 21 2512-2514 (1992).

18. R. Heitz, M. Grundmann, N. N. Ledentsov, L. Eckey, M. Veit, D. Bimberg, V. M. Ustinov, A. Y. Egorov, A. E. Zhukov, P. S. Kopev, Z. I. Alferov, *Surface Science* **362**, 1-3 770-773 (1996).

19. R. Heitz, M. Grundmann, N. N. Ledentsov, L. Eckey, M. Veit, D. Bimberg, V. M. Ustinov, A. Y. Egorov, A. E. Zhukov, P. S. Kopev, Z. I. Alferov, *Applied Physics Letters* **68**, 3 361-363 (1996).

20. K. Hess, S. J. Manion, *Journal of Applied Physics* **62**, no.12 4942-4 (15 Dec. 1987).

21. C. T. Hultgren, D. J. Dougherty, E. P. Ippen, *Applied Physics Letters* **61**, 23 2767-2769 (1992).

22. P. A. Knipp, T. L. Reinecke, *Solid-State Electronics* **40**, Si 343-347 (1996).

23. W. H. Knox, D. S. Chemla, G. Livescu, J. E. Cunningham, J. E. Henry, *Physical Review Letters* **61**, no.11 1290-3 (12 Sept. 1988).

24. W. H. Knox, R. L. Fork, M. C. Downer, D. A. B. Miller, D. S. Chemla, C. V. Shank, A. C. Gossard, W. Wiegmann, *Physical Review Letters* **54**, no.12 1306-9 (25 March 1985).

25. K. Mukai, N. Ohtsuka, H. Shoji, M. Sugawara, *Physical Review B-Condensed Matter* **54**, 8 R5243-R5246 (1996).

26. K. Mukai, N. Ohtsuka, H. Shoji, M. Sugawara, *Applied Physics Letters* **68**, 21 3013-3015 (1996).

27. R. Nagarajan, M. Ishikawa, T. Fukushima, R. S. Geels, J. E. Bowers, *IEEE Journal of Quantum Electronics* **28**, 10 1990-2008 (1992).

28. R. L. Nagarajan, Ph.D. Dissertation: Carrier Transport Effects in High Speed Quantum Well Lasers, University of California, Santa Barbara, (1992).

152

29. P. J. Price, *Annals of Physics* **133**, no.2 217-39 (2 May 1981).

30. S. Raymond, S. Fafard, S. Charbonneau, R. Leon, D. Leonard, P. M. Petroff, J. L. Merz, *Physical Review B-Condensed Matter* **52**, 24 17238-17242 (1995).

31. K. H. Schmidt, G. Medeirosribeiro, M. Oestreich M, P. M. Petroff, and G. H. Dohler. *Physical Review B (Condensed Matter)* **54** 16 11346-11353 (1996).

32. S. Schmitt-Rink, D. A. B. Miller, D. S. Chemla, *Physical Review B (Condensed Matter)* **35,** no.15 8113-25 (15 May 1987).

33. P. C. Sercel, *Physical Review B-Condensed Matter* **51**, 20 14532-14541 (1995).

34. J. Shah, *IEEE Journal of Quantum Electronics* **24**, no.2 276-88 (Feb. 1988).

35. J. Shah, *Ultrafast Spectroscopy Of Semiconductors And Semiconductor Nanostructures* (Berlin ; New York : Springer, 1996)

36. J. Singh, I. Vurgaftman, *IEEE Journal of Quantum Electronics* **30**, 9 2012-2025 (1994).

37. A. Uskov, J. Mork, J. Mark, *IEEE Journal of Quantum Electronics* **30**, 8 1769-1781 (1994).

38. J. Wang, U. A. Griesinger, H. Schweizer, *Applied Physics Letters* **69**, 11 1585-1587 (1996).

39. G. Wang, C.-K. Sun, H. R. Blank, B. Brar, J. E. Bowers, H. Kroemer, M. H. Pilkuhn, *QELS '96. Summaries of Papers Presented at the Quantum Electronics and Laser Science Conference. Vol.10 1996 Technical Digest Series. Conference Edition (IEEE Cat. No.96CH35902)* , 164-5 (1996).

40. M. Willatzen, A. Uskov, J. Mork, H. Olesen, B. Tromborg, A. P. Jauho, *IEEE Photonics Technology Letters* **3**, 7 606-609 (1991).

41. S.V. Zaitsev, and A. M. Georgievski, *Japanese Journal of Applied Physics, Part 1,* **36** no.6B (1997).

Chapter Six

Radiative Recombination in GaSb Quantum Dots

6.1 Introduction

The discussions in the previous chapters have been focused on the properties of the spatially direct excitons in the nested band alignment quantum dots. In the nested band alignment heterostructure, both the conduction band and the valence band of the quantum dot material are nested within the bandgap of a wider-gap barrier material. Electrons and holes are spatially confined together within the quantum dots. This spatial confinement of electrons and holes may be modified when a different band alignment is introduced. In a staggered band alignment quantum dot, either the conduction band or the valence band is lying outside the bandgap of surrounding material. The spatial separation of electrons and holes is a fundamental feature of the staggered band alignment heterostructure (Figure 6.1).

In a two dimensional heterojunction with a staggered band alignment, electrons and holes are localized in self-consistent quantum wells at the interface. The quantum wells are induced by the field between the spatially separated charges. Two distinct phenomenon are observed in the staggered band alignment heterointerface. First, radiative recombination can occur across the heterojunction via tunneling. Long radiative lifetimes and small exciton binding energies are the

result of a decrease in the optical matrix element due to a reduced wavefunction overlap. Second, due to the self-consistent nature of the quantum well potentials, the emission energy of the staggered heterojunction is strongly influenced by the carrier density and the external electric field. These two properties can lead to unusual dynamic and recombination properties unlike the nested band alignment structures.

Nested Band Lineup
Quantum Dots

Staggered Band Lineup
Quantum Dots

Ec

Ev

GaAs/InAs/GaAs

GaAs/GaSb/GaAs
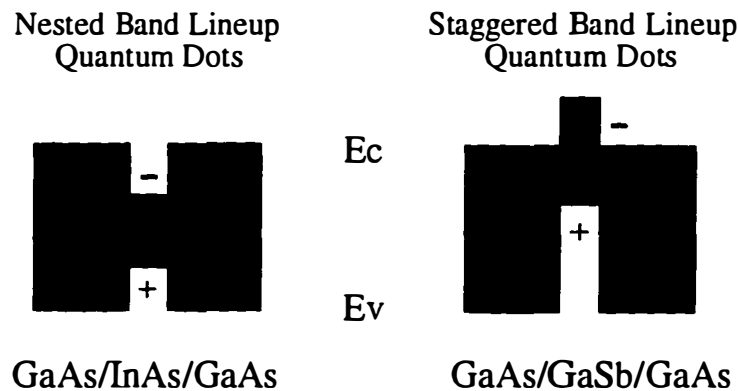
Figure 6.1 Schematic illustrations of the nested and staggered band lineups. The "-" and "+" indicate the spatially positioned electron and hole.

These similar recombination dynamics may be expected from quantum dots with a staggered band alignment such as the GaSb/GaAs system. The self-consistent quantum wells at the heterointerface are transformed into a spherical shell of negative charges in the conduction band and a core of positive charges in the valence band. This situation is analogous to an atom, where negatively charged electrons surround a positive charged nucleus.

Despite this novel concept of the artificial atom, the spatially indirect excitons in the staggered band alignment quantum dots have received limited attention. Only a few theoretical investigations of excitons in a staggered band lineup are reported. Rorison *et al.* (1993) and Laheld *et al.* (1995) have utilized variational techniques to gain theoretical understandings of the exciton binding energy vs. dot radius and effective masses in a single particle picture. The past experimental research in the staggered band alignment heterostuctures have involved only heterointerface or quantum well structures. The staggered band alignment heterojunctions have been extensively studied in the GaInAsSb/GaSb system by Mikhailova and Titkov (1994), and the recombination dynamics in the other staggered alignment heterostructures have also been thoroughly reviewed by Wilson (1988).

The lack of experimental research on these dots is mainly attributed to the absence of the staggered dot materials. With the recent advances in the growth of the self-organized quantum dots, the staggered band-lineup dots have become a reality (Sun *et al.* 1996; Benett, *et al.*, 1996; Hatami *et al.*, 1995). The advances in the molecular beam expitaxy (MBE) growth of the self-organized quantum dots have produced small coherent GaSb islands embedded in GaAs. With a giant valence band offset (Ledentsov *et al.*, 1995), the GaSb/GaAs quantum dot system created an excellent opportunity to study the properties of spatially indirect excitons in the quantum dots.

In this chapter, the experimental and theoretical investigations of the carrier dynamics in the GaSb/GaAs quantum dots are presented. In Section 6.2, the MBE growth of the GaSb quantum dot samples is summarized. The sample structures

and the associated photoluminescence are introduced. The time-correlated single photon counting (TCPC) technique is described in Section 6.3. TCPC is utilized to measure the nanosecond recombination dynamics of the spatially indirect transition. In Section 6.4, the unusual recombination dynamics of the staggered band alignment quantum dots are presented. The transition from the spatially indirect to the spatially direct exciton is investigated using a sample with a higher confinement energy. In Section 6.5 and 6.6, a space charge model is developed to explain the observed dynamics. Numerical solutions are obtained by solving the self-consistent Poisson-Schrödinger equations in the GaSb/GaAs quantum dot structure.

6.2 GaSb/GaAs Quantum Dot Samples

The GaSb/GaAs quantum dots studied in this chapter are grown on semi-insulating GaAs (100) at 530 °C using MBE. The samples are grown by Bobby Brar and Richard Blank.To avoid the replacement of the antimony atoms by the arsenic atoms at the dot interface, a lower temperature (460 °C) is used during the overgrowth of GaAs capping layer. Unlike the InAs/GaAs quantum dots, where the difference between the group III elements (In and Ga) is responsible for the formation of the dots, the different group V elements (Sb and As) contribute to the growth of the GaSb/GaAs dots. Even though the underlying growth mechanism may be slightly modified (Bennett, 1996), a dot structure similar to the InAs/GaAs quantum dot described in Section 1.3 is obtained.

Figure 6.2 shows an atomic force microscope (AFM) image of the GaSb/GaAs dots without the GaAs capping layer. With 1.4 monolayers of GaSb deposited during the dot growth, a dot density of 3.7×10^9 cm^{-2} is obtained. The

average dot height is 10 nm, and the average diameter is 84 nm with a standard

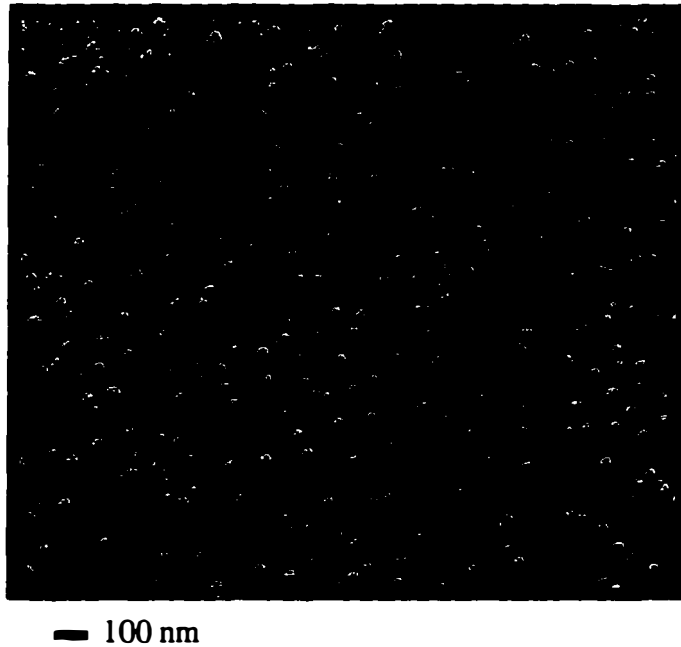deviation of 7 nm. Although the GaSb dot diameter is larger than the InAs/GaAs

■ 100 nm

Figure 6.2 Atomic force microscope (AFM) image of the GaSb/GaAs dots. Dot density shown is $4x10^9$ cm $^{-2}$. The average dot height is 10 nm, and the average diameter is 84 nm.

quantum dots, the actual size during the growth may be smaller due to the

interdiffusion of Sb with As atoms on the surface (Bennett, 1996).

Three sample structures are designed for the optical study (Figure 6.3).

Sample A consists of GaSb dots surrounded by bulk GaAs. In Sample B, GaSb

dots are surrounded by a digitally alloyed $Al_{0.5}Ga_{0.5}As$ superlattice. In Sample C,

GaSb dots are grown in the center of a 15 nm $GaAs/Al_{0.5}Ga_{0.5}As$ /GaAs quantum

well. Staggered band alignments are expected in Sample A and C, while Sample B

is expected have a nested band alignment.

Sample Structures   Expected Band Offsets
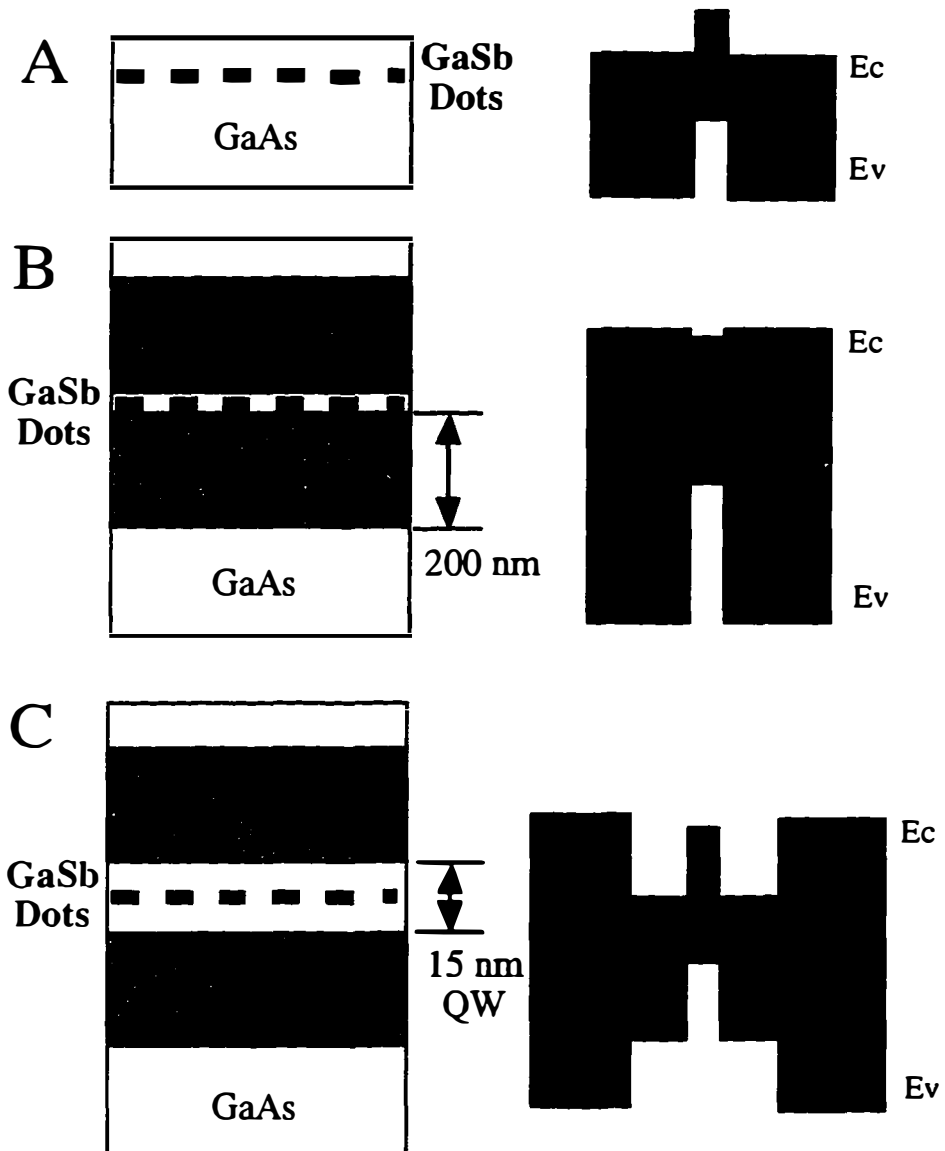
Figure 6.3 Three different GaSb/GaAs quantum dot sample structures used in the experiments.

The low temperature photoluminescence spectra of these samples are shown in Figure 6.4. The photoluminescence (PL) of the Sample A is centered near 1.3 eV. Compared to the bulk GaSb, this large shift in the emission energy is attributed to the significant hydrostatic band shift due to the large compressive strain between the GaSb and GaAs crystal. A smaller effective size may also occur due to the intermixing of antimony and arsenic atoms on the surface during the GaAs

Figure 6.4 Photoluminescence spectra of Samples A, B, and C.

160

overgrowth. Higher emission energies are observed in Sample B and C. These blue shifts are the result of the enhanced quantum confinement from the surrounding AlGaAs superlattice.

6.3 GaSb/GaAs Photoluminescence Energies
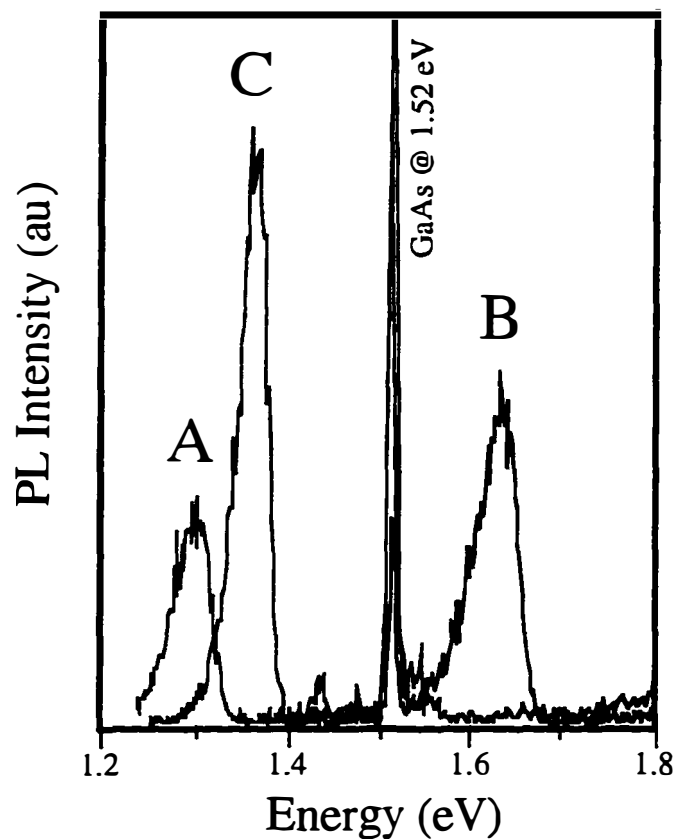
Figure 6.5 illustrates the effects of strain on the conduction and the valence band edges for the GaSb/GaAs heterostructures. The calculation is based on the model-solid theory presented by Herring *et al.* (1955), Keyes (1967), and Van de Walle (1988). The large valence band offset in the relaxed GaSb/GaAs is attributed to the large spin-orbit splitting in the GaSb. The biaxial strain occurs in the 2D GaSb/GaAs quantum well. The presence of a biaxial strain will split the energies levels of the heavy hole and the light hole, pushing the heavy hole energy level of the GaSb higher from the relaxed value. Ledentsov *et al.* (1996) have shown that the calculated band structures due to the biaxial strain underestimated the measured PL emission energies in the thin GaSb/GaAs heterostructures. An idealized isotropic strain is assumed for the quantum dots. In this case, the large hydrostatic shift of the GaSb band edge is attributed to the large volume dilation (Equation 2.5).

Figure 6.6 shows the calculated PL emission energies for the GaSb/GaAs quantum dots with different thicknesses and widths. The assumption of an isotropic strain yields a reasonable agreement with the measured PL. For the quantum dot with a lateral diameter of 84 nm, the effect of the lateral confinement is absent. The variation in the dot PL energies is completely attributed to the fluctuation in the dot thickness. The measured PL emission energies are higher than the expected value.

This discrepancy may be attributed to the extremely simplified assumptions of the dot geometry and the uniform strain. Other source of errors may due to the break down of the model-solid theory in the high strain regime.

The calculated band alignment (Figure 6.5) for the quantum dot presents an unexpected disagreement for the assumed nested band lineup in Sample B (Figure 6.3). The calculated GaSb conduction band edge is higher than the value for the $Al_{0.5}Ga_{0.5}As$. This confusion in the band alignment of the $GaSb/Al_{0.5}Ga_{0.5}As$ quantum dots will be discussed in Section 6.6.

0.1

1.06

0.64

Ec

GaSb

1.52 eV

0.81

1.03

0.3

Ev   GaAs

Relaxed
Bulk

Biaxial Strain
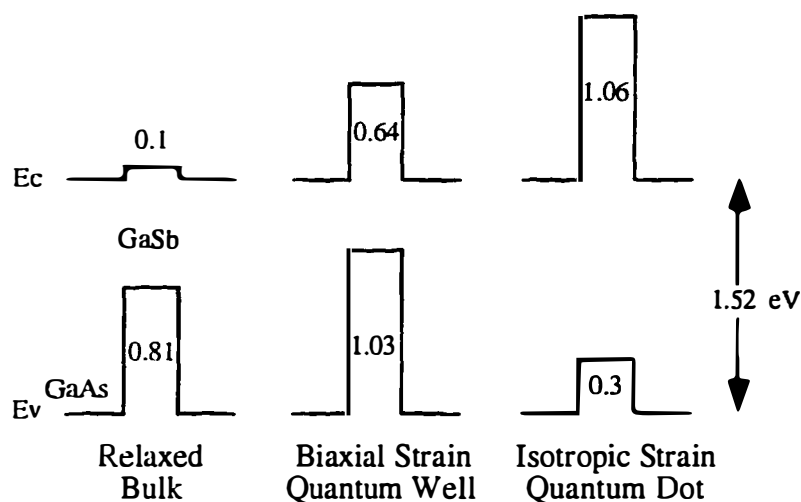Quantum Well

Isotropic Strain
Quantum Dot

Figure 6.5 Calculated GaSb/GaAs band alignment schemes for different strain situations. Calculated band offsets are indicated. All numbers are given in eV. The calculation is based on the model-solid theory (Van de Walle, 1988).
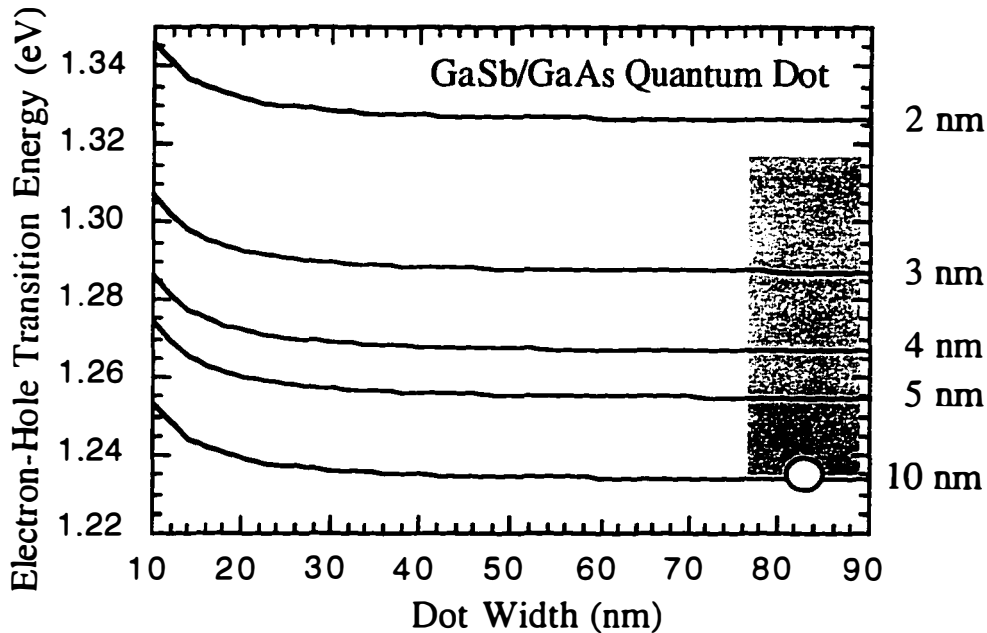
Figure 6.6 Calculated electron-hole transition energy for GaSb/GaAs quantum dot for various dot thickness and width. Isotropic strain is assumed. A flat, square quantum box model is used (see inset of Figure 2.4). The shaded area indicates the measured PL energy and dot diameter distribution. The circle indicates the average dot size measured from AFM.

6.4 Time-Correlated Single Photon Counting

The radiative decay rate of exciton is directly proportional to the wavefunction overlap between the electron and hole. For the spatially indirect exciton in the staggered band alignment quantum dot, the reduced wavefunction overlap will yield decay time longer than the spatially direct exciton. The maximum time range of the streak camera (12 ns) is insufficient to study the radiative dynamics in the GaSb/GaAs quantum dots. Instead, time-correlated single photon

163

counting (TCPC) technique (O'Conner and Philips, 1984; Fouquet, 1984) is employed.

The single photon counting measurement relies on the concept that photoluminescence decay is fundamentally a statistical process. By accumulating the time delays between the excitation pulses and the emission of a single photoluminescence photon, a probability distribution of the photoluminescence decay is collected. The measurement of the time delays between the excitation pulse and the luminescence photon requires the use of a time-to-amplitude converter (TAC). The trigger signal from the excitation pulse initiates the charging of a capacitor within the TAC. This charging process is terminated when a single photoluminescence photon is detected. The time delay between the two pulses is measured from the voltage of the capacitor. This delay time measurement is repeated until enough samples are collected to obtained a reasonable signal to noise ratio in the distribution. The relationship between the signal to noise is governed by Poisson statistics, where the noise is proportional to the square root of the collected sample number.

The schematic of the TCPC measurement setup is shown in Figure 6.7. The system is driven by a Ti:sapphire regenerative amplifier with a pulsewidth of 1 ps and a repetition rate of 250 kHz, allowing us to measure decays as long as 4 μs. An excitation wavelength of 800 nm is selected to avoid generation of carriers in the $Al_{0.5}Ga_{0.5}As$ superlattice barrier, where the slow and the indirect k-space transition may re-excite the quantum dots. To ensure the proper temporal correlation of excitation and luminescence pulses, a passive delay (Princton Model 792) is used to
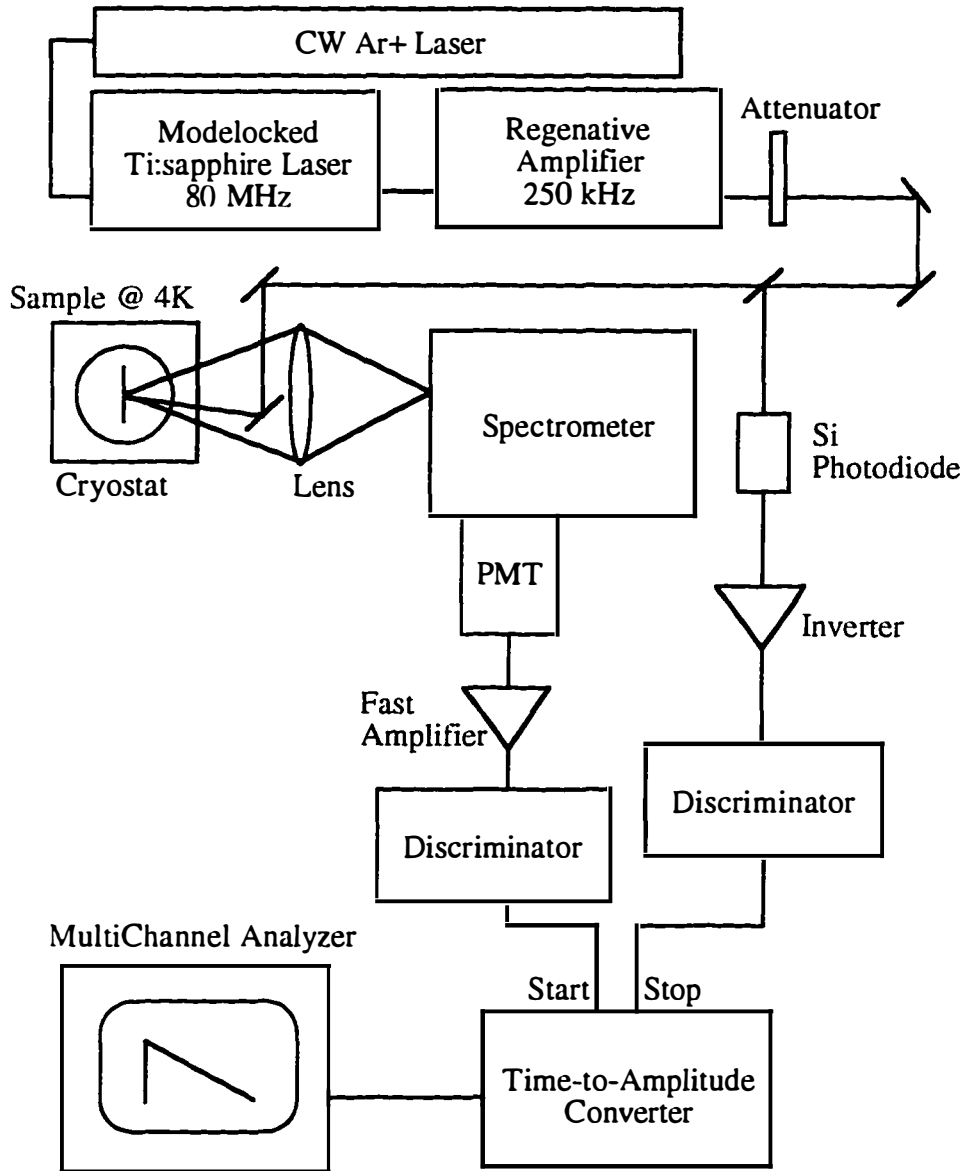
Figure 6.7 Time-Correlated Single Photon Counting (TCPC) setup.

adjust the timing position of the trigger pulse. A Hamamastu R2809 Micro Channel Plate photomultiplier tube (MCP-PMT) with a S-1 response is used to detect the photoluminescence photon. A fast amplifier (EG&G VT100) and a discriminator (Tennelec TC 454) are used to amplify, shape and filter the signal. A multichannel analysis software running on a PC is used to analyze the output of the TAC (EG&G Ortec 457). The overall time resolution of TCPC system is 250 ps, which is limited from the transient time spread of MCP-PMT and the timing jitter in the detection electronics.

6.5 Dynamics of the Spatially Indirect Excitons

The time-resolved photoluminescence of Samples A, B, and C are shown in Figure 6.8. For the GaSb/GaAs quantum dots (Sample A), unlike the InAs/GaAs quantum dots, a slow photoluminescence decay is observed. The decay is not a single exponential but exhibits two time constants of 8 ns and 30 ns. This measured lifetime is longer than the radiative lifetimes of 600 ps from a spatially direct GaSb/AlSb quantum well (Cebulla *et al.*, 1987) and 700 ps from the InGaAs/GaAs quantum dots. The measured slow decay is attributed to a reduced electron and hole wavefunction overlap, resulted from the staggered band alignment.

For Sample C, a similar slow and two-exponential luminescence decay is observed. The 150 Å quantum well provides a better confinement of electrons in Sample C. A brighter PL intensity and faster time constants of 7.5 ns and 23 ns are obtained from the curve fit.
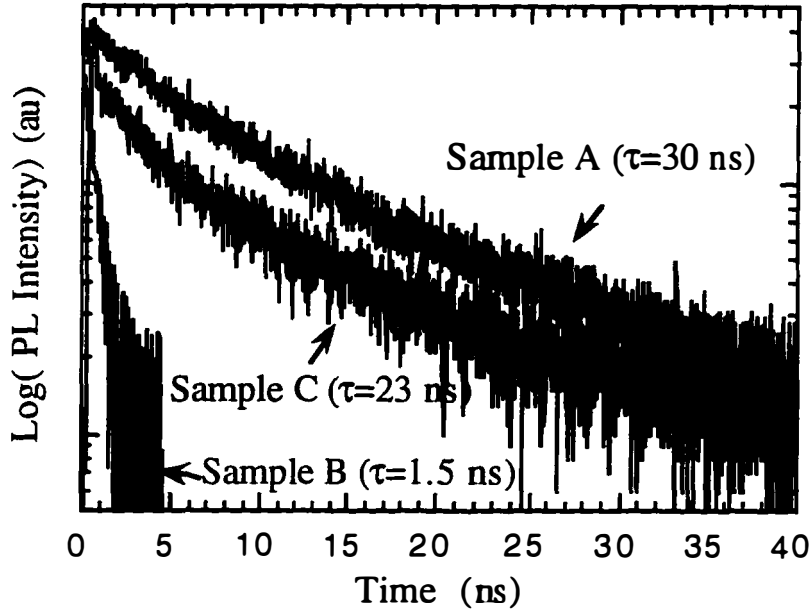
Figure 6.8 Time-resolved photoluminescence of Sample A, B, and C. A fast decay is observed in Sample B.

6.6 GaSb/Al$_{0.5}$Ga$_{0.5}$As Quantum Dots

While extremely slow decays are observed for Sample A and C, the GaSb/Al$_{0.5}$Ga$_{0.5}$As Sample B exhibiting a fast decay, limited by the TCPC system resolution. The streak camera measurement of Sample B indicates a single exponential decay time of 1.5 ns. This fast decay time is comparable to the InAs/GaAs quantum dots discussed in the previous chapters. In contrast to Sample A and C, this fast decay may suggest that a nested band alignment exists in the GaSb/Al$_{0.5}$Ga$_{0.5}$As quantum dots, where both the electrons and holes are spatially confined together.

The band alignment suggested from the measured time-resolved photoluminescence and calculated using model-solid theory is shown in Figure 6.9.

The evidence of a fast TRPL decay indicate that the large conduction band offest calculated from the model-solid theory may be incorrect. Our extremely simplified assumption of a uniform strain in dots may be invalid in this large strain case.

Two possible band alignments for GaSb/Al$_{0.5}$Ga$_{0.5}$As Quantum Dots
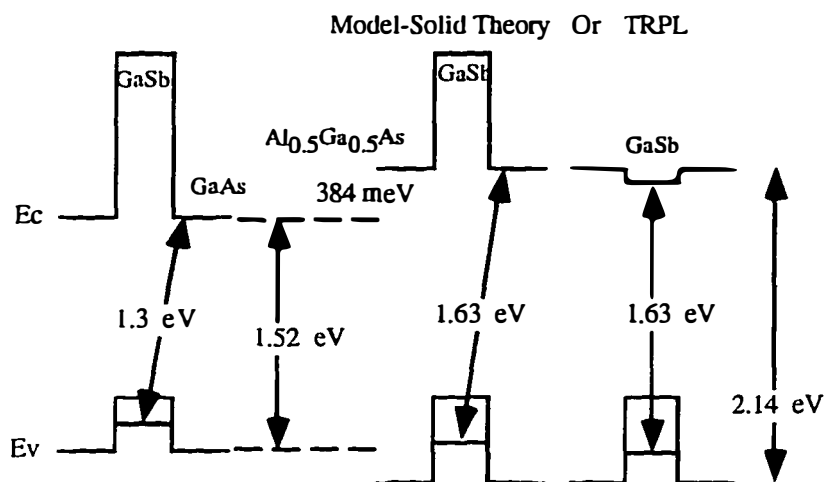
Figure 6.9 Band alignment analysis between the GaSb/GaAs and GaSb/Al$_{0.5}$Ga$_{0.5}$As quantum dots. The measured emission energy of 1.63 eV from Sample B can result from either spatially direct or spatially indirect band alignments.

6.7 Electron and Hole Wavefunction Overlap

To understand the slow, non-exponential of luminescence decays from the spatially separated electron and hole, the nature of the self-consistent electron and hole potentials needs to be carefully considered. The spatially separated charges are confined in the heterointerface due to the Coulomb attraction. The overlap between the spatially separated wavefunction at the heterointerface will determine the radiative decay rate. During the initial decay, a larger field associated with the high

charge density pulls the electron and hole wavefunctions closer together. The enhanced wavefunction overlap will lead to a faster decay time. As the charges are depleted from the heterointerface, the self-consistent field is reduced. Electron and hole wavefunctions become further apart, producing a slower radiative decay time.

The time dependent wavefunction overlap is modeled by including the Coulomb interaction between the spatially separated charges. Using the effective-mass treatment, the Hamiltonian for the GaSb/GaAs system is written as

$$H = \frac{p_e^2}{2m_e} + \frac{p_h^2}{2m_h} + V_e(r_e) + V_h(r_h) - e\Phi_{coulomb}(r_e - r_h),$$ (6.1)

where V_e and V_h are the bare potentials for the conduction band and the valence band, calculated from the model-solid theory (Figure 6.5). The self-consistent Coulomb potential Φ is obtained by solving the Poisson Equation

$$\varepsilon\nabla^2\Phi(r_e - r_h) = \rho(r_e, r_h) = Ne\left[-\psi_e^2(r_e) + \psi_h^2(r_h)\right].$$ (6.2)

where N is the number of charge pairs involved, and ψ_e and ψ_h are the wavefunctions of electron and hole. Self-consistent solutions are obtained by numerically integrating the above Poisson-Schrödinger Equations across the GaSb quantum dot structure.

Figure 6.10 a and b show the electron and hole wavefunctions calculated for Samples A and C, respectively. The solutions are shown for the cases of N=1, 5,

Sample A
Band Structures

Electron (-) and Hole (+)
Wavefunction Overlaps

N=1

GaSb

Ec

GaAs

Ev

→
R

−   +   −

N=5

Ec

Ev

−   +   −

N=10

Ec

Ev

−   +   −

Figure 6.10a Electron and hole wavefunctions calculated for the Sample A. The solutions are obtained for the cases of N=1, 5, and 10, where N is the number of charge pairs involved. Spherical dot is assumed in the model. The effect of the graded composition in ignored.

Sample C
Band Structures

Electron (-) and Hole (+)
Wavefunction Overlaps

N=1

GaSb

Ec

Al$_{0.5}$Ga$_{0.5}$As

Ev

$\longleftrightarrow$
150 Å GaAs Quantum Well

+

-                    -

N=5

Ec

Ev

+

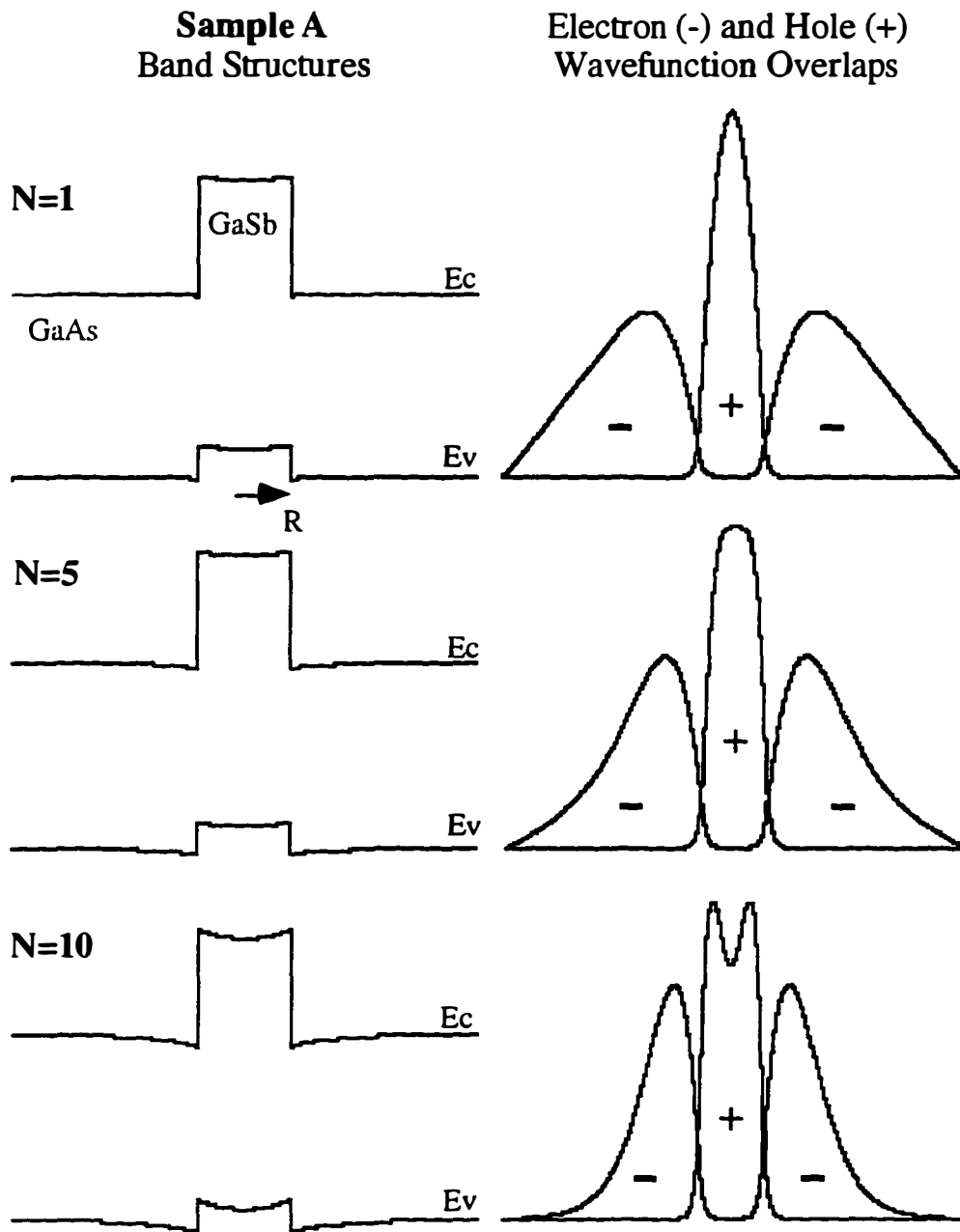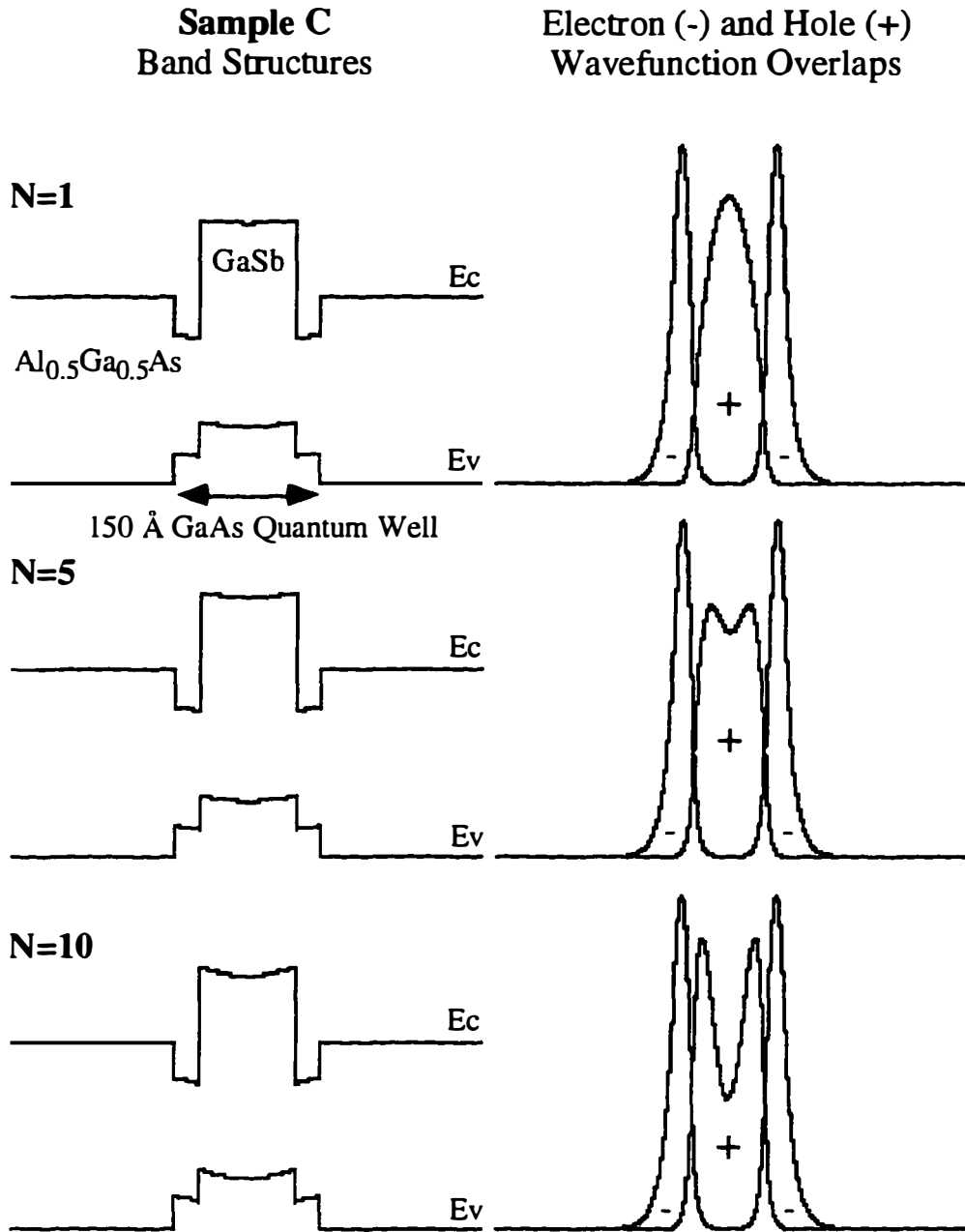-   -

N=10

Ec

Ev

+

-                    -

Figure 6.10b Electron and hole wavefunctions calculated for the Sample C. The solutions are obtained for the cases of N=1, 5, and 10, where N is the number of charge pairs involved. Spherical dot is assumed in the model. The effect of the graded composition in ignored.

and 10. An increased wavefunction overlap is observed for a higher charge density, supporting the measured non-exponential time decay. Due to the confinement of electrons in the 15 nm quantum well, a larger electron and hole wavefunction overlap is obtained for Sample C. This calculation concurs with the observed decays in Figure 6.8.

6.8 Intensity Dependent Photoluminescence

As the carrier density increases at the GaSb/GaAs interface, a steeper confinement potential is induced due to the larger number of the space charges. The effect of a steeper potential will increase the electron quantization energy. This effect is clearly observed in the intensity dependence PL as shown in Figure 6.11a. With an increased excitation intensity, the PL peak shifts toward a higher energy. A similar blue shift from the GaSb heterostructures is also observed by Ledentsov *et al.* (1995) and Glaser *et al.* (1996).

Figure 6.11a The photoluminescence of GaSb/GaAs quantum dots at various excitation intensities. The blue shift of the emission energy is the evidence of the space charge effect.
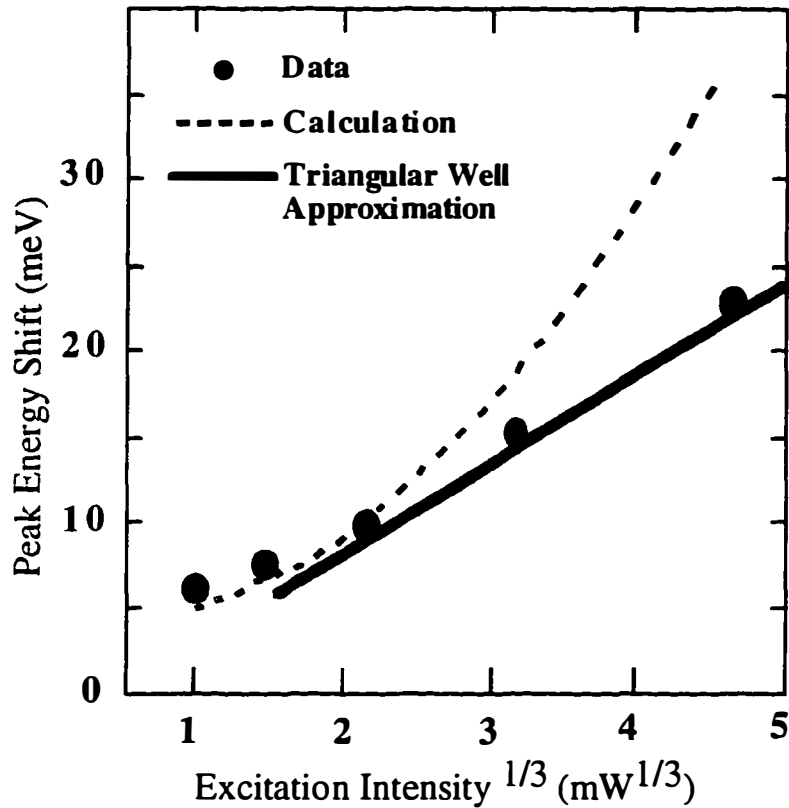
Figure 6.11b PL peak energy dependence on the cubic root of the excitation density.

Ledentsov *et al.* (1995) have suggested that the shape of the Coulomb potential may be approximated using a triangular quantum well. The quantization energy of a triangular quantum well varies linearly with the cubic root of the excitation intensity (Weisbuch and Vinter, 1991). In Figure 6.11b, the self-consistent quantization energies obtained from the Poisson-Schrödinger Equations are compared to the measured energy shifts in the PL spectra. Good agreement is obtained at low excitation intensities. At high intensity a larger shift is predicted

from the calculation. This discrepancy between the theory and the experiment may be attributed to many body effects such as charge screening. The effect of the screening can reduce the range of Coulomb potential. The cubic root dependence on the excitation density is valid only for high pump intensity, where the triangular potential may be a better approximation for the steeper Coulomb potential.

6.9 Space-Charge Dynamics

The observed non-exponential decays in Sample A and C require careful consideration of the space charge dynamics. The overlap between the electron and hole wavefunctions are modeled by considering the dependence of Coulomb potential on the charge density. Since the radiative decay rate is proportional to the square of electron and hole wavefunction overlap, the time dependent carrier density or the PL intensity may be expressed as,

$$\frac{dn}{dt} = \frac{n}{\tau(n)} \propto n \times overlap^2(n) \tag{6.3}$$

where the dependence of wavefunction overlap on the carrier density is obtained by considering the Poisson-Schrödinger Equations for the different number of the space charges (Figure 6.12).

In Figure 6.13, the numerical solutions to Equation 6.3 is compared to the measured TRPL decay at a high pump intensity. Qualitative agreement is obtained between the theoretical and the experimental results. During the initial time decay where the carrier density is high, a fast decay time is observed, indicating a larger wavefunction overlap at the interface. As the carrier density decreases, the

measured decay rate reduces as the result of a weaker Coulomb potential at the

interface.
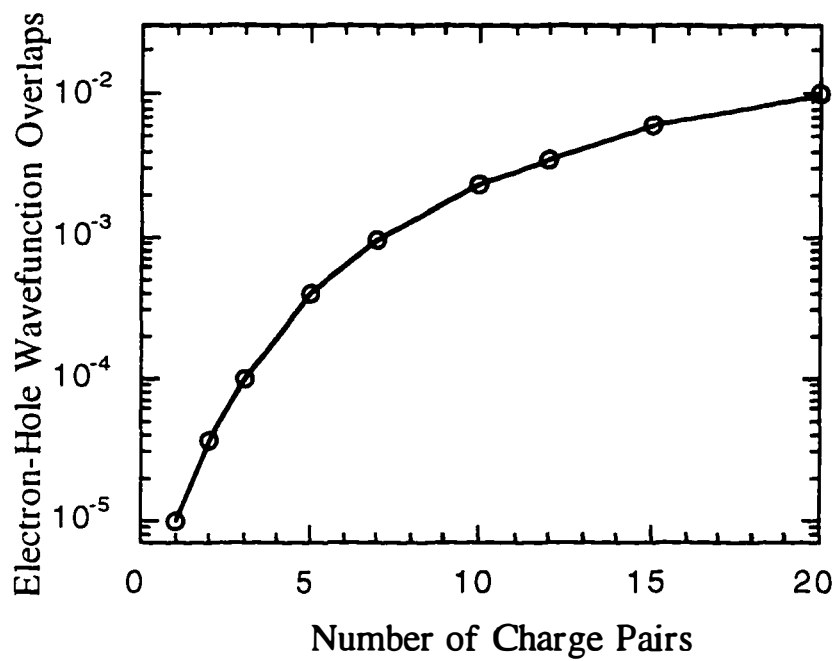
Figure 6.12 Electron and hole wavefunction overlap as a function of
the space charge pair. At high carrier density, a larger wavefunction
overlap can lead to a faster decay rate.
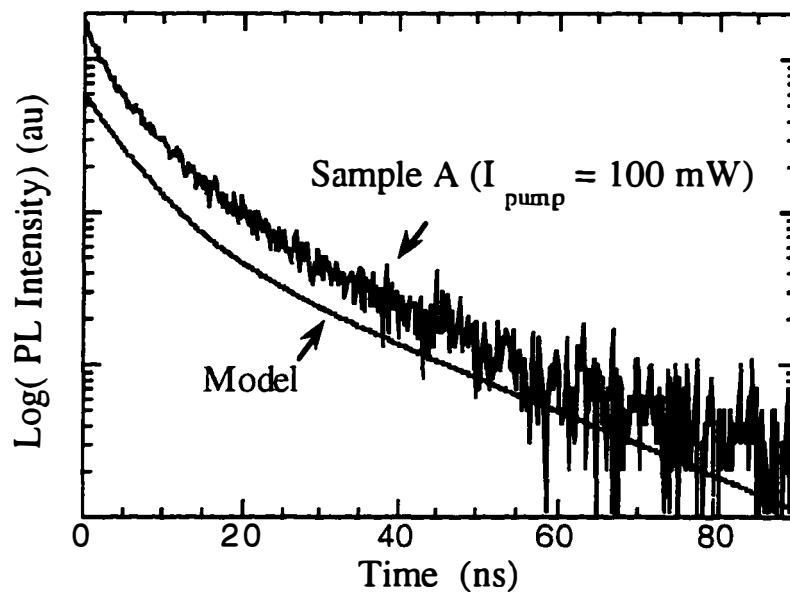
Figure 6.13 Calculated (Equation 6.3) and measured TRPL decays for the GaSb/GaAs quantum dots. The calculated curve is offset for clarity.

6.10 Summary

Traditionally, the application of the GaSb materials are limited to wavelength longer than 2 μm range. Utilizing the effects of strain, near-infrared emission wavelength is achieved in GaSb/(Al)GaAs quantum dots. Optoelectronic devices suitable for the telecommunication may be achieved using this novel GaSb/GaAs quantum dot material.

Although the GaSb/GaAs quantum dots are structurally similar to the InAs/GaAs quantum dots, their optical properties are distinctly different. The spatial separation of the electrons and the holes can lead to an increased radiative lifetimes, an intensity dependence of PL emission energy, and a non-exponential TRPL decay. These results support the staggered band alignment estimated from the model-solid theory where luminescence originates from the radiative recombination between the spatially separated electron and hole pair.

References

1. B. R. Bennett, P. M. Thibado, M. E. Twigg, E. R. Glaser, R. Magno, B. V. Shanabrook, L. J. Whitman, *Journal of Vacuum Science & Technology B* **14**, 3 2195-2198 (1996).

2. B. R. Bennett, B. V. Shanabrook, R. Magno, *Applied Physics Letters* **68**, 7 958-960 (1996).

3. J. Fouquet, Ph.D. Dissertation: Recombination Dynamics in Quantum Well Semiconductor Structures, Stanford University, (1986).

4. E. R. Glaser, B. R. Bennett, B. V. Shanabrook, R. Magno, *Applied Physics Letters* **68**, 25 3614-3616 (1996).

5. F. Hatami, *et al.*, *Applied Physics Letters* **67**, 5 656-658 (1995).

6. W. Herring, T. Geballe, J. Kunzler, *Bell Sys. Tech. J.* **38**, 657 (1959).

7. R. Keyes, *Solid State Phys* **11**, 149 (1960).

8. P. S. Kopev, S. V. Ivanov, N. N. Ledentsov, B. Y. Meltser, M. Y. Nadtochii, V. M. Ustinov, *Soviet Physics Semiconductors-USSR* **24**, 4 450-451 (1990).

9. U. E. H. Laheld, F. B. Pedersen, P. C. Hemmers, *Physical Review B-Condensed Matter* **52**, 4 2697-2703 (1995).

10. N. N. Ledentsov, J. Bohrer, M. Beer, F. Heinrichsdorff, M. Grundmann, D. Bimberg, *Physical Review B-Condensed Matter* **52**, 19 14058-14066 (1995).

11. M. P. Mikhailova, A. N. Titkov, *Semiconductor Science and Technology* **9**, 7 1279-1295 (1994).

12. D. V. O'Connor, D. Phillips, *Time-Correlated Single Photon Counting* (Academic Press, London-Orlando, 1984).

13. J. M. Rorison, *Physical Review B-Condensed Matter* **48**, 23 17651-17651 (1993).

14. C. K. Sun, G. Wang, J. E. Bowers, B. Brar, H. R. Blank, H. Kroemer, M. H. Pilkuhn, *Applied Physics Letters* **68**, 11 1543-1545 (1996).

178
16. C. G. Van de Walle, *Physical Review B (Condensed Matter)* **39**, no.3 1871-83 (15 Jan. 1989).

17. C. Weisbuch, B. Vinter, *Quantum Semiconductor Structures : Fundamentals and Applications* (Academic Press, Boston, 1991).

18. B. A. Wilson, *IEEE Journal of Quantum Electronics* **24**, no.8 1763-77 (Aug. 1988).

Chapter Seven

Summaries and Conclusions

7.1 Looking at the Present

The present understanding of carrier dynamics in quantum dots mostly derived from theoretical calculations. The contribution of this disseration is to provide some inital experimental evidences to justify the existing theoretical understanding of quantum dot carrier dynamics. The objective of this chapter is to summarize what we have learned from the previous chapters. Since the present research on the carrier dynamics in self-organized quantum dots is incomplete in scope and idealized in assumption, open questions and future research opportunities will be addressed.

From the experiments in the previous chapters, we have gained some basic understandings of carrier dynamics which are intrinsic to the self-organized quantum dots. Section 7.1 of this chapter will summarize our experimental results. Some of the ideas for the future research will be discussed in Section 7.2. Based on the dynamic processes we have studied, Section 7.3 of this chapter will consider the implication for the design of quantum dot lasers. The effects on optical gain and modulation responses will be shown in Section 7.4 and 7.5, respectively. Section 7.6 will conclude this dissertation by summarizing the design considerations for the quantum dots lasers.

7.1.A. Carrier Capture/Relaxation Process: Phonon Bottleneck

From the photoluminescence efficiency (Chapter 4) and the ultrafast absorption spectroscopy (Chapter 5), we find that the effect of phonon-relaxation bottleneck is not as severe as the phonon-relaxation bottleneck theory (Benisty *et al.* 1991) has predicted. The experimental results have shown that the quantum dot PL efficiency is comparable to the reference quantum well, and the measured carrier capture/relaxation time is similar to the values reported for GaAs quantum well (Knox, 1986). This observed fast carrier capture and relaxation process in the self-organized quantum dot indicates that the dominant relaxation mechanism in the quantum dots is still not clarified, and that relaxation processes based on other scattering mechansims such as Auger-like processes (Bocklemann *et al.*, 1992; Efros *et al.*, 1995) need to be carefully considered.

From the temperature dependent radiative lifetime study (Section 4.9), we observed a reduction in the carrier-LA phonon scattering, qualitively supporting the calculation of Bockelmann and Bastard (1992).

7.1.B. Radiative Recombination Process

From the time-resolve photoluminescence of quantum wells and quantum dots, we understand that the observed longer radiaitve lifetimes of the self-organized quantum dots can be attributed to the effect of localization. The radiative lifetime of quantum structure is determined by three factors: 1. material oscillator strength, 2. wavefunction overlap of the electron and hole pair, and 3. the ratio of coherence length to the Bohr radius of exciton. By comparing our measurement results with the published quantum dot carrier lifetimes (Table 3.3), we understand

that the radiative recombination rate in quantum dots is significantly reduced by the effect of carrier localization.

7.1.C. Thermionic Emission Process

The temperature dependent study has taught us that the effect of thermionic emission is significant. The quenching of PL efficiency at high temperature is attributed to the onset of thermionic emission process. From the good agreement between our experimental results and theory (Bacher *et al.* 1991), we understand the height of the confinement barrier will govern the dynamics of thermionic emission process.

7.1.D. GaSb/GaAs Quantum dots

The study of the spatially indirect exciton in GaSb/GaAs quantum dots demonstrated the wide wavelength range of the self-organized quantum dots. Traditionally, the application of the GaSb materials are limited to wavelength longer than 2 μm range. Utilizing the effects of strain, near IR emission wavelength is achieved in GaSb/(Al)GaAs quantum dots.

A reduction of radiative recombination rate is observed in the GaSb/GaAs quantum dots, which is attributed to the spatially indirect exciton induced from the staggered band alignment. A significant space charge effect is seen from the intensity dependence photoluminescence and time resolved photoluminescence. At a higher excitation intensity, a blue shift of the PL emission and a faster decay is measured. This space field effect may be utilized to construct tunable quantum dot devices in the near IR region.

7.2 Future Research

The present research on the carrier dynamics in self-organized quantum dots is incomplete in scope and idealized in assumption. There are many un-explored areas that can offer future research opportunities.

A more detailed study of the scattering mechanism in quantum dots would require a higher signal-to-noise ratio than the experiment present in this disseration. With the improvement of the dot growth control, multiple layers of the quantum dots with a brighter PL intensity and a higher absorption may allow us to better resolve the PL decay and the absorption dynamics on the femtosecond scale.

The idealized assumption of isotropic strain in the quantum dots needs to be further explored. A proper understanding of the strain profile will be necessary for the engineering and design of the quantum dot devices. The heights of conduction band and valence band offsets are critical to the carrier dynamics and the optical gain of the quantum dot materials.

The study of the spatially indirect exciton in GaSb/GaAs quantum dots demonstrated the wide wavelength range of the self-organized quantum dots. Traditionally, the application of the GaSb materials are limited to wavelength longer than 2 um range. Utilizing the effects of strain, near IR emission wavelength is achieved in GaSb/(Al)GaAs quantum dots. The space field effect in these dots can be utilized to construct tunable laser in the near IR region.

Today's material research is driven by potential device applications. Novel materials like quantum dots are expected to fuel the industry's thirst for better device performance. One of the ultimate goal of quantum dot research is to provide improved material properties for optoelectronic applications. The carrier dynamic

studied in this dissertation will influence the potential device parameters. The rest of this chapter will discuss how our understanding of quantum dot carrier dynamics will affect the performance parameters of quantum dot laser.

7.3 Quantum Dot Lasers: Looking into the Future

Semiconductor quantum dot lasers are expected to have a larger differential gain, a lower threshold current (Asada *et al.*, 1986), and an improved temperature characteristic (Arakawa and Sakaki, 1982). Because many aspects in the fabrication of the quantum dot lasers are identical to the quantum well lasers, many research groups have already successfully demostrated lasing using self-organized quantum dot materials (Table 7.1).

Despite this rapid progress, it is clear that the device performance for these first generation quantum dot lasers is far from the quantum well lasers. In this chapter, the implications of the carrier dynamics studied in this dissertation will be summarized by investigating the potential and the limitations in the quantum dot laser. Section 7.4 will discuss the effect of the carrier capture and emission on the optical gain in the quantum dot material. The rapid thermal carrier emission process in the quantum dots can lead to vastly different optical gain profiles. In Section 7.5, following the analysis of high speed quantum well lasers, the effect of carrier transport on the high speed potential of the quantum dot laser will be analyzed. Section 7.6 will summarize the design criteria for efficient and wide bandwidth quantum dot lasers.

Reference	T (K)	Material	Threshold A/cm^2	Notes
Moritz *et al.*	300	$Ga_{0.52}In_{0.48}P/InP$	23*	optical pump
Zaitsev *et al.*	300	$In_{0.5}Ga_{0.5}As/Al_{0.15}Ga_{0.85}As$	15	high ηi
Mirin *et al.*	300	$In_{0.3}Ga_{0.7}As/GaAs$	500	low temperature dependent lasing wavenegth
Saito *et al.*	300	$In_{0.5}Ga_{0.5}As/Al_{0.25}Ga_{0.75}As$	5120	VCSEL
Fafard *et al.*	77	$In_{0.64}Al_{0.36}As/Al_{0.3}Ga_{0.7}As$	700	visible
Kirstaedter *et al.*	77	InA/GaAs	20	high gain

* kW/cm^2.

Table 7.1 The summary of published self-organized quantum dot laser results. All references are dated in 1996.

7.4 Optical Gain in Quantum Dots

The expression for the optical gain in semiconductor material is given by (Yan, Corzine, and Coldren, 1990):

$$g(E) = \frac{4\pi^2 e^2}{3\hbar c} \frac{1}{\sqrt{\varepsilon}} \frac{P^2}{E} \rho(E)(f_c - f_v) \qquad (7.1)$$

where P^2 is the Kane matrix element, and ρ is the reduced density of states. The f_c and f_v are the distribution functions of electrons in the conduction band and holes in the valence band. In the bulk and the quantum well materials, the occupation probability which minimizes the free energy of the free electron (or hole) gas is given by the Fermi-Dirac distribution:

$$f_{n,p} = \frac{1}{1 + e^{(E-E_f)/kT}} \qquad (7.2)$$

where E_f is the quasi-Fermi level in the conduction band or the valence band, defined within a continous energy states. In a single quantum dot, since the energy levels and the distribution function become discrete, the definition of the Fermi energy and the concept of the free electron gas require careful considerations.

The Fermi energy (or the chemical potential) of a free electron gas is defined as $E_f \cong \partial U/\partial N$, which is the energy change required when adding or removing another electron in the next empty state. For a quantum dot with only a single bound state, the chemical potential of the quantum dot is given by the energy of the confinement barrier. Therefore, the occupation probability in a quantum dots is simply given by $(E-E_f) = (-\Delta E)$ in Equation 7.2.

The above result can also be determined analytically from the carrier dynamics model of the thermal emission and capture. The occupation probability is obtained by solving the steady state rate equation in a quantum dot.

$$\frac{\partial f}{\partial t} = \frac{1-f}{\tau_{capture}} - \frac{f}{\tau_{escape}} - \frac{f}{\tau_{radiative}} = 0 \qquad (7.3)$$

where $\tau_{radiative}$ is the spontaneous emission lifetime, $\tau_{capture}$ is the carrier capture time, and τ_{escape} is the thermionic emission time. Assuming the spontaneous emission rate is several orders less than the carrier capture rate, an expression for $f(E)$ is obtained.

$$f(E) = \frac{1}{1 + \dfrac{\tau_{capture}}{\tau_{escape}} + \dfrac{\tau_{capture}}{\tau_{radiative}}} \approx \frac{1}{1 + \dfrac{\tau_{capture}}{\tau_{escape}}} \equiv \frac{1}{\chi} \qquad (7.4)$$

Equation (7.4) may be further simplified by employing the thermionic emission theory discussed in Chapter 4 (Equation 4.1).

$$f(E) = \frac{1}{1 + e^{-\Delta E/kT}}. \qquad (7.5)$$

where ΔE is the confinement energy of the quantum dot. This result is identical to the one obtained from the statistical arguement. From Equation (7.4) and (7.5), two distinct carrier distributions can occur in the inhomogenously broadened quantum dot ensemble. The optical gain resulted from the two different cases will dictate the

187

device properties of the quantum dot lasers, such as internal quantum efficiency, differential gain, spectral position, and temperature characteristics.

7.4.A Strong Confinement / Low Temperature ($e^{-\Delta E/kT} \ll 1$)

For the case of strongly confined carriers, the gain profile essentially follows the size distribution of the quantum dots (Figure 7.1a). Peak gain occurs at the maximum of the dot size distribution. Since the occupation probabilities are identical in all dots, the increase of the material gain requires the filling of all quantum dot states.
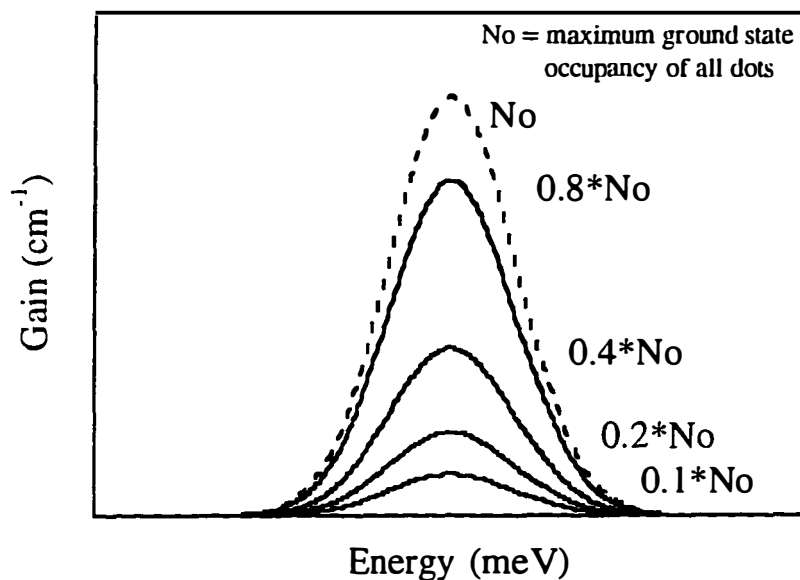

Figure 7.1a Gain spectra vs. carrier density in quantum dots with a strong quantum confinement. These theoretical curves is obtained from Equation (7.1) and (7.5), in the limit of $e^{-\Delta E/kt} \ll 1$.

7.4.B Weak Confinement / High Temperature ($e^{-\Delta E/kT} \gg 1$)

For the case of shallow confinement, the effect of the thermionic emission will lead to the redistribution of carriers in the quantum dot ensemble. Quantum dots with a lower energy will have the highest occupation probability. Figure 7.1b illustrates the gradual filling of carriers in the quantum dot distribution.
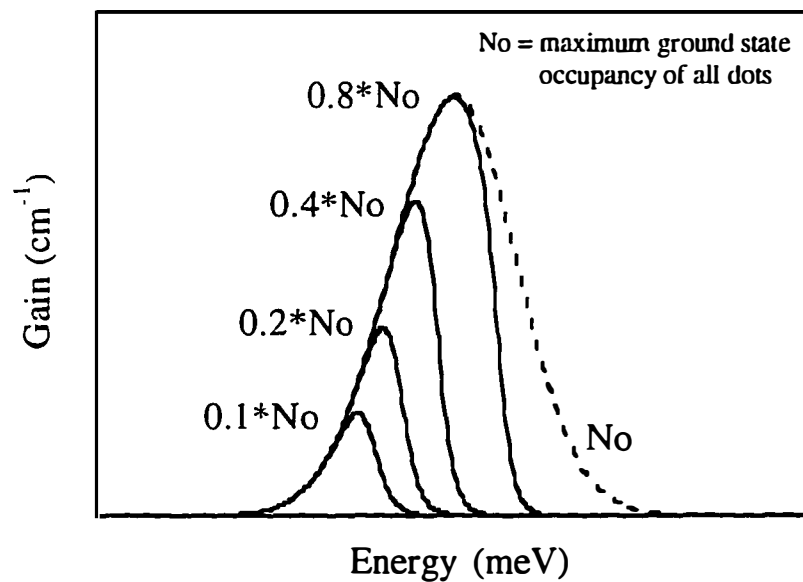

Figure 7.1b Gain spectra vs. carrier density in quantum dots with a weak quantum confinement. These theoretical curves is obtained from Equation (7.1) and (7.5), in the limit of $e^{-\Delta E/kT} \gg 1$.

7.4.C Differential Gain

The peak gain vs. carrier density from Figure 7.1 a and b is plotted in Figure 7.2. For the case of the shallow carrier confinement, a higher differential gain is observed at lower carrier density. The peak gain saturates once 50 % of dots are filled. Higher gain can only be obtained from the filling of the excited states.

Unlike the shallow confinement case, the peak gain in the strong confinement case can be reached only when all dots are filled. A higher quantum efficiency is obtained from the shallow confinement case. Less carriers are required to achieve the threshold condition.
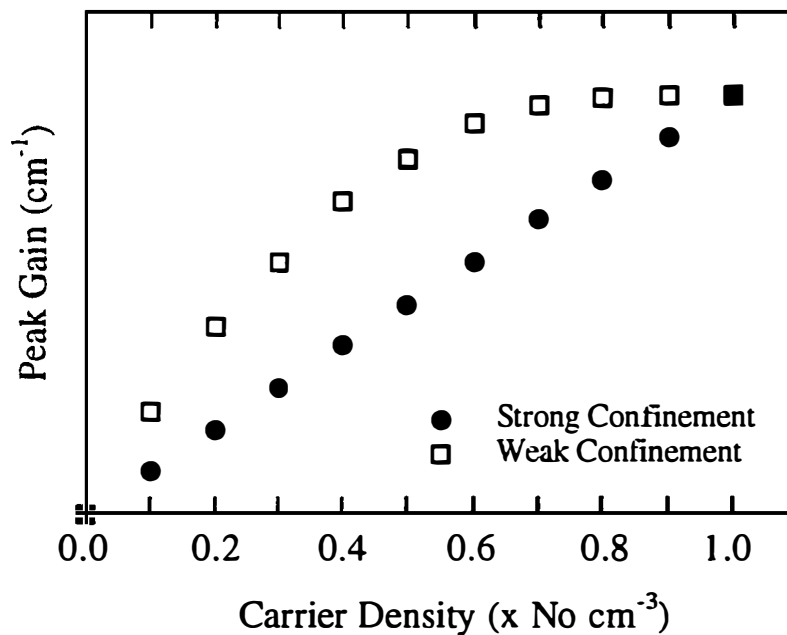

Figure 7.2 Peak gain vs. carrier density in the quantum dot lasers. Solid dots are strong confinement case (Figure 7.1a), and open square are the weak confinement case (Figure 7.1b). Higher differential gain can be obtained from the weaker confinement case.

7.5 Transport Effect on Modulation Reponse of Quantum Dot Lasers.

In spite of the higher quantum efficiency may be obtained from the shallow confinement case, the effect of the fast thermionic emission can limit the modulation response. Nagarajan *et. al.* (1992) have derived the modulation response for the quantum well lasers by considering the effect of carrier transport.

$$M(\omega) \propto \left(\frac{1}{1 + j\omega\tau_{capture}} \right) \frac{1}{\omega_r^2 - \omega^2 + j\omega\gamma} \qquad (7.6)$$

where

$$\omega_r^2 = \frac{(v_g g_o / \chi) S_o}{\tau_p (1 + \varepsilon S_o)} \left[1 + \frac{\varepsilon}{(v_g g_o / \chi)(\chi\tau_{spon})} \right]$$

$$\gamma = \left[\tau_p + \frac{\varepsilon}{(v_g g_o / \chi)} \right] \omega_r^2 + \frac{1}{\chi\tau_{spon}} \qquad (7.7)$$

where ω_r is the resonance frequency, γ is the damping factor, S_o is the photon density, g_o is the differential gain, and ε is the gain saturation factor. The transport factor χ in Equation (7.7) is identical to the occupation probability derived in Equation (7.4). Equation (7.6) and (7.7) suggest several potential high speed limitations of the quantum dot laser.

1. The roll-off of the frequency response is dependent on the carrier capture time in the quantum dot. A servere reduction of 3 dB bandwidth can occur if the effect of a phonon relaxation bottleneck is significant.

2. For the case of a quantum dot laser with a shallow confinement, the effect of transport will significantly reduce the differential gain and increase the spontaneous emission lifetime, resulting in reductions in the 3 dB bandwidth and damping factor.

3. Due to the limited packing density and the small dot volume, the effect of the gain saturation may be important at a high photon density. Other possible contributing effects such as spectral hole burning and carrier heating have yet to be explored in the quantum dot laser.

7.6 Quantum Dot Laser Design Considerations

To properly design the quantum dot laser for its potential application, one needs to carefully consider the carrier dynamics presented in the previous chapters. The radiative lifetime of the carriers in the quantum dots will govern the threshold properties of the quantum dot laser. A longer upper state lifetime will enhance the population inversion and lead to a lower threshold current. The carrier lifetime is determined not only from the oscillator strength of the material but also the coherence area and overlap of the wavefunctions.

To minimize the potential bandwidth reduction due to the phonon-relaxation bottleneck, a fast carrier capture time may be obtained by selecting the confinement energy of the lasing dots to be a multiples of LO phonon energy.

For the high speed design of the quantum dot laser, one needs to reduce the effect of thermionic emission by selecting a larger confinement energy. Because the

threshold gain condition requiring the filling of all dots, this isolation of the carriers in the quantum dots will increase the threshold current and reduce the quantum efficiency. This trade off of threshold current and quantum efficiency can only be circumvented by improving the size distribution of the quantum dots. Increasing the dot density by using multiple layers of quantum dots or high packing density can only increase the threshold carrier density by creating excess energy levels do not contribute to the peak gain.

For the case of the quantum dot laser with shallow confinement energies, the efficient transport of the carriers to the lasing dots can occur due to the fast thermionic emission process in the non-lasing dots. A lower threshold and a higher quantum efficiency may be obtained in CW operation than the larger confinement case. In this case, higher material gain can be obtained using multiple layers of dots since the excess energy levels above the lasing mode does not need to be filled.

Despite the difficulties in attaining an efficient quantum dot laser that is comparable to the performance of a quantum well laser, there are other incidental adventages associated with the self-organized quantum dot lasers. Because the significantly larger strain can exist in the self-organized quantum dot than quantum well. a wider wavelength range may be achieved by extending the limits for misfit dislocations by lateral strain relief. Quantum dot photolumiescence at 1.3 μm has been demonstrated by Mirin et al. (1996) using InGaAs/GaAs material. Using GaSb/GaAs quantum dots, we have observed 0.9 μm light emission. These wavelengths cannot be obtained previously from quantum well structures using similar materials. The complete spectral range of the self-organized quantum dot material has yet to be explored fully. The idea of obtaining 1.3 μm light source

using only GaAs materials may ease the integration of high speed optoelectronic sources with high speed circuits.

The temperature dependence of lasing wavelength can also be modified significantly. Mirin *et al.* (1996) have shown that an improved temperature dependence of lasing wavelength can be obtained using self-organized quantum dots. By balancing the temperature dependent bandgap energy shift with the level filling effect in quantum dots, a flat temperature dependent lasing wavelength can be achieved.

The major improvement in the area of the quantum dot laser will depend significantly on the growth control and the reduction of size flucutation. Without this progress, quantum dot lasers cannot utilize the desired advantage derived from the 0D confinement. On the other hand, the broad spectral width of spontaneous emission is uncharacteristic among the semiconductor materials. One may utilize this large bandwidth to produce wavelength tunable and modelocked quantum dot lasers.

The future applications of the quantum dot materials are limited only by our knowledge of the fundamental physics. With the proper understanding of the self-organized quantum dots, the potential uses of these artificial atoms are only limited by our imaginations.

References

1. Y. Arakawa, H. Sakaki, *Applied Physics Letters* **40**, no.11 939-41 (1 June 1982).

2. M. Asada, Y. Miyamoto, Y. Suematsu, *Journal of Quantum Electronics* **QE-22**, no.9 1915-21 (Sept. 1986).

3. S. Fafard, K. Hinzer, S. Raymond, M. Dion, J. McCaffrey, Y. Feng, S. Charbonneau, *Science* , to be published in 1997.

4. N. Kirstaedter, *et al.*, *Applied Physics Letters* **69**, 9 1226-1228 (1996).

5. R. Mirin, A. Gossard, J. Bowers, *Electronics Letters* **32**, 18 1732-1734 (1996).

6. A. Moritz, R. Wirth, A. Hangleiter, A. Kurtenbach, K. Eberl, *Applied Physics Letters* **69**, 2 212-214 (1996).

7. R. Nagarajan, M. Ishikawa, T. Fukushima, R. S. Geels, J. E. Bowers, *IEEE Journal of Quantum Electronics* **28**, 10 1990-2008 (1992).

8. H. Saito, I. Ogura, Y. Sugimoto, *Photonics Technology Letters* **8**, 9 1118-1120 (1996).

9. R. H. Yan, S. W. Corzine, L. A. Coldren, I. Suemune, *Journal of Quantum Electronics* **26**, 2 213-216 (1990).

10. S. Zaitsev, A. Georgievski, N. Gordeev, V. Kopchatov, V. Ustinov, A. Zhukov, A. Egorov, D. Bimberg, *Proc. SPIE Int Conf Optical Dimension, Kiev, Ukraine* , 287 (1995).